April 29, 1957

To the Graduate Council:

I am submitting herewith a thesis written by John William Prados entitled "The Analysis of Two-Dimensional Laminar Flow Utilizing a Doubly Refracting Liquid." I recommend that it be accepted in partial fulfillment of the requirements for the degree of Doctor of Philosophy with a major in Chemical Engineering.

F. N. Peebles
Major Professor

We have read this thesis
and recommend its acceptance:

W. O. Harms

R. M. Boarts

Edgar D. Eavis

H. L. Johnson

E. E. Stansbury

Hilton A. Smith

Abb Jury

Accepted for the Council:

Charles P. White for
Dean of the Graduate School

THE ANALYSIS OF TWO-DIMENSIONAL LAMINAR FLOW UTILIZING A DOUBLY REFRACTING LIQUID

A THESIS

Submitted to
The Graduate Council
of
The University of Tennessee
in
Partial Fulfillment of the Requirements
for the degree of
Doctor of Philosophy

---

by

John William Prados

June 1957

Experiment Station. The author wishes to thank these agencies for the opportunity of conducting graduate research under their support.

Thanks are due to Mr. E.H. Honeycutt, Laboratory Supervisor, and his staff for their aid in the construction and modification of the experimental equipment. Mr. H. B. Thompson performed the difficult task of constructing the flow test channels and the equipment benches, and provided many helpful suggestions in the design of the flow system components. Messrs. B. L. McGill, T. A. Long, and O. V. Prater were of great assistance in the modification and maintenance of the refrigeration and fluid circulation systems.

The author's association with the staff and graduate students of the Department of Chemical Engineering has been an invaluable experience, and has been of considerable aid, directly and indirectly, in his work under the present investigation. Particular thanks are due to Dr. H. F. Johnson and Mr. C. R. Brooks for their advice on problems of photography.

Mrs. Dorothy Norton undertook the arduous task of typing the final draft of this report. Her careful typing and excellent suggestions for improvement of the format are gratefully acknowledged. The skillful draftmanship of Mr. J. C. Eubanks in the preparation of the difficult drawings for Figure 16 of this document is also recognized with thanks.

Finally, the author wishes to express deepest appreciation to his wife, Lynn B. Prados. She has made many major contributions to this thesis, among them the typing of the original draft. Her chief contribution, however, has been her continued support and her cheerful acceptance of the major and minor inconveniences occasioned by her husband's graduate study.

ABSTRACT

The optical characteristic exhibited by certain liquids known as flow double refraction offers attractive features in the analysis of two-dimensional laminar flow situations, especially those in which measuring probes are undesirable. Such liquids become anisotropic to the passage of light when set in motion; and when they are viewed in polarized light while flowing through a transparent channel, visible interference patterns are observed. These patterns may be related to the magnitude and direction of the shearing stresses set up by two-dimensional laminar flow, and from suitable calibration under known flow conditions they may be used to determine the stress distribution in an unknown flow situation.

Attempts made by previous investigators to apply this technique to the analysis of flow have not yielded promising results. The doubly refracting test liquids used have been either very unstable or extremely viscous. Also, results have been analyzed under the assumption that doubly refracting properties could be correlated directly in terms of streamline directions and velocity gradients, rather than in terms of the direction and magnitude of the shearing stresses in the liquid. This assumption appears questionable in the light of certain experimental facts noted in this investigation, except for flow cases involving parallel streamlines.

The objectives of the present investigation were two-fold: (a) the development of methods for predicting streamline directions and velocity gradients from the stress distributions obtained from double refraction measurements, thus avoiding the necessity of any direct correlation between the gradients themselves and the doubly refracting properties, and (b) the experimental application of these methods to two-dimensional laminar flow situations, and the checking of results by independent means whenever possible.

The desired analytical methods were developed, and experimental studies were carried out for the following situations: (a) flow between parallel plates, (b) converging and diverging flow between flat, non-parallel plates, and (c) flow about a cylindrical obstacle in a bounded channel. In case (a), streamlines were determined by the parallel channel walls. In case (b), streamlines were assumed to be straight lines emanating radially from the point of intersection of the non-parallel walls. In case (c), streamlines were determined from information on stress directions obtained from the flow double refraction patterns. The doubly refracting liquids employed were aqueous solutions of a commercial dye, milling yellow, which remain stable over a period of approximately two weeks, and which have viscosities in the neighborhood of twenty centipoises. They show Newtonian behavior under shearing stresses less than 5 dynes per

square centimeter, the range of interest of this investigation. Correlation of doubly refracting properties with stress was obtained by observation of the known flow situation in the annular space between fixed and rotating concentric cylinders. The flow test channel was made of Plexiglas and was of rectangular cross section with a high aspect ratio (ratio of width to depth) in order to approximate two-dimensional flow. The channel was five inches wide and contained 1-inch and $\frac{1}{2}$-inch deep sections joined by a converging section.

A velocity profile obtained from double refraction measurements for plane parallel flow was checked with that predicted by the theoretical formula for flow between plane parallel plates, and all points agreed within $\pm$ 3.0 per cent. Velocity profiles in plane parallel, converging, and diverging flow were integrated to yield total discharges which were compared with experimentally measured discharges for each case. Agreement was within a maximum deviation of $\pm$ 10.0 per cent and a mean square deviation of 4.2 per cent for all plane parallel flow cases, and within a maximum deviation of $\pm$ 13.5 per cent and a mean square deviation of 7.8 per cent for all converging and diverging flow cases. The experimental discharge was required in the analysis of flow about a cylindrical obstacle, and could not be used for comparison. However, the viscous drag coefficient for the cylinder was calculated from flow double refraction measurements and compared

with theoretical and experimental literature values. Agreement was found within 2.0 per cent with the theoretical value and within 10.5 per cent with the experimental value. The range of flow rates covered was from 20 to 200 cu.cm./sec., and corresponded to Reynolds numbers from approximately 1 to 10.

In conclusion, it appears that the technique offers attractive possibilities for the analysis of complex two-dimensional laminar flow situations, and with certain experimental refinements, should be capable of even better results than those reported above.

TABLE OF CONTENTS

CHAPTER		PAGE
I.	INTRODUCTION	1
II.	FLOW ANALYSIS FROM DOUBLE REFRACTION MEASUREMENTS	5
	General Considerations	5
	Mathematical Relationships	13
III.	EXPERIMENTAL EQUIPMENT	28
	The Optical System	30
	The Flow Test Channel	34
	The Fluid Circulation System	36
	The Calibration Equipment	39
IV.	THE EXPERIMENTAL TECHNIQUE	43
	The Optical Calibration	43
	The Photographing of the Flow Test Patterns	48
	The Measurement of the Flow Photographs . .	51
	Supporting Experimental Activities	54
V.	THE ANALYSIS OF THE FLOW PATTERN PHOTOGRAPHS AND REPRESENTATIVE RESULTS	57
	Straight Parallel Flow	57
	Converging and Diverging Flow	63
	Flow about a Cylindrical Obstacle	70
VI.	TABULATED RESULTS AND DISCUSSION	76
	Flow in Straight Channels	76

CHAPTER PAGE

VI. (continued)

Convergent and Divergent Flow 78

Flow about a Cylindrical Obstacle 84

Recommended Improvements 86

Parallel and Future Investigations 88

VII. CONCLUSIONS AND RECOMMENDATIONS 89

LIST OF REFERENCES 91

APPENDIXES 96

A. The Shearing Stress in a Viscous Fluid in Terms of Velocity Space Derivatives 97

B. Transformation of Deformation Components from Cartesian to Stream Coordinates 100

C. Experimental Data 105

D. Sample Calculation: Straight Parallel Flow . 136

E. Sample Calculation: Converging Flow 139

F. Sample Calculation: The Cylindrical Obstacle 149

G. Calculation of the Viscous Drag Coefficient . 155

H. Optical Calibration Data 161

J. Notation 163

LIST OF TABLES

TABLE		PAGE
I.	Distribution of Velocity and Velocity Gradient across a Straight Channel of Aspect Ratio 10:1	61
II.	Distribution of Velocity and Velocity Gradient across a Straight Channel of Aspect Ratio 5:1	62
III.	Calculated Velocity Profiles across a Divergent Channel	67
IV.	Calculated Velocity Profiles across a Convergent Channel	69
V.	Agreement between Observed Discharges and Those Calculated from Double Refraction Measurements for Flow in Straight Channels .	77
VI.	Agreement between Observed Discharges and Those Calculated from Double Refraction Measurements for Flow in Convergent and Divergent Channels	79
VII.	Experimental Data Recorded while Photographing Isochromatic Patterns	106
VIII.	Experimental Data Recorded while Photographing Isoclinic Patterns	108
IX.	Measured Positions of Isochromatic fringes in Straight Channels	109

TABLE		PAGE
X.	Measured Positions of Isochromatic Fringes in Converging Channels	117
XI.	Measured Positions of Isochromatic Fringes in Diverging Channels	120
XII.	Measured Position of Isochromatic Fringes along Vertical Grid Lines about Cylinder . .	123
XIII.	Values of the Isoclinic Angle along Vertical Grid Lines about Cylinder	129
XIV.	Sample Calculations for Straight Parallel Flow	137
XV.	Sample Calculation for Convergent Flow	142
XVI.	Stream Function, ψ, Upstream from Cylinder . .	150
XVII.	Calculation of the Viscous Drag Force on a Cylindrical Obstacle	158

LIST OF FIGURES

FIGURE		PAGE
1.	Typical Light Interference Patterns Produced by Flow Double Refraction in Aqueous Milling Yellow Solutions	7
2.	Relationships between Coordinates and Velocity Components in Rectangular Cartesian and Stream Coordinate Systems	15
3.	Stream Coordinates in Straight, Converging or Diverging Flow	23
4.	Photographs of the Flow Facility	32
5.	Schematic Representation of the Optical System .	33
6.	Photographs of the Flow Test Channel	35
7.	Schematic Representation of the Fluid Circulating System	38
8.	Schematic Representation of the Concentric Cylinder Polariscope	41
9.	Appearance of the Isoclinic and Isochromatic Fringes in the Flow Cell of the Concentric Cylinder Polariscope	45
10.	Flow Pattern Photograph and Plots of Velocity Gradient and Velocity versus Distance for a Straight Channel of 10:1 Aspect Ratio	58

FIGURE PAGE

11. Flow Pattern Photograph and Plots of Velocity Gradient and Velocity versus Distance for a Straight Channel of 5:1 Aspect Ratio 59

12. Comparison of Velocity Profiles Calculated from Equation (25) and Obtained from Flow Double Refraction Measurements 64

13. Photograph and Developed Velocity Profiles for Flow in a Diverging Channel 66

14. Photograph and Developed Velocity Profiles for Flow in a Converging Channel 68

15. Tabulation of the Values of the x-Component of the Rate of Deformation, E_{xy}, and the Stream Function, ψ, at the Corners of the Co-ordinate Grid 71

16. Steps in the Development of Streamlines about a Cylinder 74

17. Flow Patterns Produced in a Converging Channel from Plane and Circularly Polarized Light at Comparable Flow Rates 81

18. Square Element of a Continuum, Subjected to a Generalized Two-Dimensional Stress System . . 97

19. Relationships between Coordinates and Velocity Components in Rectangular Cartesian and Stream Coordinate Systems 100

FIGURE PAGE

20. Interpolation Plot of Rate of Deformation versus Distance from Center of Channel along a Circular Arc; Convergent Flow 148

21. Interpolation Plot for Isoclinic Angle and Rate of Deformation along Vertical Grid Line Number 6 151

22. Tabulation of Intermediate Data at the Corners of the Coordinate Grid 152

23. Viscous Drag Forces on a Circular Cylinder . . . 156

24. Optical Calibration Curves for Test Solutions T-7 and T-8 162

CHAPTER I

INTRODUCTION

During the last century a number of techniques (5)* have been developed for the visual study of fluid motion. These have been of particular use in the analysis of flow situations which are too complex to analyze mathematically, and which at the same time are unsuited for the more common experimental measuring devices such as the pitot tube or hot-wire anemometer. In many instances the insertion of a probe of any type into the flowing fluid will distort the flow, and render the results of measurements questionable.

The majority of visual techniques yield only qualitative information about the fluid motion. However, there exists a method which may be used for quantitative study of two-dimensional laminar flow. This method makes use of an optical property exhibited by certain liquids known as flow double refraction and depends on the occurrence of visible light interference patterns related to the viscous stresses in the moving liquid. These patterns are observed when a doubly refracting liquid is caused to flow through a transparent channel and is viewed in plane or circularly polarized

---

*Numbers in parentheses refer to the List of References, page 91.

light. Under known flow conditions, a quantitative relationship can be established between the observed interference pattern and the rate of deformation in the flowing fluid. This relationship may then be applied to determine the rates of deformation from the interference pattern set up by an unknown flow situation.

In spite of the quantitative possibilities of the flow double refraction technique, the majority of previous investigations (6)(7)(20)(21)(32) have been qualitative in nature, and most of the few existing quantitative treatments (9)(15)(16)(34)(35) have been based on questionable assumptions. Moreover, previous investigators (1)(9)(32) have been hampered by the undesirable properties of their doubly refracting liquids, i.e., extremely high viscosity or marked instability on contact with most common materials of construction.

It was felt that this method offered unique advantages for the analysis of complex two-dimensional laminar flow situations, and the present work was undertaken in an attempt to overcome some of the previous difficulties and place the analysis of results on a sounder basis. Specifically, the objectives were twofold: (a) the development of mathematical techniques for flow analysis from double refraction measurements based on more generalized assumptions than those previously employed, and (b) the application of these techniques

to the experimental analysis of a number of two-dimensional laminar flow situations. It was also desired to check the experimental results by independent means wherever possible.

To achieve these objectives, a mathematical analysis was made to relate desired flow parameters to quantities which could be obtained from flow double refraction measurements. Next an experimental study was carried out for three types of two-dimensional laminar flow: (a) flow between parallel plates in which case the streamlines are straight and parallel, (b) flow in convergent and divergent channels in which cases the streamlines are straight but not parellel, and (c) flow about a cylindrical obstacle in which case the streamlines are neither straight nor parallel. The results were analyzed in the light of the previous analysis and some suggestions by Rosenberg (27) which enable one to avoid the questionable assumptions made by former investigators.

The doubly refracting liquid used in the present study was an aqueous solution of a commercially available organic dye, milling yellow. Stable, satisfactory working solutions of this dye can be prepared with viscosities not over twenty times that of water. They exhibit marked flow double refraction in concentrations as low as 1.2 per cent dye by weight. Their use in flow studies was first reported by Peebles, Garber, and Jury (23).

In order to inform those who are not familiar with flow double refraction phenomena, a qualitative description will be presented in the following chapter together with a brief summary of the work of past investigators. In the same chapter, the method of analyzing flow situations from the double refraction measurements will be developed. This will be followed by descriptions of the experimental equipment and procedures, and finally the results of the flow analyses themselves will be presented. Mathematical derivations, sample calculations, experimental data, and notation will be found in the appendix.

CHAPTER II

FLOW ANALYSIS FROM DOUBLE REFRACTION MEASUREMENTS

General Considerations

The Observed Phenomena

Flow double refraction in liquids is analogous to the photoelastic behavior exhibited by many solids. In either case, a marked alteration in optical properties is observed when the substance is subjected to shearing stresses. In liquids, these stresses are the result of viscous forces arising from motion. Such liquids are isotropic with respect to the passage of light when at rest, but become anisotropic when set in motion. A beam of plane polarized light entering such a moving liquid is broken up into two rays vibrating at right angles to one another and traveling at different velocities. The difference in velocities between these rays is related to the maximum shearing stress set up by the liquid motion, and hence the total retardation of the slow ray behind the fast is dependent on the length of the light path in the liquid and the average maximum shear stress along the light path. If, now, the light leaving the liquid is passed through an analyzer (a piece of polarizing material whose axis of polarization is set at right angles to that of the light entering the liquid) only the resultant component of

the two rays in the plane of polarization of the analyzer can pass through. Hence regions of light interference and reinforcement result which appear as a pattern of light and dark bands. The dark bands are known as isochromatics, and for a given liquid depth, they correspond to constant values of the maximum shearing stress. These appear whether the incident light is plane or circularly polarized. They are black when a monochromatic source is employed, but take on the colors of the spectrum in white light.

Also, when the maximum shearing stress makes a certain angle with the axis of polarization of the incident light, other dark regions occur known as isoclinics. These isoclinics appear only when plane polarized light is employed, and are black whether the light source is monochromatic or white.

Typical light interference patterns for flow in various geometries are shown in Figure 1. The flow is laminar in all cases, and the light source is monochromatic (sodium vapor).

The quantitative relationships which govern the appearance of the isochromatics and isoclinics have been treated on a macroscopic basis by a number of authors (13)(14)(25)(27). The microscopic explanation of the phenomena is still a matter of great uncertainty. A number of theoretical developments based on various microscopic models have been made, and reviews of these are presented by Edsall (10), Cerf and

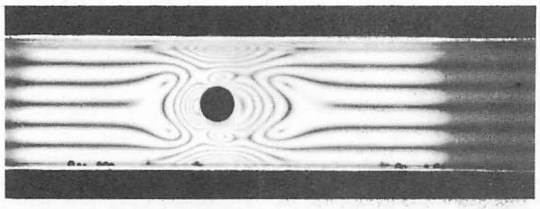

a. Flow about a cylindrical obstacle at an intermediate flow rate; circularly polarized light

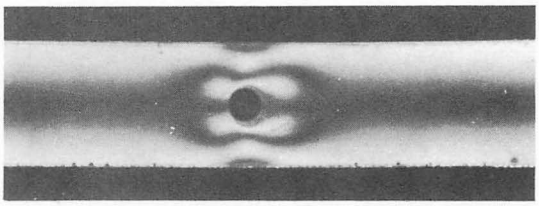

b. Flow about a cylindrical obstacle at a low flow rate; plane polarized light

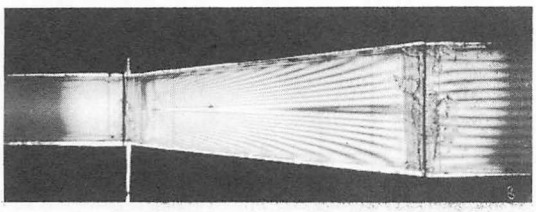

c. Flow in a diverging channel at a high flow rate; circularly polarized light

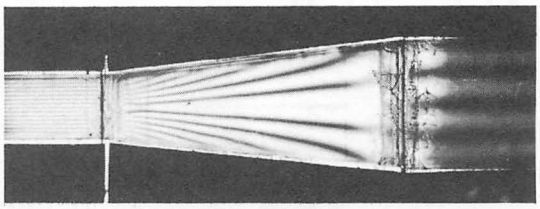

d. Flow in a diverging channel at a low flow rate; circularly polarized light

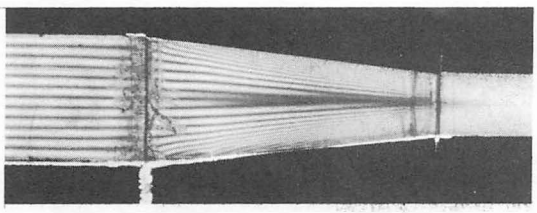

e. Flow in a converging channel at a high flow rate; plane polarized light

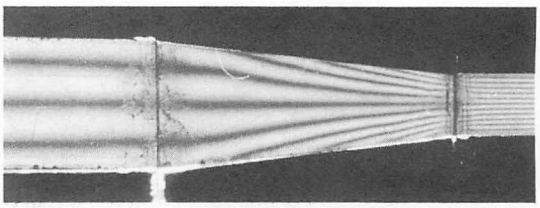

f. Flow in a converging channel at a low flow rate; plane polarized light

Figure 1. Typical light interference patterns produced by flow double refraction in aqueous milling yellow solutions

Scheraga (8), Prados and Peebles (25), and others. In general these theories will explain the behavior of certain systems but fail with others, and none as yet has been devised which will predict the behavior of all doubly refracting liquids.

The Technique of Analysis

The complete analysis of a flow situation should provide two pieces of information: (a) the streamline directions and (b) the velocity distribution. The interference patterns produced by flow double refraction do not yield this information directly, but instead give the magnitude and direction of the maximum shearing stress at each point in the flowing liquid. In order to obtain the streamlines and velocity distribution, therefore, it is necessary to determine how the direction of the maximum shearing stress is related to the direction of the streamlines and how the maximum shearing stress itself is related to the velocity gradient normal to the streamlines. These relationships are developed in the latter half of the present chapter.

From suitable optical calibration of a given liquid, one may obtain the value of the maximum shearing stress corresponding to a given isochromatic, and the angle between the maximum shearing stress and the axis of polarization of the incident light along an isoclinic. (This angle is, in general,

a function of the shearing stress itself.) This calibration is usually carried out in a concentric cylinder polariscope as described by Prados and Peebles (24).

In actual practice, it is more convenient to relate optical properties to the maximum rate of deformation, E, which is defined as the ratio of the maximum shearing stress, τ, at a point in the fluid to the fluid viscosity, μ. This permits studies to be made without complete knowledge of the viscous behavior of the doubly refracting liquid. It is an unfortunate fact that most doubly refracting liquids exhibit non-Newtonian viscosities.

When the calibrated liquid is caused to flow through a transparent channel of given geometry and viewed in plane polarized light, both isochromatics and isoclinics are visible. By inserting two suitably oriented quarter-wave plates in the light system, the light incident on the channel can be circularly polarized, and only the isochromatics will be visible. Photographs of a given flow situation, with and without the quarter-wave plates in position, can be used to determine which of the dark bands are isoclinics and which are isochromatics. The order of the isochromatics may be determined from geometric considerations, and their position accurately measured with respect to the channel boundaries.

The order of the isochromatics and the optical calibration may then be combined to specify the magnitude of the

maximum rate of deformation throughout the field of flow. The isoclinics, obtained at various orientations of the axis of light polarization, may be used to determine the direction of the maximum rate of deformation throughout the field. These data can then be treated by the mathematical techniques of the present chapter in order to obtain the desired streamline directions and velocity distribution.

Previous Investigations

A large amount of literature on flow double refraction is in existence, and extensive reviews may be found in references (8), (10), and (24). Attention will be confined here to those investigators who applied flow double refraction to the analysis of fluid motion.

The earliest of these investigators appears to have been Humphry (20) in 1923. Using a vanadium pentoxide sol he was able to demonstrate qualitatively the difference between laminar and turbulent flow. Alcock and Sadron (1) in 1936 attempted quantitative measurements of the velocity profiles of sesame oil flowing between parallel plates, and obtained reasonable agreement with theory. They were limited by the extremely high viscosity and low optical sensitivity of their liquid.

By far the most extensive of the earlier investigations were those reported by Hauser and Dewey (9)(15)(16) between

1940 and 1942. Using bentonite sols they made quantitative and qualitative studies of velocity profiles in two dimensional laminar flow. However, in the analysis of their results, two questionable assumptions were made: (a) that the direction of the streamlines could be obtained directly from the isoclinics and (b) that the isochromatics were an indication of the velocity gradient normal to the streamlines rather than the total rate of deformation in the liquid. Some calculations presented by Rosenberg (27) and some experimental observations made during the present investigation strongly indicate that these assumptions are invalid.

Weller et al. (34)(35) in 1943 carried out some studies similar to those of Hauser and Dewey using a solution of ethyl cellulose in a commercial solvent "Methyl Cellosolve" instead of bentonite. Ullyott (32) in 1947 described work similar to that of Hauser and Dewey and of Weller, but made no attempt to interpret his results quantitatively.

In 1945 Leaf (21) reported an interesting qualitative application of flow double refraction. By observing the flow of doubly refracting bentonite sols through a transparent model of a locomotive fire box, he was able to predict the flow behavior of the hot gases in the prototype and to recommend procedures for eliminating erosion of boiler tubes by ash suspended in these gases. In 1945 and 1947 Binnie (6)(7) reported the use of a doubly refracting benzopurpurin sol to

determine the point of onset of turbulence in a long circular tube. Balint (5) in 1953 presented a review of methods of visual flow analysis including flow double refraction.

A careful study of fluid flow analysis by the double refraction technique was presented by Rosenberg (27) in 1952. He showed that the direction of maximum rate of deformation in fluids and the direction of the streamlines are not coincident except for the case of parallel streamlines, and suggested a method for analyzing a general two-dimensional flow situation in which the streamlines are not parallel. No experimental measurements were reported by Rosenberg, nor did he carry out any actual flow analyses; but some of his suggestions have been extended and incorporated into the present work.

A recent investigation of interest was reported by Wayland (33) in 1955. Using both colloidal bentonite sols and pure ethyl cinnamate he studied the flow in the annular space between a fixed and a rotating cylinder. Careful investigations were carried out to yield laminar velocity distributions across the annular gap both for cases in which the inner cylinder rotated and in which the outer cylinder rotated. Measurements were also made in the transition region where the flow changes from laminar to turbulent including a regime of stable vortex formation predicted by Taylor (30). Definite breaks in the curves of amount of double refraction

versus rate of shear were found at these transition points.

Mathematical Relationships

As was pointed out earlier in this chapter, the successful determination of streamline directions and velocity distributions from double refraction measurements will require two relationships: (a) that between the maximum rate of deformation and the velocity gradient normal to the streamlines of flow and (b) that between the direction of the maximum rate of deformation and the direction of the streamlines. These relationships are developed in the following pages for the general case of two-dimensional laminar flow. The results are then applied to the calculation of the velocity profiles for various simplified situations involving known streamline directions or parallel streamlines. Finally a method is shown whereby one may calculate the Stokes stream function throughout the field for general two-dimensional laminar flow. Such specification of the stream function is equivalent to specification of velocity profiles and streamline directions, although additional computations are needed for the calculation of point velocities.

The Relationship between the Maximum Rate of Deformation and the Velocity Gradient

Consider a generalized two-dimensional laminar flow

situation specified in terms of two coordinate systems:

(1) Rectangular Cartesian (x,y)

Where x = horizontal coordinate

y = vertical coordinate

(2) Streamline coordinates (s,n)

Where s = distance along a streamline

n = distance along a curve normal to a set of streamlines

Other related quantities are:

θ = angle made by the direction of the maximum rate of deformation with the positive x axis

ϕ = angle made by a streamline with the positive x axis

u = component of fluid velocity in the x direction, $\frac{dx}{dt}$

v = component of fluid velocity in the y direction, $\frac{dy}{dt}$

V = fluid velocity along a streamline, $\frac{ds}{dt}$

r = radius of curvature of a streamline

r' = radius of curvature of a curve normal to a set of streamlines

The various coordinate relationships are illustrated in Figure 2, page 15. Note that both the streamline and the normal shown are considered to have positive curvature in the present work.

A combination of the theories of elasticity and viscous flow yield the following expression for the shearing stress

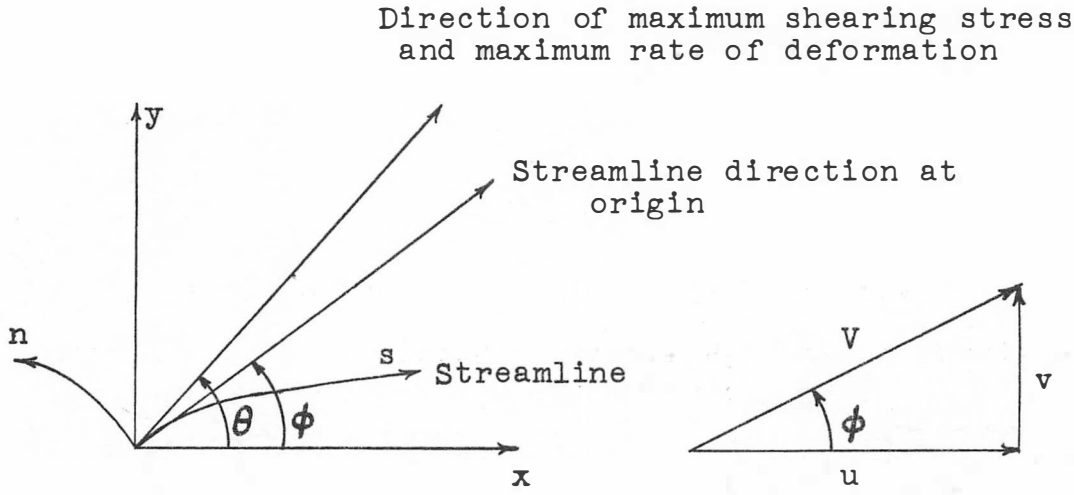

Figure 2. Relationships between coordinates and velocity components in rectangular Cartesian and stream coordinate systems

acting on a plane inclined at an angle ξ to the positive x axis in a viscous fluid in two-dimensional laminar motion (see Appendix A):

$$\tau_\xi = -\mu\left(\frac{\partial u}{\partial x} - \frac{\partial v}{\partial y}\right) \sin 2\xi + \mu\left(\frac{\partial u}{\partial y} + \frac{\partial v}{\partial x}\right) \cos 2\xi \qquad (1)$$

where

τ_ξ = shearing stress acting on a plane inclined to the horizontal with angle ξ

μ = fluid viscosity

Further, from the general two-dimensional definition of viscosity

$$\tau_\xi = \mu E_\xi \qquad (2)$$

where

E_ξ = the rate of deformation in the fluid along the plane of action of τ_ξ .

It should be noted here that equations (1) and (2) and subsequent equations involving the viscosity require the use of consistent units. To use mixed units one should replace the viscosity by the ratio $\frac{\mu}{g_c}$ where g_c is the force-mass conversion factor for the units to be employed.

One may now transform the equations (1) and (2) into stream coordinates with the following result (see Appendix B for details):

$$E_\xi = -\left[\left(\frac{\partial V}{\partial s}-V\frac{\partial \phi}{\partial n}\right) \cos 2\phi - \left(\frac{\partial V}{\partial n} + V\frac{\partial \phi}{\partial s}\right) \sin 2\phi\right] \sin 2\xi + \left[\left(\frac{\partial V}{\partial n} + V\frac{\partial \phi}{\partial s}\right) \cos 2\phi + \left(\frac{\partial V}{\partial s} - V\frac{\partial \phi}{\partial n}\right) \sin 2\phi\right] \cos 2\xi \quad (3)$$

By collecting terms and applying trigonometric identities one obtains

$$E_\xi = \left(\frac{\partial V}{\partial n} + V\frac{\partial \phi}{\partial s}\right) \cos (2\phi - 2\xi) + \left(\frac{\partial V}{\partial s} - V\frac{\partial \phi}{\partial n}\right) \sin (2\phi - 2\xi) \quad (4)$$

which may be slightly simplified by noting that

$$\frac{\partial \phi}{\partial s} = -\frac{1}{r} \; ; \; \frac{\partial \phi}{\partial n} = \frac{1}{r'} \quad (5)$$

where

ϕ = angle made by streamline with the positive x axis

r = radius of curvature of the streamline

r' = radius of curvature of the normal curve to the streamlines

In stream coordinates, the rate of pure shear is given by

$$G = \frac{\partial V}{\partial n} - \frac{V}{r} \tag{6}$$

where

G = rate of pure shear strain in the moving fluid

Also the law of continuity may be written as

$$\frac{\partial V}{\partial s} + \frac{V}{r'} = 0 \tag{7}$$

so that by analogy with (6) one may define the rate of dilation of the flow (a measure of the degree of convergence or divergence of the streamlines) as follows:

$$D = \frac{\partial V}{\partial s} - \frac{V}{r'} \tag{8}$$

where

D = rate of dilation

Note that from (7)

$$D = -\frac{2V}{r'} \tag{8a}$$

From substitution of the results of equations (5) through (8) into equation (4) one obtains

$$E_\xi = G \cos (2\phi - 2\xi) + D \sin (2\phi - 2\xi) \tag{9}$$

In order to find the orientation of the maximum shear stress (and rate of deformation), one differentiates equation (9) with respect to ξ and sets the derivative equal to zero. Two possible values of ξ will result, π radians apart. Obviously these specify the same plane, the only difference arising in the direction of positive action of stress, one corresponding to a maximum value and the other to a negative maximum (or minimum) value. This differentiation is performed,

$$\frac{dE}{d\xi} = 2G \sin (2\phi - 2\xi) - 2D \cos (2\phi - 2\xi) \qquad (10)$$

Equation (10) is equated to zero and rearranged. If one now notes that $\xi = \theta$, he arrives at

$$\tan (2\phi - 2\theta) = \frac{D}{G} \qquad (11)$$

When this result is substituted into (9)

$$E = \frac{G^2}{\sqrt{G^2 + D^2}} + \frac{D^2}{\sqrt{G^2 + D^2}} = \sqrt{G^2 + D^2} \qquad (12)$$

and G and D are substituted from (6) and (8a) the final result,

$$E = \sqrt{\left(\frac{\partial V}{\partial n} - \frac{V}{r}\right)^2 + \frac{4V^2}{r'^2}} \qquad (12a)$$

is obtained.

Equation (12a) provides the desired relationship between

the maximum rate of deformation and the velocity gradient normal to the streamlines. One is usually interested in calculating $\frac{\partial V}{\partial n}$ from values of E obtained by flow double refraction measurements. Hence equation (12a) is rearranged to obtain

$$\frac{\partial V}{\partial n} = \frac{V}{r} \pm \sqrt{E^2 - \frac{4V^2}{r'^2}} \qquad (13)$$

with the sign determined from the direction of travel along the normal according as V is increasing or decreasing.

Use of equation (13) to analyze general two-dimensional flow situations is complicated by the necessity of knowing the radii of curvature of both streamline and normal curves throughout the field. In other words one needs the streamline pattern first before he can use equation (13) for the calculation of velocity profiles. Hence, it will be in order here to develop the relationship between the direction of maximum rate of deformation and the direction of the streamlines.

The Relationship between the Direction of Maximum Rate of Deformation and the Streamline Direction

The desired relationship can be obtained almost directly from equation (11) by taking the arctangent of both sides:

$$2\phi - 2\theta = \arctan \frac{D}{G} \qquad (14)$$

Solving for θ and substituting for D and G

$$\theta = \phi - \tfrac{1}{2} \arctan \left[\frac{-\frac{2V}{r'}}{\frac{\partial V}{\partial n} - \frac{V}{r}} \right] \qquad (15)$$

where

θ = angle made by the direction of maximum rate of deformation with the horizontal

ϕ = angle made by streamline with the horizontal

Equations (14) and (15) show that the streamline directions coincide with the direction of maximum rate of deformation only for cases where the rate of dilation is zero, i.e., the normal curves to the streamlines are straight lines, indicating that the streamlines are parallel and no convergence or divergence of flow is occurring. If one takes only principal values for the arctangent it is seen that the maximum difference in these directions which can occur is $\frac{\pi}{4}$ radians and will be manifested in situations where the rate of pure shear is zero, but the rate of dilation is not. Such a situation would be found along the center line of a symmetrical convergent or divergent channel.

Equation (15) indicates that if the isoclinic positions are determined by the maximum rate of deformation, as results of the present study suggest, they will be of little use in determining the streamline patterns in cases where convergence or divergence of the flow occurs. Hence equation

(13) can be used only to determine the velocity distribution for cases where: (a) the streamline pattern is known from the channel configuration, (b) it is known that no divergence or convergence of flow occurs and the streamline patterns can be developed from the isoclinics, or (c) the streamline patterns can be obtained from some source other than double refraction measurements. The use of equation (13) in some specific situations is illustrated below.

Calculation of Velocity Distributions for Specified Cases

Case I, parallel straight streamlines. For laminar flow between flat plates, the streamlines are straight and parallel. This situation is approximated experimentally by flow in a straight rectangular channel of high aspect ratio (ratio of width to depth). In this case the terms $\frac{V}{r}$ and $\frac{V}{r'}$ vanish, and the streamlines are determined by the channel walls. Equation (13) reduces to

$$\frac{dV}{dn} = \pm E \qquad (16)$$

From isochromatic patterns, E may be specified throughout the field of flow. Equation (16) can then be integrated numerically or graphically along a stream normal to obtain the velocity distribution. Necessary boundary conditions are provided by the fact that V = 0 at the channel walls.

Case II, parallel curved streamlines. For the case of parallel but curved streamlines, one sees that $\frac{V}{r'} = 0$ and $\theta = \phi$. Hence the isoclinic patterns may be used to obtain the streamlines throughout the flow field. A graphical or numerical method will be needed to determine their radius of curvature at each point. Equation (13) becomes

$$\frac{\partial V}{\partial n} = \pm E + \frac{V}{r} \tag{17}$$

Having calculated r from the isoclinics and determined E from the isochromatics for each point in the field, one may integrate equation (17) numerically to obtain the velocity distribution. Integration is performed along a streamline normal, subject to the boundary conditions of zero velocity at the walls.

Case III, non-parallel straight streamlines. Flow between two non-parallel walls provides a situation in which the streamlines are straight but not parallel, and the dilation component of the flow does not vanish. A good approximation to this case in practice is found in a symmetrical convergent (divergent) section joining two rectangular channels of the same width but different depths. One considers that the streamlines are radial lines emanating from the line at which the non-parallel walls would converge, if extended, as shown in Figure 3.

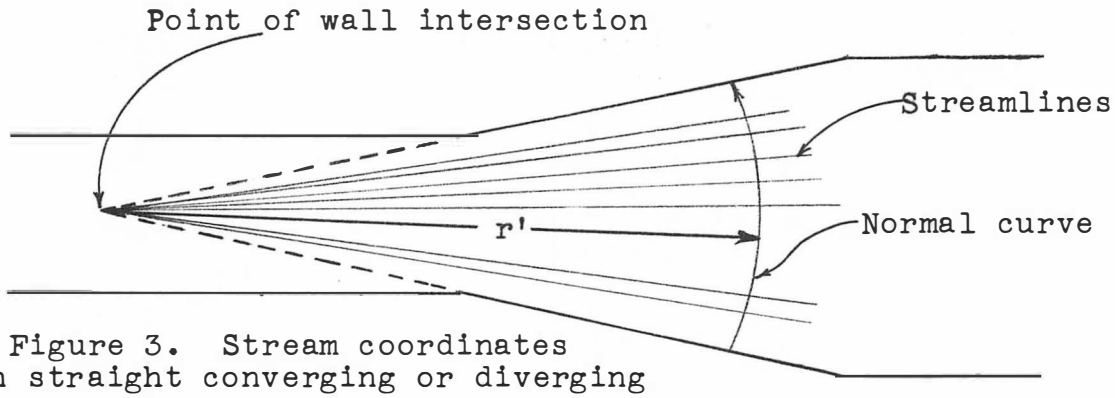

Figure 3. Stream coordinates in straight converging or diverging flow

In the present case, equation (13) becomes:

$$\frac{\partial V}{\partial n} = \pm\sqrt{E^2 - \frac{4\,V^2}{r'^2}} \tag{18}$$

which must be integrated numerically along a normal curve (here the arc of a circle whose center is the point of convergence of the walls). E is obtained from the isochromatics; and r' from the channel configuration. The usual boundary conditions of zero velocity at the walls are used, and a check is provided in the fact that $\frac{\partial V}{\partial n}$ should vanish at the center of the channel for a symmetrical situation.

Case IV, general two-dimensional flow with known streamlines. Situations may arise in which the streamlines are neither straight nor parallel, but are known throughout the flow field from some source other than double refraction measurements. One can obtain r and r' by a graphical or numerical method for each point in the field, and then apply

equation (13) directly.

$$\frac{\partial V}{\partial n} = \frac{V}{r} \pm \sqrt{E^2 - \frac{4\,V^2}{r'^2}} \qquad (13)$$

Numerical integration is performed along a streamline normal, subject to the zero velocity conditions at the walls.

A Method for Analyzing a Generalized Two-Dimensional Laminar Flow Situation

In accordance with a suggestion of Rosenberg (27) a method is presented for the analysis of two-dimensional laminar flow for a case in which the streamlines are unknown and are neither straight nor parallel. The analysis requires the introduction of the Stokes stream function, ψ, which will be defined by the following relationships:

$$u = -\frac{\partial \psi}{\partial y}$$

$$v = \frac{\partial \psi}{\partial x} \qquad (19)$$

where

ψ = the Stokes stream function

u = fluid velocity component in the x direction

v = fluid velocity component in the y direction

The definition of viscosity in two dimensions may be expressed in the form (29):

$$\tau_{xy} = \mu\left(\frac{\partial u}{\partial y} + \frac{\partial v}{\partial x}\right) \tag{20}$$

where

τ_{xy} = shearing stress acting in the positive x direction on a surface facing the positive y direction

When the stream function is introduced into equation (20) one finds that

$$\tau_{xy} = \mu\left(\frac{\partial^2 \psi}{\partial x^2} - \frac{\partial^2 \psi}{\partial y^2}\right) \tag{21}$$

From the theory of elasticity (13) it may be shown that

$$\tau = \tau_{xy} \cos 2\theta \tag{22}$$

where

τ = maximum shearing stress in the liquid

θ = angle made by maximum shear stress with the positive x axis

If equations (21) and (22) are combined, together with the original definition of viscosity, equation (2), the following is obtained:

$$\frac{\partial^2 \psi}{\partial x^2} - \frac{\partial^2 \psi}{\partial y^2} = E \cos 2\theta \tag{23}$$

An important property of the stream function, ψ, should be noted at this point; the difference in ψ values

between two points in the field of flow is numerically equal to the volumetric flow rate across a curve connecting the points. Two direct consequences of this property are that: (a) curves of constant stream function values are the streamlines themselves and (b) the stream function is constant along any solid boundary. Furthermore, for the case of unidirectional flow, the value of ψ may be obtained across a flow channel by direct integration of the appropriate equation (19).

Hence if one considers a situation in which the flow starts out as unidirectional in a straight channel, he may assign an arbitrary value to ψ along one of the channel boundaries and calculate the distribution of ψ across to the other boundary by integration of (19). Now having the value of ψ along both channel boundaries, and across the channel at some distance upstream from the region of interest, one is in possession of the necessary boundary conditions to begin a numerical solution of the second order partial differential equation (23). The values of E and θ may be obtained throughout the field of flow from the isochromatic and isoclinic patterns respectively.

Numerical solution of equation (23) requires that it first be placed in finite difference form. If one assumes that the flow field is divided up into a square grid of equal spacing, h, in both x and y directions, the following

difference equation results. Details may be found in many texts on applied mathematics, such as Hildebrand (17).

$$\psi(x+h,y) + \psi(x-h,y) - \psi(x,y+h) - \psi(x,y-h) = h^2 E \cos 2\theta \qquad (24)$$

One may start from the known values of ψ along the boundaries, and employ a simple iteration procedure to obtain ψ at each corner of the grid of spacing h. Graphical interpolation may be applied to determine curves of constant ψ (streamlines) and numerical differentiation will yield the velocity components if desired. This procedure will be demonstrated in Chapter V.

CHAPTER III

EXPERIMENTAL EQUIPMENT

The observation of the flow double refraction interference patterns requires a relatively simple experimental arrangement. The doubly refracting liquid must be caused to flow through a transparent channel, and the channel itself must be placed between two suitably oriented polarizing plates. A light source is placed outside one of the polarizing plates, and the observer looks from the opposite side through one plate, the channel, and the other plate in series.

The production of flow patterns which can be analyzed quantitatively presents somewhat more difficulty. Early attempts to analyze the flow through channels of square cross section were wholly unsuccessful. Completely anomalous flow patterns were observed, and independent checks disagreed with the double refraction measurements by as much as 100 per cent. However, the flow through a channel of rectangular cross section whose aspect ratio (ratio of width to depth) was 3:1 was treated with better results. Observations in this case were made with the light path parallel to the long dimension of the channel. These investigations are reported in detail by Farrow (12).

It was concluded that the poor results in the square

channel were due to: (a) large velocity gradients (and hence shearing stresses) along the line of sight and (b) large variations in velocity gradient perpendicular to the line of sight. Hence the flow was not truly two-dimensional. Attempts were then made to analyze the double refraction interference effects for a three-dimensional system, but these were unsuccessful. It was finally decided that two-dimensional flow would have to be produced experimentally, by use of a channel of high aspect ratio.

It is shown by Purday (26) that when laminar flow occurs in a rectangular channel of high aspect ratio, the velocity along the long dimension is almost constant over the majority of the distance, falling off to zero only near the walls. For a channel aspect ratio 5:1, the velocity distribution is uniform within 10 per cent over 72 per cent of the long dimension, and for a channel aspect ratio 10:1 the velocity distribution is uniform within 10 per cent over 85 per cent of the long dimension. Hence a rectangular channel constructed with these aspect ratios (or higher ones) will provide an almost two-dimensional flow situation across the short dimension when they are viewed parallel to the long dimension. Such channels were used in the present investigation.

The apparatus used for fluid motion analysis by flow double refraction consisted of three major sub-systems:

(a) the optical system, (b) the flow test channel, and (c) the fluid circulation system. These will be discussed in the order named, followed by a brief description of the equipment used for optical and viscous calibration of the doubly refracting test liquid. Reference will also be made to the important pieces of auxiliary equipment.

The Optical System

The optical system used in the flow double refraction studies was of the type used in polariscopes for solid photoelastic analyses. It consisted of a light source, two collimating lenses, two polarizing plates, two quarter-wave plates, and a two-section optical bench. These components were purchased from the Polarizing Instrument Company, Irvington-on-Hudson, New York. An Exakta 35 millimeter camera manufactured by the Ihagee Camera Works of Dresden, Germany, was used to record the visible flow patterns.

The light source and one collimating lens were mounted in a single housing. Two separate lamps were provided, an 85 watt sodium vapor lamp for the production of monochromatic light, and a 500 watt projection lamp for the production of white light. The lamps were mounted at opposite ends of a platform which could be rotated to place either lamp at the focal point of the lens in order to provide parallel rays of

light. A two-inch circular aperture between the lamps and the lens aided in the production of parallel rays by causing the lamps to approximate point sources of light more closely.

The lenses, polarizing plates, and quarter-wave plates were circular and about ten inches in diameter. Each polarizing plate could be rotated on ball bearing rollers, and had a scale laid off in degrees along its outer circumference so that its axis of polarization could be varied by known amounts. One polarizing plate and one quarter-wave plate were mounted in a single holder. The quarter-wave plates were mounted on sliding tracks in the holder so that they could be moved in and out of the light path at will.

Two tables were provided for supporting the optical components. A section of the optical bench was placed on each table, one carrying the lamp-lens housing, the other carrying the separate lens. Each table had a polarizing and quarter-wave plate holder assembly bolted to one end. These tables were set on opposite sides of and perpendicular to a third table which supported the flow test channel. The overall arrangement is shown in the photographs of Figure 4. The arrangement of optical components is shown schematically in Figure 5.

The camera was mounted on the table holding the individual lens. The mount consisted of a heavy metal base, fitted with a vertical rod and an adjustable clamp, which held

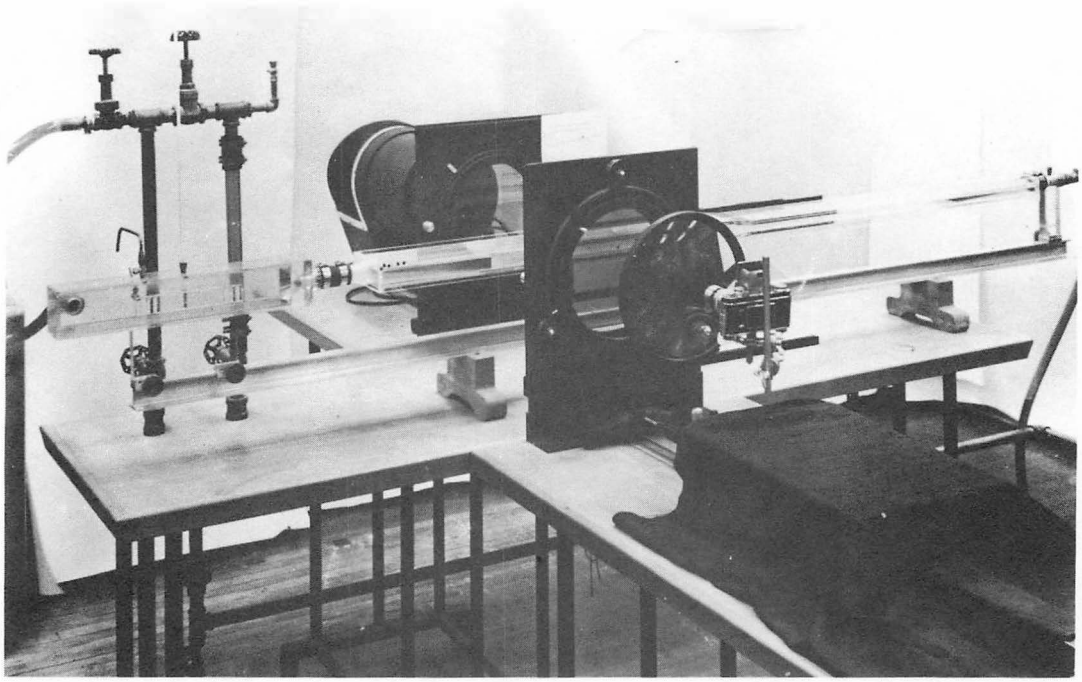

a. Flow test channel, calming box and optical components

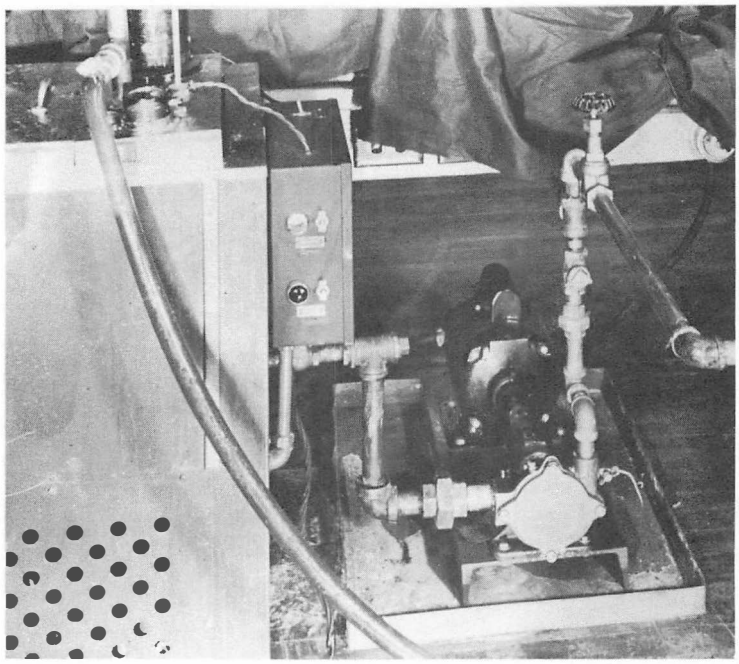

b. Pump and constant temperature bath

Figure 4. Photographs of the flow facility

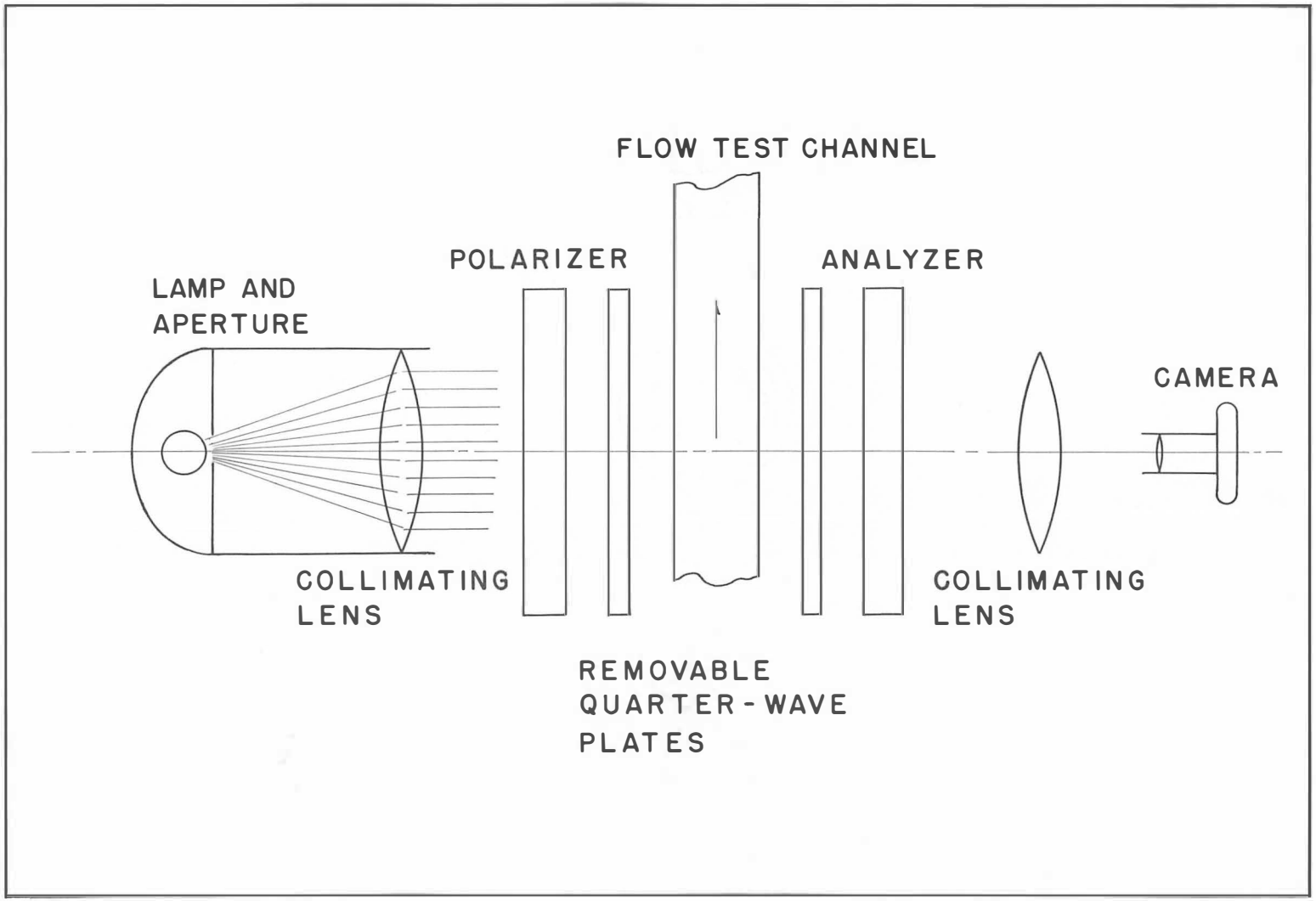

Figure 5. Schematic representation of the optical system

an adapter screwed into the camera's tripod fitting. The camera was of the single-lens reflex type, and was equipped with a 10 centimeter focal length f/2.8 telephoto lens. Kodak Tri-X, Plus X, and Micro-File films were used in photographing the flow patterns. Plus-X film developed with fine-grain Kodak Microdol developer appeared to give the best combination of high film speed along with low film graininess and good contrast.

The Flow Test Channel

Photographs of the flow test channel are shown in Figure 6. The channel was made of 3/8 inch thick Plexiglas and provided a rectangular cross-section for flow. The aspect ratio (ratio of width to depth) was kept high in order to more closely approximate a two-dimensional flow situation. Flow patterns were observed through the wide dimension of the channel as indicated in Figure 4.

The channel consisted of two sections of uniform rectangular cross section, one measuring 12.41 cm. x 2.546 cm., the other 12.49 cm. x 1.250 cm. These were joined by a straight-walled converging section. The converging section was symmetrical about the center line of the two uniform sections and the converging walls made an angle of five degrees and fifty-eight minutes with the horizontal. Diffuser vanes

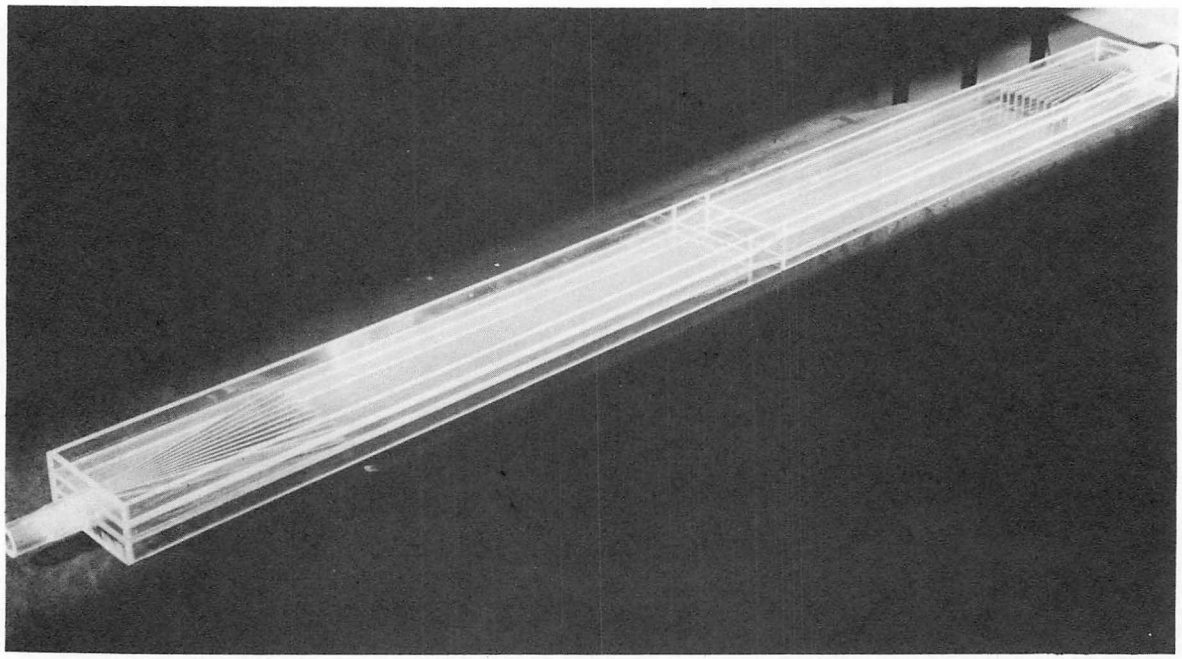

a. Flow test channel before installation of the cylindrical obstacle

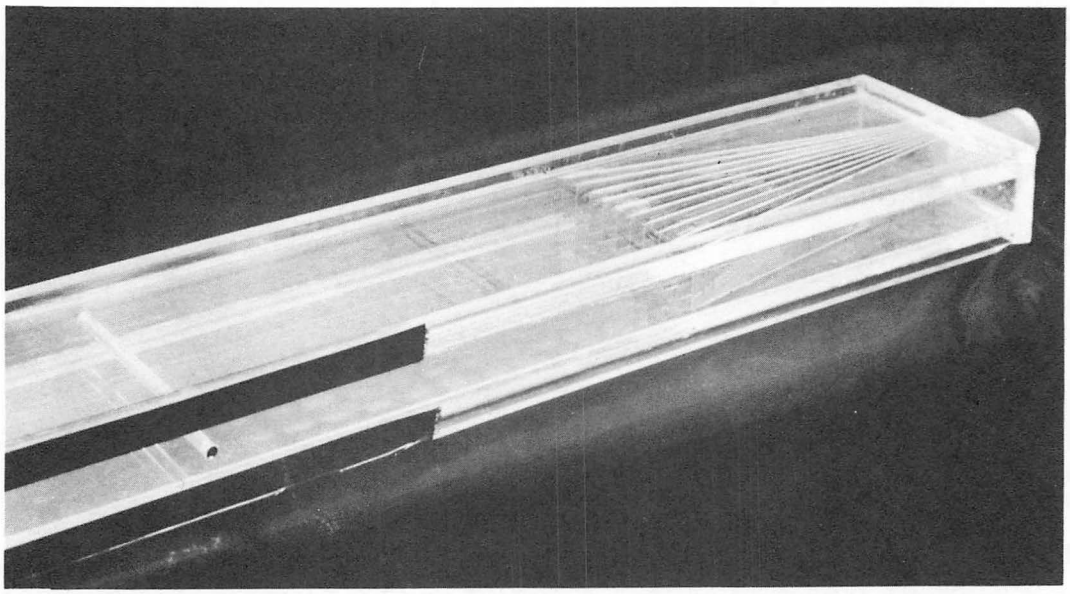

b. Deep end of channel showing flow diffuser vanes and cylindrical obstacle installed

Figure 6. Photographs of the flow test channel

were provided at each end of the system to s pread the flow across the wide dimension and aid in rapid establishment of the two-dimensional velocity profiles. The channel was mounted on an aluminum rail and was attached to the upstream calming box and downstream return line with short sections of rubber radiator hose. The hose was secured with circular clamps, and the entire assembly could be moved back and forth along the rail.

This test channel provided an opportunity for observing flow in uniform channels of different aspect ratios (5:1 and 10:1) and in straight convergent and divergent sections. In addition a 0.718 cm. O.D. cylindrical rod was inserted in the 2.546 cm. deep section about midway along its length. The rod was mounted perpendicular to the side walls of the channel and extended all the way across the flow path, thereby permitting a study of the two-dimensional flow about a cylindrical obstacle. These details may be observed in Figure 6.

The Fluid Circulation System

Aqueous milling yellow dye solutions, the doubly refracting test liquids used, have optical and viscous properties which are extremely sensitive to variations in temperature. Therefore the entire flow system was installed in an

air-conditioned laboratory in which the temperature was maintained at 25.0 ± 0.5°C. Furthermore, a constant temperature bath was included in the fluid circulation system to maintain the fluid temperature at 25.0 ± 0.1°C. The constant temperature bath was manufactured by the American Instrument Company, Silver Spring, Maryland. It had a capacity of 16 gallons, was refrigerated and heated, and had a control range of -30°C to+ 72°C. The temperature control system employed a bimetallic strip sensing element which opened and closed a set of contact points as the temperature in the bath rose and fell respectively. The containing tank was copper.

Fluid circulation was provided by an Eco Centrichem centrifugal pump. The pump was driven by a 3/4 horsepower, 110 volt, 60 cycle A.C. motor. The pump itself had a Carpenter 20 stainless steel casing and impeller, and a mechanical shaft seal. Flow lines were 1-inch brass schedule 40 pipe and 1-inch O.D. 3/4-inch I.D. Tygon hose. A glass rotameter containing a stainless steel plummet measured the flow rate, and a precision thermometer reading to 0.05°C for measuring fluid temperature was mounted in a calming box just upstream from the flow test channel. An overall view of the flow system is provided in Figure 4, and the fluid circulating system is shown schematically in Figure 7.

The dye solutions themselves were designated T-7 and T-8 and were prepared from commercial lots of milling yellow

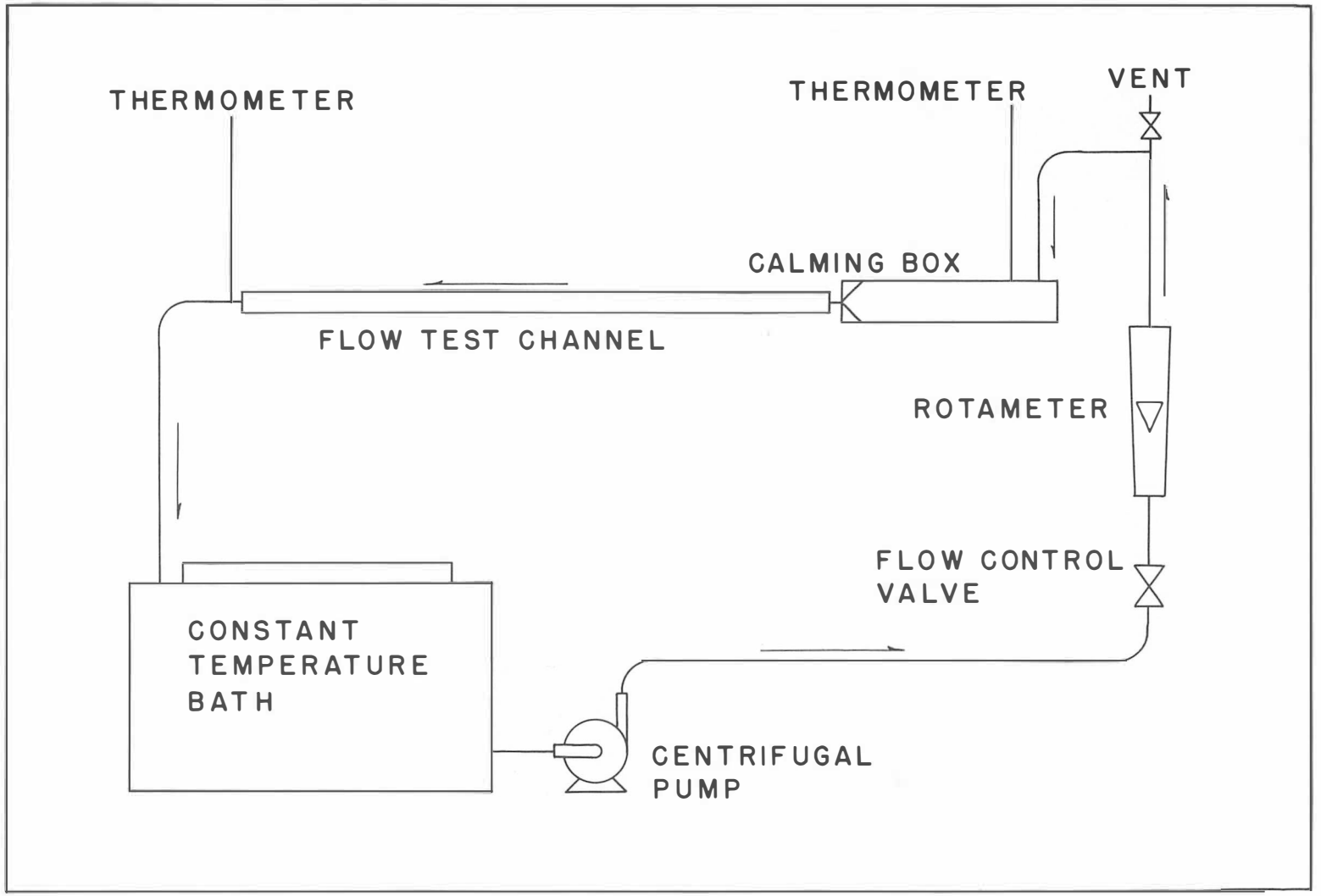

Figure 7. Schematic representation of the fluid circulating system

dye powder, obtained from the National Aniline Division of the Allied Chemical and Dye Company. Solution T-7 also contained a small amount of a salt-free dye powder purchased on special order from the National Aniline Division.

The Calibration Equipment

In order to carry out a successful flow analysis by the double refraction technique it is necessary to measure certain optical properties of the doubly refracting test liquid as functions of the deformation rate. These properties are most conveniently measured in a concentric cylinder polariscope. The viscous behavior of the fluid is also of considerable importance to the analysis, and a capillary viscometer with a continuously varying pressure head provides a convenient means of measuring this behavior over the stress range of interest for double refraction studies. These pieces of equipment will be described briefly here.

The Concentric Cylinder Polariscope

The concentric cylinder polariscope has been discussed in detail by a number of authors (11)(25), and no extensive discussion of its theory of operation will be reproduced here. It consists of an optical system almost identical with that previously described for the flow test facility. The fluid to be calibrated is placed in the annular space between two

concentric cylinders in which a known rate of deformation can be set up by causing the outer cylinder to rotate while the inner one remains stationary. Light from the optical system passes through the fluid parallel to the axis of the cylinders. The arrangement is shown schematically in Figure 8. The device permits one to calibrate the order of the isochromatic fringes against the rate of deformation and to calibrate the angle between maximum shear stress and light polarization axes at which isoclinics appear against the rate of deformation. The concentric cylinder polariscope used to calibrate doubly refracting liquids for the present study was manufactured by the Rao Instrument Company, Brooklyn, New York.

The Capillary Viscometer

A capillary viscometer system similar in principle to that described by Maron, Krieger, and Sisko (22) was used to determine the viscous behavior of one of the doubly refracting test liquids. The viscometer was of the type used by Honeycutt and Peebles (19) but the driving pressure for flow was provided by a difference in level of the liquid being tested in extended arms of the viscometer, rather than by external gas pressure. The capillary had a length of 20.18 cm. and a radius of 0.0529 cm. The pressure head varied from 0.37 to 9.44 cm. of water providing a wall shear stress of 0.476 to 12.155 dynes per square centimeter. A water jacket

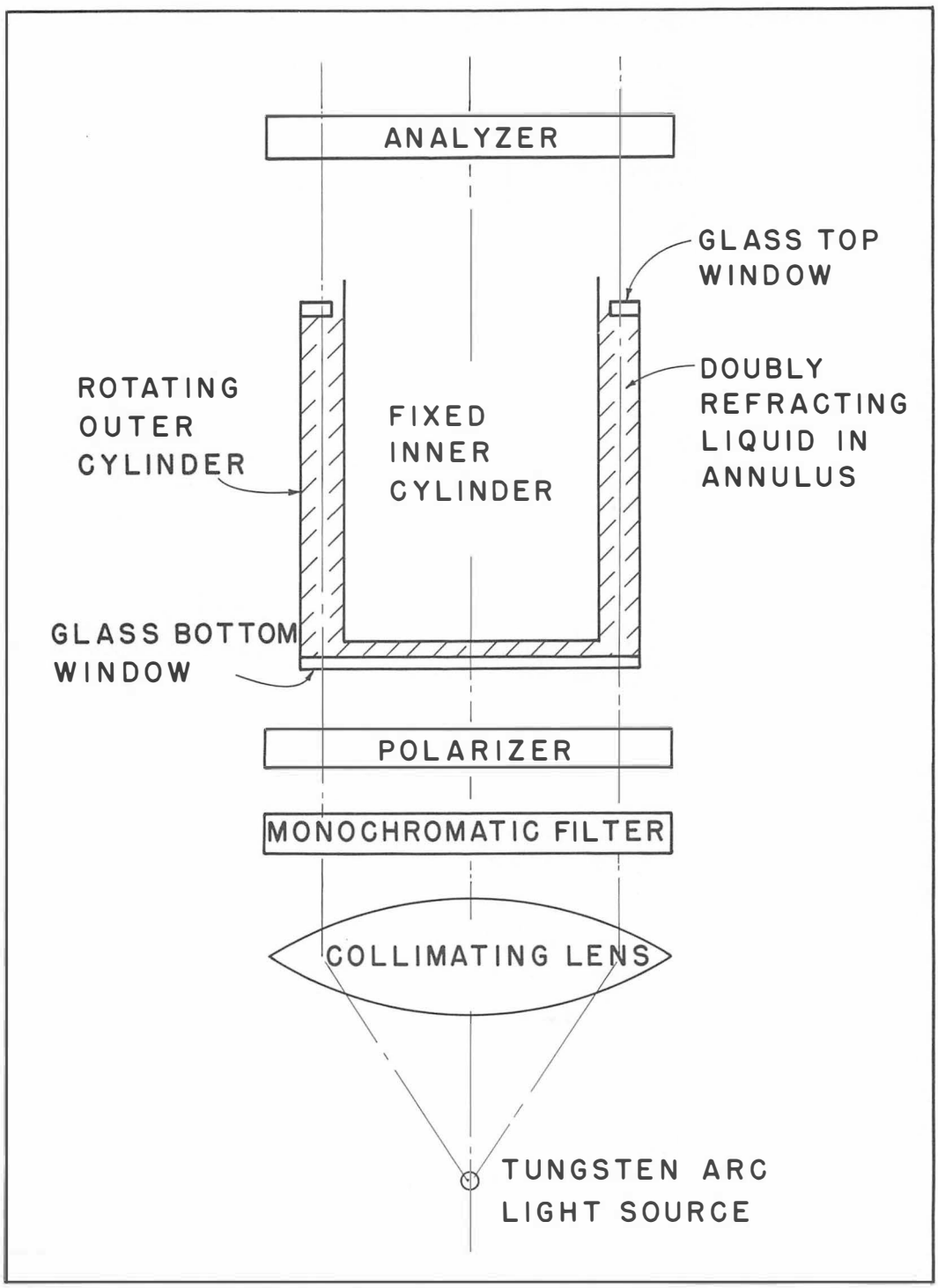

Figure 8. Schematic representation of the concentric cylinder polariscope

fed from a constant temperature bath maintained the temperature of the capillary at 25.00° ± 0.05°C. during a viscosity determination. A complete description of the instrument and its operation is given by Havewala (17).

CHAPTER IV

THE EXPERIMENTAL TECHNIQUE

The experimental techniques of flow analysis by double refraction methods fall into three major categories: (a) the optical calibration of the doubly refracting liquid, (b) the photographing of interference patterns produced by the calibrated liquid in the flow test channels, and (c) the measurement of these photographs to obtain the spatial distribution of isochromatic and isoclinic curves throughout the field of flow. These operations are normally performed in the order mentioned, and hence it will be logical to discuss them in that order.

The Optical Calibration

As long as consideration is restricted to laminar flow, the amount of double refraction in a doubly refracting liquid is a monotonic, increasing function of the rate of deformation in the plane normal to the light path (25). The flow cell of the concentric cylinder polariscope provides a light path of constant length, and a nearly uniform rate of deformation normal to that light path. This rate of deformation can be varied at will by varying the speed of rotation of the outer cylinder.

Isochromatic Calibration

When the fluid is at rest, no double refraction is present and the flow field appears dark. When the outer cylinder is set in motion, the flow field becomes bright and remains so as the speed of rotation is increased until a point is reached where a dark band appears in the field (the so-called "first order" isochromatic). This is the result of a given amount of double refraction in the liquid producing a relative retardation between the fast and slow light rays, of such magnitude that light interference occurs at the analyzer. The amount of double refraction necessary to cause this effect can be calculated from the liquid depth and the wavelength of light used (25). As the rate of deformation is further increased, the field brightens again until a second dark band appears (the "second order" isochromatic). Isochromatics of still higher order appear when the rate of deformation is increased further. By noting the speed of rotation at which each band appears, one may make a calibration plot of isochromatic order (and hence amount of double refraction) versus speed of rotation (and hence rate of deformation) for a given liquid. The appearance of the isochromatic bands in the calibration cell is shown in Figure 9.

Such a calibration curve may then be used to obtain the rate of deformation to be associated with an isochromatic of known order in the flow interference patterns. The order

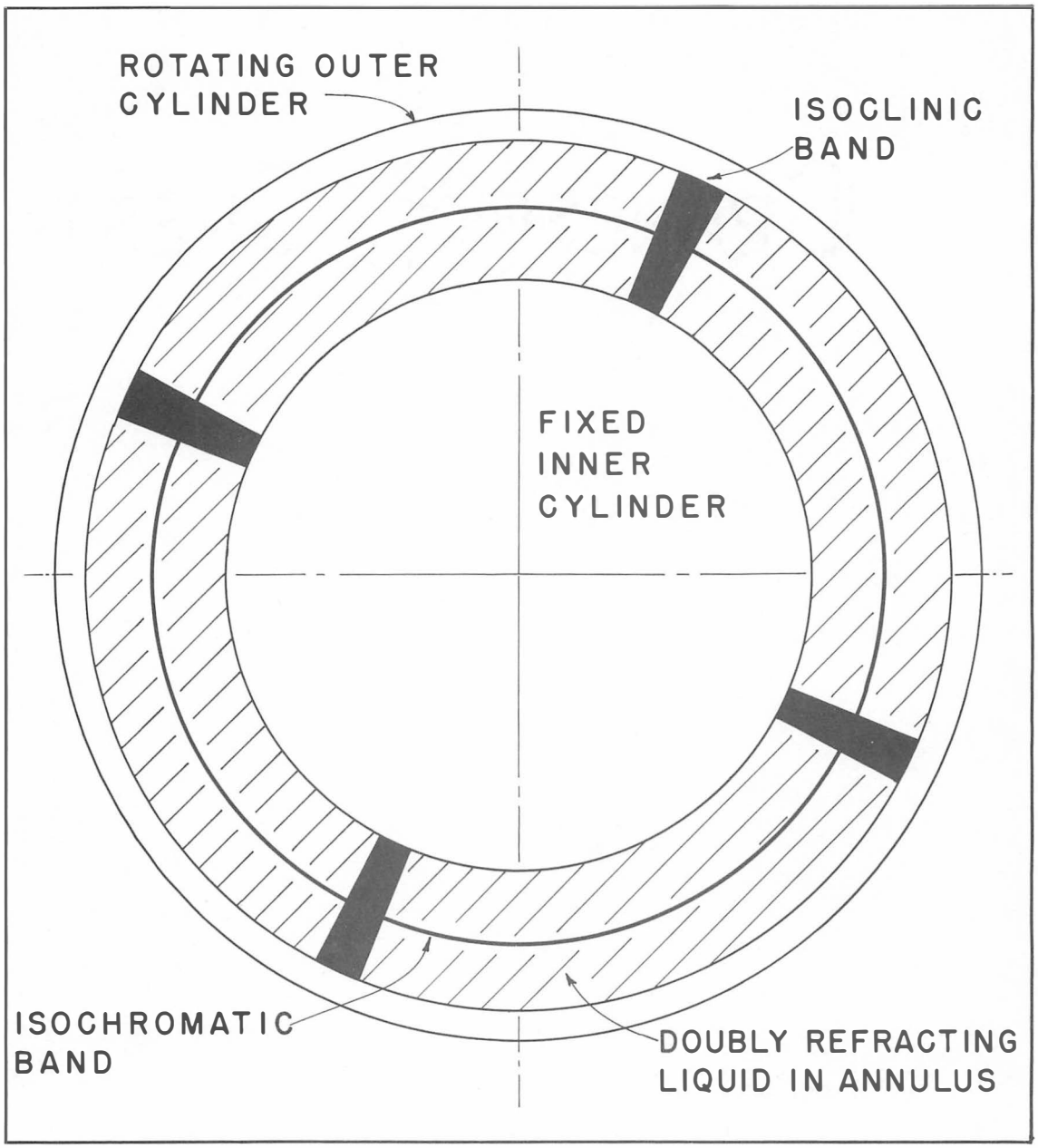

Figure 9. Appearance of the isoclinic and isochromatic fringes in the flow cell of the concentric cylinder polariscope

of the isochromatics in the flow patterns must be obtained by consideration of the physical situation present. In a straight, parallel-walled channel, the zero order isochromatic (corresponding to a zero rate of deformation) occurs at the center of the channel and the other isochromatics increase in order monotonically toward the walls. In all of the flow situations studied, these isochromatics of known order could be identified in the undisturbed flow upstream or downstream from the region of interest and followed directly into that region. Isochromatics not directly connected with these could be identified by noting that adjacent isochromatics must be of adjacent order, since the rate of deformation in the flow field is a continuous function of position.

Calibration curves were prepared on the flow test solutions at temperatures of 24.75°, 24.95°, 25.00°, and 25.20°C. Graphical interpolation was used to obtain calibration values at other temperatures.

Isoclinic Calibration

Isoclinic bands appear in the flow patterns at points where the optic axis of the fluid makes an angle of 0, 90, 180, or 270 degrees with the axis of the polarization of the incident light. The optic axis is a direction characteristic of the optical orientation of the doubly refracting liquid

and forms a given angle with the direction along which the maximum rate of deformation acts. This angle is known as the extinction angle and is frequently a function of the rate of deformation itself. (See Prados and Peebles (25) for a fuller discussion of these quantities.)

Since the annular flow cell of the concentric cylinder polariscope provides a circular flow channel of parallel streamlines, the direction of the plane of maximum rate of deformation varies through a full 360 degrees and is known at each point in the cell. There are four points in the cell where isoclinics appear, corresponding to the angles of 0, 90, 180, and 270 degrees made by the optic axis of the fluid with the axis of polarization of the incident light. These isoclinics appear as four dark areas, like the arms of a cross superimposed on the isochromatic bands in the flow cell. The polariscope is provided with a calibrated set of cross hairs so that the angle made by these isoclinics with the plane of polarization can be measured, and from it the extinction angle can be calculated. These measurements made at various speeds of rotation allow one to plot a second calibration curve of extinction angle versus rate of deformation. This curve may be used along with the isochromatics to calculate the angle between the direction of maximum shear and the axis of light polarization indicated by a given isoclinic in the flow test channel. The appearance of the isoclinic

regions in the flow cell is shown in Figure 9.

The Photographing of the Flow Interference Patterns

With the flow system set up as shown in the preceding chapter, the obtaining of the photographs of flow patterns was a relatively simple procedure. The flow channel was first positioned so that the section of interest was directly in the center of the light path. The channel was then leveled with a hand level. Next the temperature of the constant temperature bath was adjusted as nearly as possible to 25.0°C. The pump was started and the flow rate adjusted until the desired pattern was produced in the field of view. The flow rate was regulated by the valve just before the rotameter.

The camera and second collimating lens were adjusted until a sharp image of the flow pattern appeared on the ground glass reflex screen of the camera. The light path through the liquid was approximately five inches long and the depth of focus of the lens system was not sufficient to bring both channel walls and interference bands into sharp focus with the diaphragm opened wide. However, when the lens was stopped down to approximately f/11, the depth of focus was increased sufficiently to give sharp images throughout the field.

With the channel in sharp focus, a series of pictures was taken at various flow rates. For each picture the flow

rate and temperature were recorded, the temperature being read from the precision thermometer in the calming box just upstream from the flow test section.

The optimum exposure time and lens aperture were obtained by trial and error for each film used. The following appeared to give the best results:

Film	Exposure Time	Lens Stop
Tri-X	1.0 sec.	between 11 and 16
Plus X	4.0 sec.	between 11 and 16
Micro File	12.0 sec.	8

Kodak Microdol developer was used for the Plus X, Micro File, and some of the Tri-X photographs. Kodak DK-50 developer was used for the remainder of the Tri-X photographs. The microdol developer produced a photograph of finer grain than was produced by the DK-50. This was of considerable importance to the final photographic results, since each negative was enlarged to approximately 200 times its original area. Photographs were obtained for flow in shallow and deep straight channel sections, in the converging and diverging sections, and about the cylindrical obstacle.

Most of the photographs of the isochromatic patterns were made using circularly polarized, monochromatic light, i.e., with quarter-wave plates in place and the sodium vapor lamp in use. Some isochromatic patterns, particularly in

the convergent and divergent sections, were photographed using monochromatic plane polarized light by sliding the quarter-wave plates out of the light path. In all cases the axis of polarization of the polarizer was vertical and that of the analyzer was horizontal.

In photographing the isoclinic patterns it was necessary to use white light so that the black isoclinics could be distinguished from the colored isochromatics. Plane polarized light of various orientations was provided by rotating the polarizer and analyzer together, keeping them crossed all the while. Isoclinic photographs were made for flow about a cylindrical obstacle at various orientations of polarizer and analyzer, but at a single flow rate and fluid temperature. The polarizer and analyzer were rotated together in a counter-clockwise direction (looking toward the light source). Photographs were made at rotations of 0, 15, 30, 45, 60, 75, 90, and -15 degrees. The -15 and 75 degree patterns were identical, as were the 0 and 90 degree patterns.

Because of marked changes over a period of two weeks in the optical response of the solutions while they remained in the flow system, samples were withdrawn on each day photographs were made. These were stored in glass bottles for later calibration.

The Measurement of the Flow Photographs

The accurate location of the isochromatic bands in the field of flow was necessary in order to allow the specification of the maximum rate of deformation throughout the field. Slightly different techniques were employed for locating these patterns in the three different types of flow studied. These methods will be discussed independently.

Straight Parallel Flow

For analysis of the flow in the stright channel sections it was necessary to know the position of the isochromatics along a vertical line across the channel. This information was obtained by means of a vernier caliper equipped with a double cross-hair sighting glass to eliminate parallax. The vernier could be read to 0.001 inch. Distances read from the photographs were converted to actual distances in the flow channel by direct proportion, using the ratio of the actual distance from top to bottom of the flow channel to measured distance from top to bottom in the photograph as a conversion factor.

Convergent or Divergent Flow

The method of treating the data from these situations required that the position of the isochromatics be known along a curve normal to the streamlines--here the arc of a

circle centered at the hypothetical point of intersection of the non-parallel walls. This was done as follows. First the photograph was attached to a drawing board, the non-parallel walls of the channel were carefully extended with a straight edge, and their point of intersection was located. A circular arc was then struck between the non-parallel walls with a compass, using this point of intersection as the center. Finally a drafting machine protractor was used to measure the angle made with the horizontal by the intersection of each isochromatic with the circular arc. This information, coupled with the known radius of the arc, allowed the calculation of linear distances along the arc to the various points of intersection by isochromatics. The protractor had a vernier which could be read to one minute.

Checks on the measurements were provided by the knowledge of the true angle of convergence (divergence) of the channel, and by the fact that for photographs taken in plane polarized light an isoclinic appears along the horizontal center line of the channel. Conversion to true channel distances was made in the same manner as for the case of straight parallel flow.

Flow about a Cylindrical Obstacle

For analysis of this generalized two-dimensional flow situation values of the maximum deformation rate were needed

at each corner of a rectangular grid set up in the field of flow. The photograph was first laid off into a square grid, eight units vertically by eighteen units horizontally. Next, the position of the isochromatics along each vertical line of the grid was carefully measured using a scale divided into 1/60-inch intervals. A graphical interpolation plot of deformation rate (obtained from the isochromatic measurements) versus distance was prepared for each vertical line. From these interpolation plots, the values of the deformation rate at each corner of the grid could be obtained.

The angle made by the plane of maximum deformation rate with the horizontal was also required. This was obtained from the isoclinic photographs made at different orientations of the polarizer and analyzer. A sheet of tracing vellum was laid off in a grid identical to that on the isochromatic photograph. On this were traced the isoclinics from each photograph made at different orientations of light polarization. The position of each isoclinic was located along the vertical grid lines, and graphical interpolation plots were prepared just as in the case of the isochromatics. From these plots, the angle between the optic axis of the fluid and the horizontal could be obtained at each point on the grid. Since the rate of deformation was known at each point, the extinction angle calibration curves could be used to obtain the angle made by the optic axis with the plane of

maximum deformation. The two angles could then be combined to yield the desired angle between the plane of maximum deformation and the horizontal.

Supporting Experimental Activities

In support of the major experimental activities just described it was necessary to carry out a considerable amount of additional work. This included the preparation of test solutions, the calibration of the flow meter, and the determination of the viscous behavior of the dye. These procedures will be discussed below.

Solution Preparation

Solutions of milling yellow dye exhibit a flow double refraction in the concentration range from about 1.2 to 2.0 per cent dye by weight. Because of the low solubility of the dye at room temperature the solution cannot be prepared directly. The technique followed was to heat a quantity of distilled water to the boiling point and then add enough of the dye powder to form about a 1.0 per cent solution. After solution of the dye, boiling was continued until a concentration in the neighborhood of 1.5 per cent was attained. The dye solution was then cooled and transferred to the flow system. Its concentration was adjusted with distilled water until suitable double refraction properties (as determined by

visual examination of flow patterns produced) were obtained. These contained about 1.3 per cent dye by weight.

Because of the rather long light path (approximately five inches) in the solution, any slight darkening of color obscured the flow patterns. Such darkening would occur in the solutions after about two weeks of use, and a fresh solution would be prepared. The flow system contained about twenty gallons of dye solution. Preparation of fresh solutions was accomplished in a thirty-gallon steam-heated bath.

Flow Meter Calibration

The total discharge in the system was metered by a glass rotameter containing a stainless steel plummet. This instrument was calibrated by a gravimetric technique. Flow was diverted into a tared container, and the time required for a given mass of dye to flow into the container was measured for various plummet elevations. The density of the dye solution was determined on a specific gravity balance. The results were plotted as a calibration curve of discharge in cubic centimeters per second versus rotameter reading.

Viscosity Determination

Doubly refracting solutions of milling yellow are known to exhibit marked non-Newtonian behavior when subjected to shearing stresses greater than five or ten dynes per

square centimeter (19). However, no data were available on these solutions at very low stresses, such as were produced in the flow test channel. Hence the viscous behavior of the dye was investigated using a variable-head capillary viscometer designed on the operating principle set forth by Maron, Krieger, and Sisko (22). The dye was introduced into the viscometer and allowed to rise about halfway up the extended manometer legs. Air pressure was applied to cause the dye to rise in one leg and fall in the other, producing a differential head across the capillary. Then the pressure was removed and the rate of fall (or rise) in each manometer leg was measured with a cathetometer and a stopwatch. The data were treated by the method of Maron, Krieger, and Sisko (22). Details of the experimental arrangement and data treatment are given by Havewala (17).

CHAPTER V

THE ANALYSIS OF THE FLOW PATTERN PHOTOGRAPHS AND REPRESENTATIVE RESULTS

A presentation will now be made of the methods used to analyze the measurements taken from photographs of the flow double refraction patterns. The methods used differed for the three types of flow analyzed, and hence a separate discussion will be given for each type of flow.

Straight Parallel Flow

The measurements taken from the photographs of straight parallel flow gave the location of each isochromatic along a vertical line from the top to the bottom of the flow channel. From the optical calibration curve for the test liquid, a rate of deformation was associated with each isochromatic, and hence the rate of deformation could be plotted versus distance across the channel. Such photographs and plots are shown in Figures 10 and 11.

For straight parallel flow, the rate of deformation and velocity gradient are equal. Hence graphical integration of the curve of rate of deformation versus distance was used to obtain a similar curve of values of velocity versus distance across the channel. This unidirectional velocity distribution curve was then integrated to yield the total

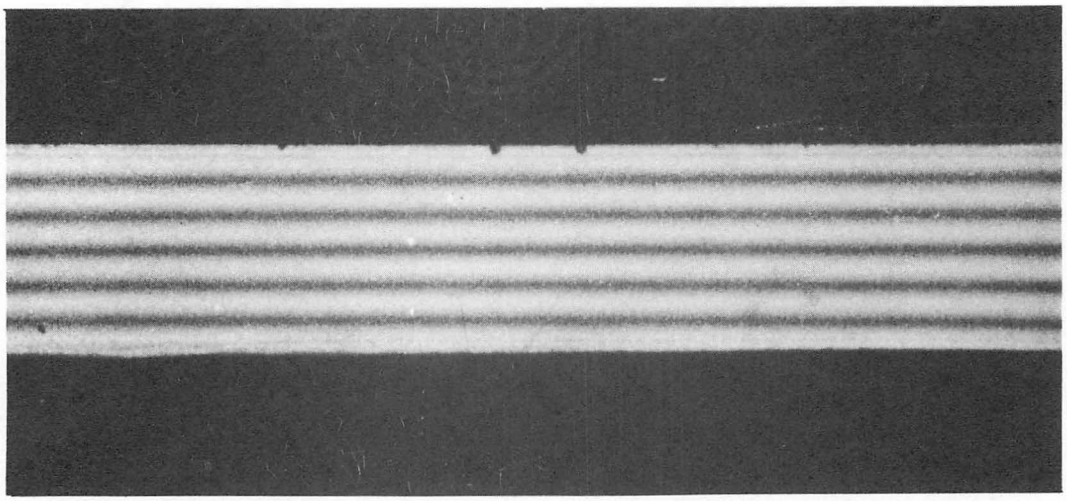

Photograph designation 98T11
Channel depth: 1.250 cm.
Solution calibration: T-7, 25.00°C
Measured discharge 18.1 cu.cm./sec.
Calculated discharge 18.1 cu.cm./sec.

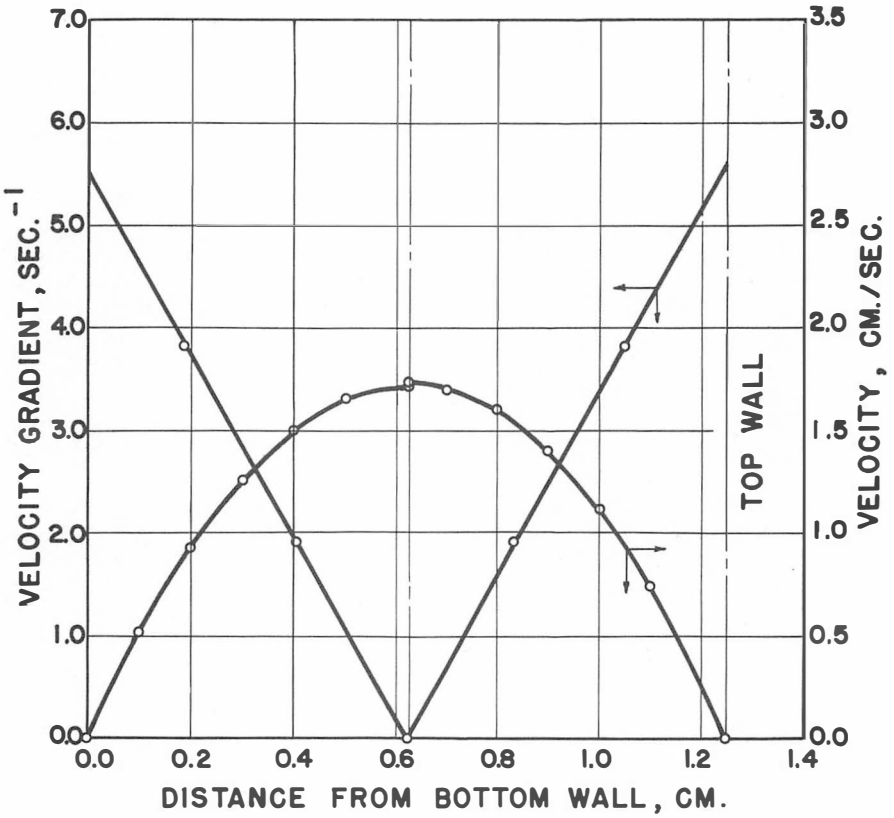

Figure 10. Flow pattern photograph and plots of velocity gradient and velocity versus distance for a straight channel of 10:1 aspect ratio

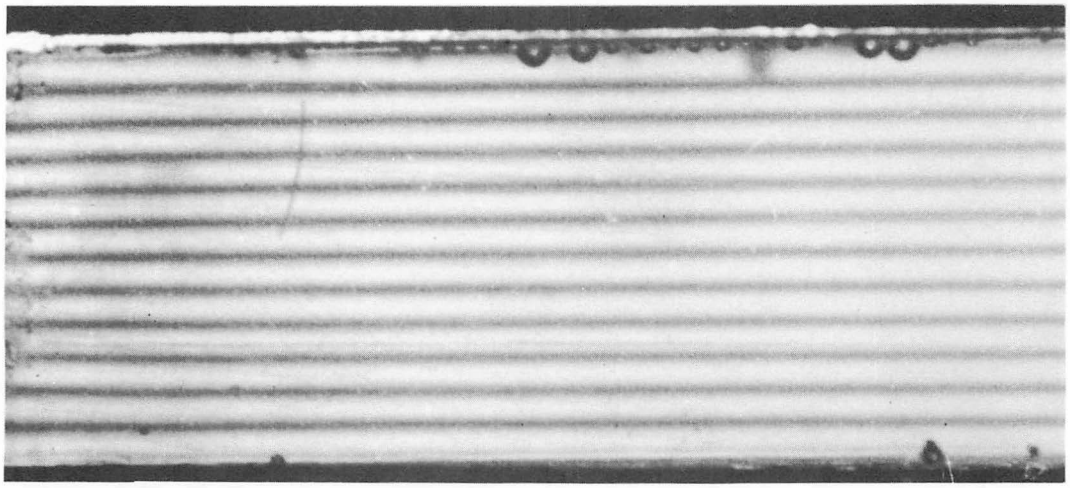

Photograph designation 97B13
Channel depth: 2.546 cm.
Solution calibration: T-7, 24.80°C
Measured discharge: 143.3 cu.cm./sec.
Calculated discharge: 142.1 cu.cm./sec.

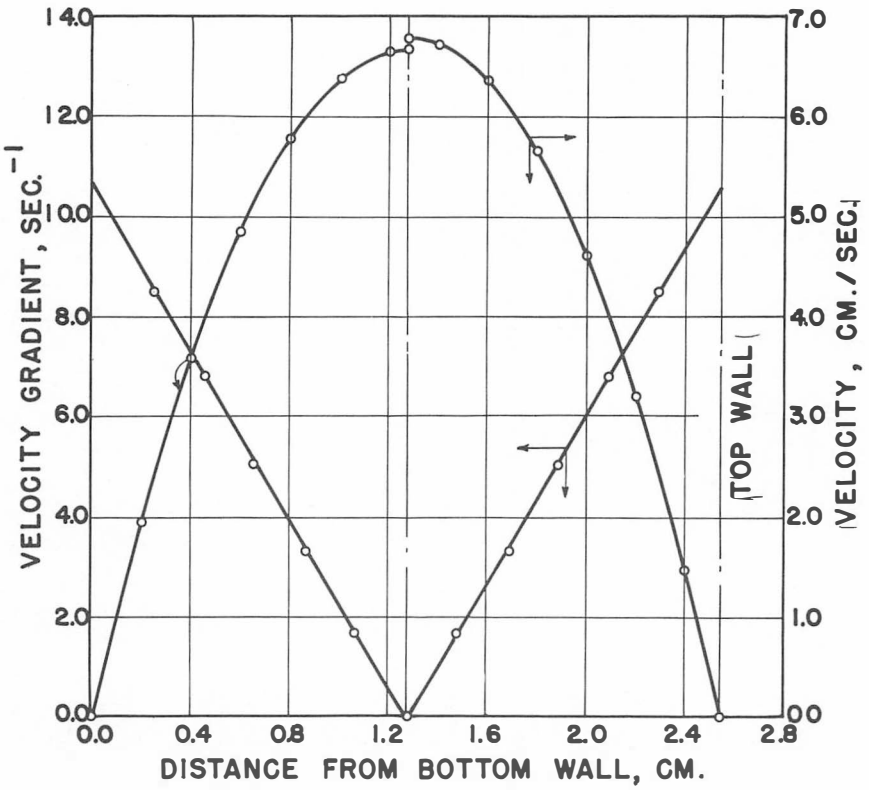

Figure 11. Flow pattern photograph and plots of velocity gradient and velocity versus distance for a straight channel of 5:1 aspect ratio

discharge through the channel. The results of these calculations for the cases illustrated in Figures 10 and 11 are tabulated in Tables I and II.

In addition the velocity distribution in the 10:1 aspect ratio channel was compared with that calculated from viscous information. The results of the viscosity determinations showed that the test solution used behaved as a Newtonian fluid with a viscosity of 17.13 centipoises at rates of deformation from twelve down to two reciprocal seconds (the range of interest of the present investigation). Hence, the formula for velocity distribution of a Newtonian fluid flowing between two parallel plates,

$$u = \frac{3}{4} \frac{Q}{ab} \left[1 - \left(\frac{y}{a}\right)^2\right] \qquad (25)$$

where

u = linear velocity in the positive x direction, cm./sec.

Q = discharge, cu.cm./sec.

b = width of channel, cm.

y = vertical distance coordinate measured from center of channel, cm.

a = distance from center of channel to wall, cm.

was assumed to hold for the high aspect ratio channel and was used to calculate the velocity profile. Equation (25) is

TABLE I

DISTRIBUTION OF VELOCITY AND VELOCITY GRADIENT ACROSS A STRAIGHT CHANNEL OF ASPECT RATIO 10:1

Distance from Bottom cm.	Velocity Gradient sec^{-1}	Calculated Velocity $cm_s/sec.$
0	5.56	0
0.1	4.67	0.514
0.2	3.74	0.934
0.3	2.85	1.262
0.4	1.95	1.502
0.5	1.08	1.654
0.625	0	1.720
0.7	0.65	1.715
0.8	1.53	1.606
0.9	2.42	1.409
1.0	3.32	1.123
1.1	4.23	0.744
1.250	5.58	0

Calculated Discharge: 18.1 cu.cm./sec.

TABLE II

DISTRIBUTION OF VELOCITY AND VELOCITY GRADIENT ACROSS A STRAIGHT CHANNEL OF ASPECT RATIO 5:1

Distance from Bottom cm.	Velocity Gradient sec^{-1}	Calculated Velocity cm./sec.
0	10.44	0
0.20	8.95	1.972
0.40	7.21	3.586
0.60	5.54	4.862
0.80	3.82	5.794
1.00	2.17	6.390
1.20	0.53	6.656
1.273	0	6.796
1.40	1.06	6.729
1.60	2.67	6.355
1.80	4.35	5.655
2.00	6.05	4.619
2.20	7.82	3.225
2.40	9.55	1.491
2.546	10.33	0

Calculated Discharge: 142.1 cu.cm./sec.

derived in most basic fluid mechanics texts as, for example, Purday (26).

Agreement between velocities calculated from equation (25) and the flow double refraction measurements was excellent. A comparison of the two is shown in Figure 12.

Converging and Diverging Flow

Photographic measurements of convergent and divergent flow gave the isochromatic positions along circular arcs centered and the hypothetical point of convergence of the non-parallel channel walls. The rate of deformation along such an arc could be obtained from the optical calibration curve of the test liquid, but here the velocity gradient was no longer equal to rate of deformation. The velocity profile could be obtained, however, by direct numerical integration of equation (18)

$$\frac{\partial V}{\partial n} = \pm\sqrt{E^2 - \frac{4\,V^2}{r'^2}} \qquad (18)$$

where

V = velocity along a streamline, cm./sec.

n = distance along circular arc normal to flow, cm.

E = rate of deformation, sec^{-1}

r' = radius of circular arc, cm.

subject to the boundary conditions of zero velocity at the

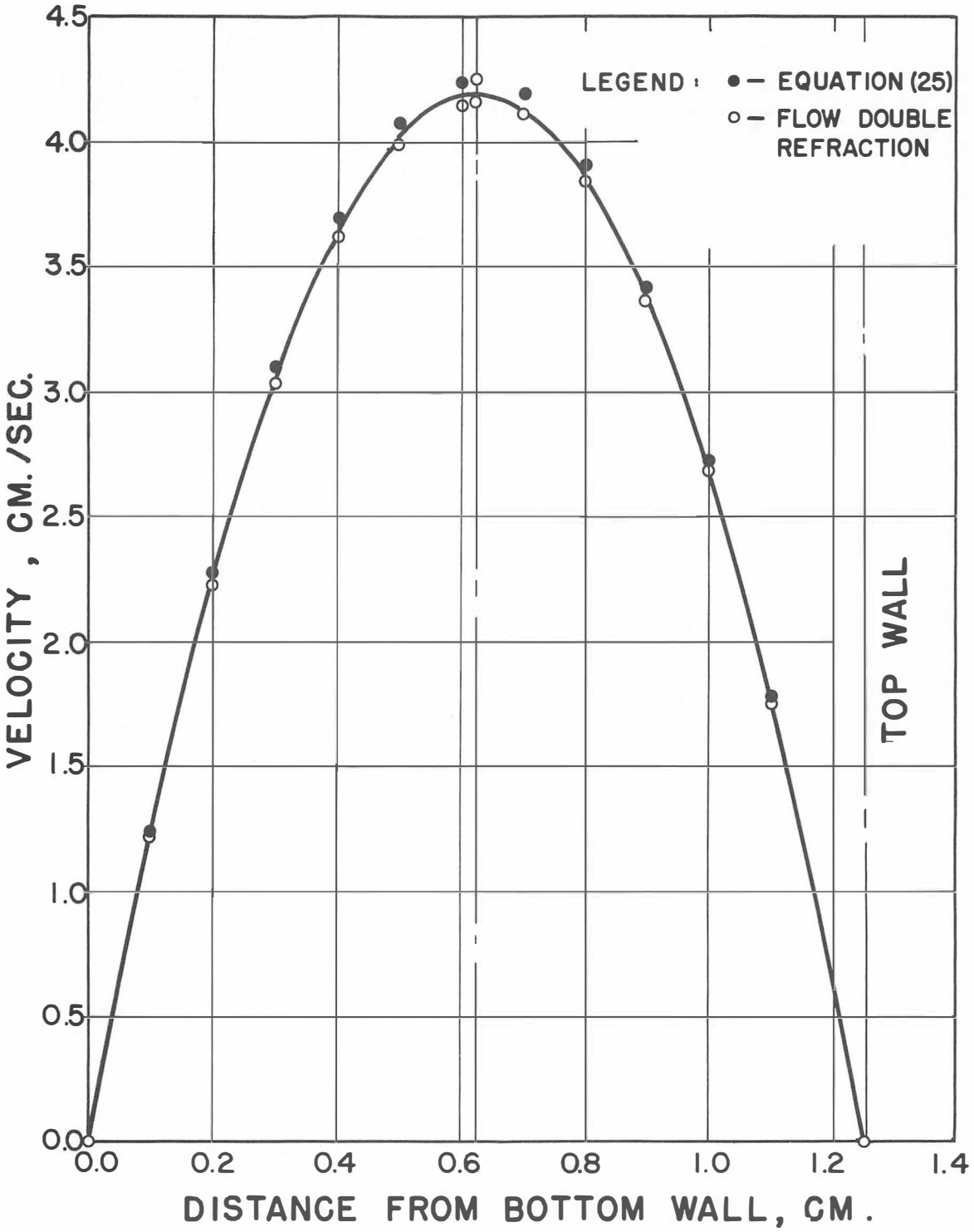

Figure 12. Comparison of velocity profiles calculated from equation (25) and obtained from flow double refraction measurements

walls. Integration was carried out by the method of Runge and Kutta (28). The results of such integrations at three locations along a divergent channel are shown graphically in Figure 13 and are tabulated in Table III. Similar results for flow in a convergent channel are given in Figure 14 and Table IV.

Since flow across a closed curve in two dimensions is equal to the velocity component normal to the curve times the length of curve, the discharge through a converging or diverging channel of high aspect ratio can be calculated from the expression:

$$Q = b\int_{o}^{N} V\,dn \qquad (26)$$

where

Q = discharge, cu.cm./sec.

b = width of channel, cm.

V = velocity component normal to circular arc (velocity along a streamline), cm./sec.

n = distance coordinate from wall measured along circular arc, cm.

N = total distance from wall to wall along circular arc, cm.

Discharges calculated from equation (26) are given in Figures 13 and 14.

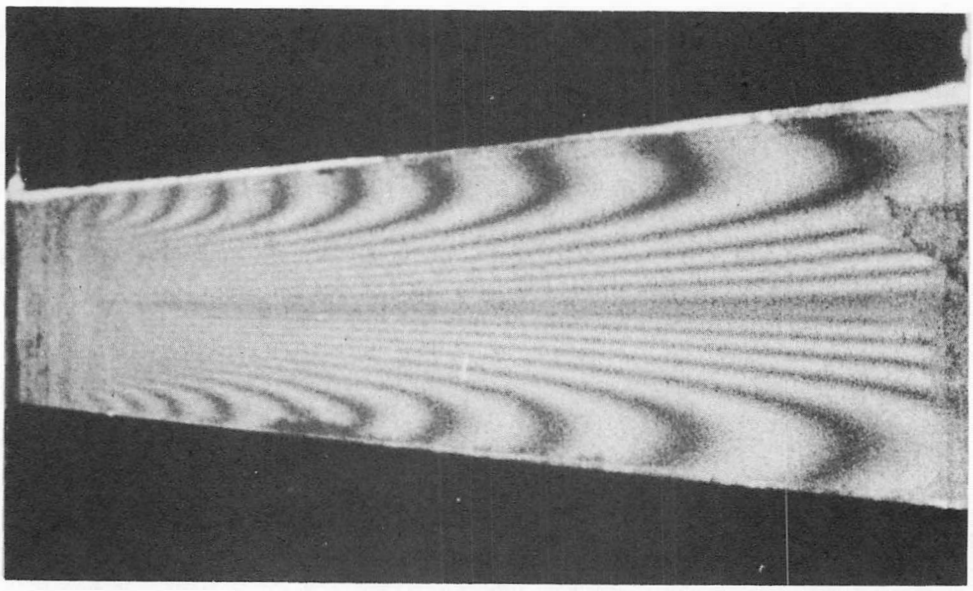

Photograph designation 98B19
Solution calibration: T-7, 24.85°C
Measured discharge: 134.6 cu.cm./sec.
Calculated discharge:
r' = 8.81 cm. Q = 136.4 cu.cm./sec.
r' = 10.31 cm. Q = 138.7 cu.cm./sec.
r' = 11.31 cm. Q = 139.7 cu.cm./sec.

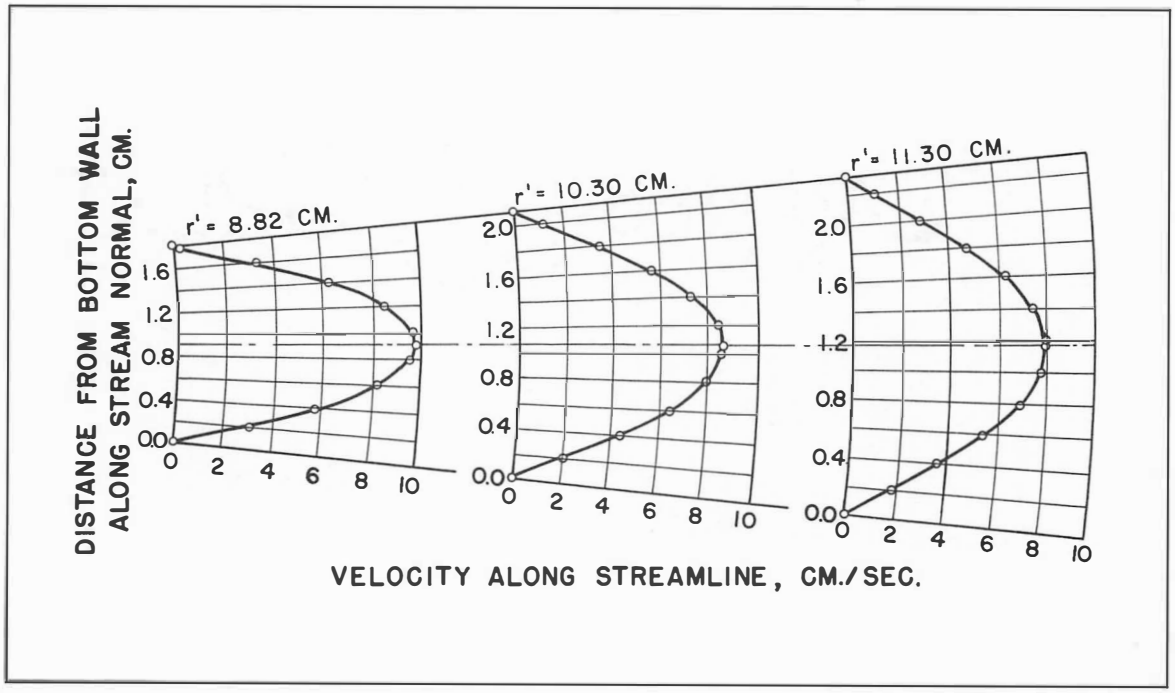

Figure 13. Photograph and developed velocity profiles for flow in a diverging channel

TABLE III

CALCULATED VELOCITY PROFILES ACROSS A DIVERGENT CHANNEL

Radius of Stream Normal, r' 8.81 cm.		Radius of Stream Normal, r' 10.31 cm.		Radius of Stream Normal, r' 11.31 cm.	
Distance from Wall along Stream Normal n cm.	V cm./sec.	Distance from Wall along Stream Normal n cm.	V cm./sec.	Distance from Wall along Stream Normal n cm.	V cm./sec.
0	0	0	0	0	0
0.108	1.604	0.261	2.841	0.164	1.476
0.308	4.586	0.461	5.008	0.364	3.314
0.508	7.265	0.661	6.912	0.564	5.097
0.708	9.104	0.861	8.213	0.764	6.646
0.908	9.719	1.061	8.657	0.964	7.676
1.108	9.187	1.261	8.194	1.164	8.012
1.308	7.337	1.461	6.895	1.364	7.695
1.508	4.595	1.661	5.003	1.564	6.657
1.708	1.601	1.861	2.842	1.764	5.099
1.816	0	2.122	0	1.964	3.316
				2.164	1.476
				2.328	0

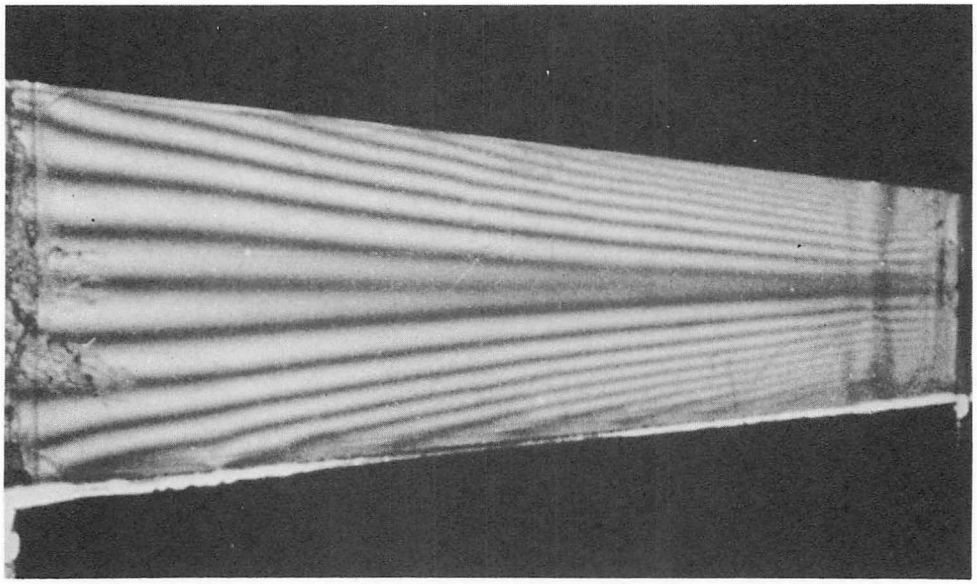

Photograph designation 97B14
Solution calibration: T-7, 24.90°C
Measured discharge: 81.2 cu.cm./sec.
Calculated discharge:

r'	= 8.40 cm.	Q = 91.5 cu.cm./sec.
r'	= 10.00 cm.	Q = 91.9 cu.cm./sec.
r'	= 10.97 cm.	Q = 88.8 cu.cm./sec.

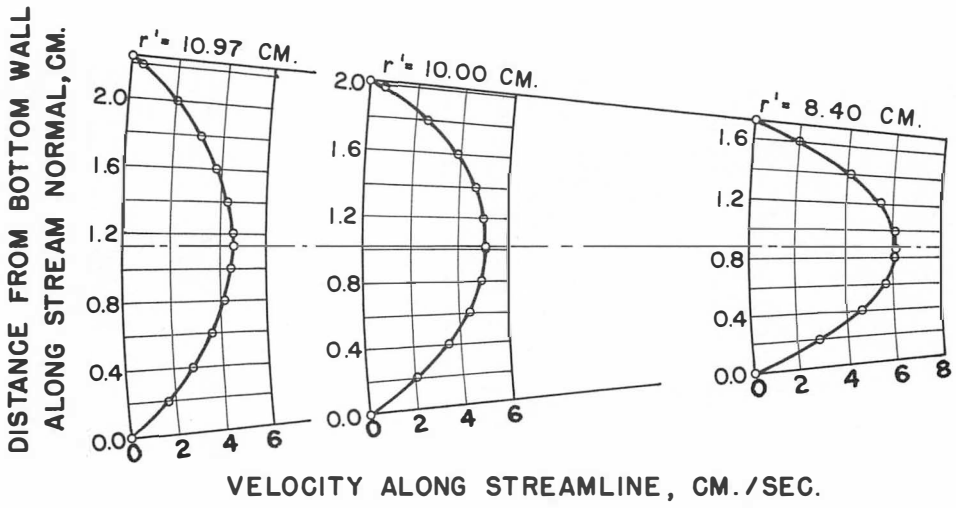

Figure 14. Photograph and developed velocity profiles for flow in a converging channel

TABLE IV

CALCULATED VELOCITY PROFILES ACROSS A CONVERGENT CHANNEL

Radius of Stream Normal, r' 8.40 cm.		Radius of Stream Normal, r' 10.00 cm.		Radius of Stream Normal, r' 10.97 cm.	
Distance from Wall along Stream Normal n cm.	V cm./sec.	Distance from Wall along Stream Normal n cm.	V cm./sec.	Distance from Wall along Stream Normal n cm.	V cm./sec.
0	0	0	0	0	0
0.118	1.730	0.133	1.382	0.132	1.149
0.268	3.511	0.333	3.055	0.332	2.501
0.468	5.043	0.533	4.164	0.532	3.442
0.668	5.853	0.733	4.831	0.732	4.048
0.868	6.064	1.033	5.146	1.132	4.604
1.068	5.870	1.333	4.806	1.532	4.055
1.268	5.055	1.533	4.150	1.732	3.446
1.468	3.508	1.733	3.051	1.932	2.501
1.618	1.729	1.933	1.381	2.132	1.149
1.736	0	2.066	0	2.264	0

Flow about a Cylindrical Obstacle

The preceding chapter discussed the method by which the maximum rate of deformation and angle made by this maximum rate with the horizontal could be obtained from the flow photographs. These values were found at each corner of a square grid of 144 points, eighteen units along the channel by eight units across the channel. The value of the component of deformation acting in the positive x direction was found from the relationship below, which follows directly from equation (22)

$$E_{xy} = E \cos 2\theta \tag{27}$$

where

E = maximum rate of deformation in the fluid

E_{xy} = component of deformation rate acting in the positive x direction

θ = angle made by plane of maximum deformation with the positive x direction

These quantities were obtained from the extinction angle, isoclinic angle, and isochromatic fringes as shown in Appendix F. The values of E_{xy} obtained at the corners of the grid are tabulated in Figure 15. The values were then used in the numerical integration of the equation

VERTICAL COORDINATE	0	1	2	3	4	5	6	7	8	9	10	11	12	13	14	15	16	17	18
8	-3.59 -1.900	-3.59 -1.900	-3.61 -1.900	-3.72 -1.900	-4.05 -1.900	-4.62 -1.900	-6.09 -1.900	-8.19 -1.900	-9.50 -1.900	-9.50 -1.900	-8.33 -1.900	-6.27 -1.900	-4.99 -1.900	-4.32 -1.900	-3.82 -1.900	-3.67 -1.900	-3.60 -1.900	-3.59 -1.900	-3.59 -1.900
7	-2.62 -1.731	-2.62 -1.731	-2.58 -1.733	-2.52 -1.726	-2.50 -1.712	-2.51 -1.700	-1.81 -1.648	-2.55 -1.326	-4.39 -1.261	-4.70 -1.367	-4.35 -1.520	-3.80 -1.489	-3.05 -1.632	-2.62 -1.685	-2.62 -1.712	-2.62 -1.730	-2.62 -1.730	-2.62 -1.733	-2.62 -1.731
6	-1.72 -1.299	-1.72 -1.299	-1.62 -1.296	-1.51 -1.290	-1.19 -1.273	-0.080 -1.206	1.32 -0.943	2.60 -0.751	0.68 -0.348	0.16 -0.441	0.50 -0.769	0.76 -0.867	0.42 -0.965	-0.26 -1.179	-1.00 -1.250	-1.38 -1.277	-1.55 -1.298	-1.70 -1.296	-1.72 -1.299
5	-0.82 -0.690	-0.82 -0.690	-0.83 -0.692	-0.64 -0.690	0.74 -0.663	0.99 -0.508	2.04 -0.443	2.56 -0.228	3.00 -0.049	3.58 -0.072	3.70 -0.150	2.57 -0.322	1.37 -0.457	0.78 -0.504	0.67 -0.643	-0.51 -0.678	-0.71 -0.686	-0.79 -0.692	-0.82 -0.690
4	0 0	0 0	0 0	0 0	0 0	0 0	0 0	0 0			0 0	0 0	0 0	0 0	0 0	0 0	0 0	0 0	0 0
3	0.82 0.690	0.82 0.690	0.81 0.687	0.64 0.688	-0.83 0.659	-0.97 0.449	-2.84 0.450	-4.49 0.163	-3.00 -0.048	-3.36 0.159	-1.47 0.286	-1.03 0.419	-0.93 0.476	-0.66 0.517	-0.65 0.629	0.35 0.673	0.73 0.685	0.78 0.687	0.82 0.690
2	1.70 1.294	1.70 1.294	1.62 1.296	1.48 1.281	1.20 1.268	0.21 1.207	-0.67 0.947	-1.35 0.853	-0.63 0.546	-0.70 0.585	-0.66 0.727	-1.71 0.866	-0.64 1.030	0.72 1.172	1.02 1.259	1.41 1.259	1.62 1.289	1.70 1.296	1.70 1.294
1	2.62 1.728	2.62 1.728	2.62 1.724	2.54 1.726	2.60 1.707	2.81 1.698	3.21 1.678	4.29 1.467	5.05 1.502	3.84 1.483	3.92 1.454	3.18 1.511	2.83 1.627	2.77 1.699	2.73 1.719	2.70 1.729	2.68 1.726	2.62 1.724	2.62 1.728
0	3.61 1.893	3.61 1.893	3.69 1.893	3.72 1.893	4.20 1.893	4.77 1.893	6.12 1.893	8.22 1.893	9.60 1.893	9.60 1.893	8.48 1.893	6.63 1.893	5.31 1.893	4.53 1.893	4.03 1.893	3.83 1.893	3.68 1.893	3.61 1.893	3.61 1.893

HORIZONTAL COORDINATE

Vertical order of tabulation: (top to bottom in a square)

x-component of deformation rate, E_{xy}

stream function, ψ

Figure 15. Tabulation of values of the x-component of the rate of deformation, E_{xy}, and the stream function, ψ, at the corners of the coordinate grid

$$\frac{\partial^2 \psi}{\partial x^2} - \frac{\partial^2 \psi}{\partial y^2} = -E \cos 2\theta \qquad (23)$$

where

ψ = the Stokes stream function

This equation was integrated in difference form (see Chapter II, page 27), and required as boundary conditions the values of ψ along the top and bottom of the channel and along two adjacent vertical grid lines upstream and two downstream from the obstacle. These values were obtained as follows.

For undisturbed unidirectional flow, the stream function, ψ, can be calculated across the channel from the following relationships

$$u = -\frac{d\psi}{dy} \quad \text{and hence} \quad \psi(y) = \psi(o) - \int_o^y u\,dy \qquad (28)$$

where

u = velocity component in the positive x direction, cm./sec.

Since ψ may only be specified with reference to an arbitrary constant, the value of ψ was chozen as zero at the center of the channel and other values of ψ out to the top and bottom walls were calculated from equation (28). Then use was made of the fact that ψ is constant along streamlines and solid

boundaries. This immediately specified ψ along the top and bottom of the channel, and from symmetry considerations, along the center line of the channel and the cylinder boundary as well. These calculations are shown in Appendix F.

From the nature of the difference form of equation (23) it was necessary to perform iteration starting along both upstream and downstream edges of the grid and working toward the middle. The results of the iteration process are shown in tabular form in Figure 15. Graphic interpolation was used to determine curves along which ψ has a constant value. These are the streamlines of flow about the obstacle. The photographs and curves of Figure 16 illustrate the steps in the development of these streamlines from the flow photographs. Calculation procedures and intermediate results appear in Appendix F.

Unfortunately the results of the calculation could not be checked by calculating the discharge, since the flow through the channel was already fixed by fixing the values of the stream function along the boundaries. A number of theoretical results (2)(3)(31) for flow of a viscous fluid about a cylinder were examined, but they were all developed for either the case of unbounded flow (31) or for a Reynolds number of the order of 0.1 (3). The Reynolds number calculated for the present situation was 3.81, calculated as follows:

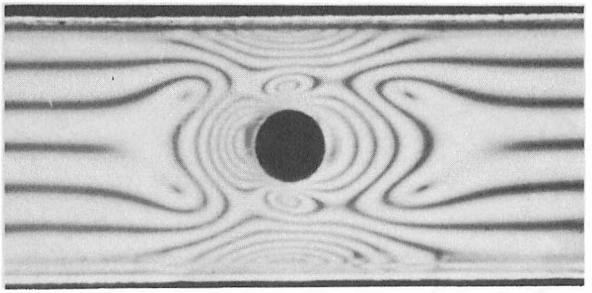

a. Isochromatic photograph

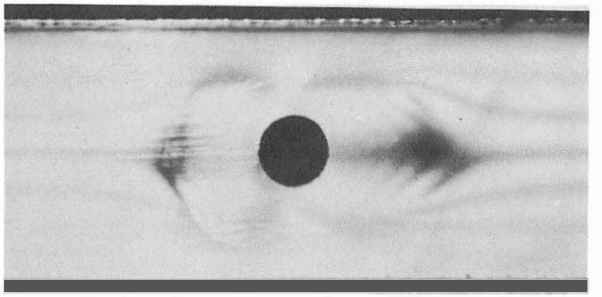

b. Isoclinic photograph, 0°, 90°

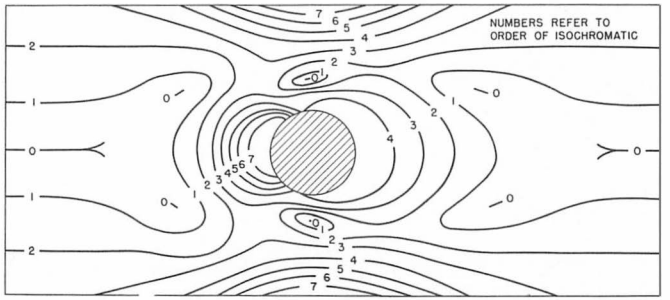

c. Isochromatic tracing

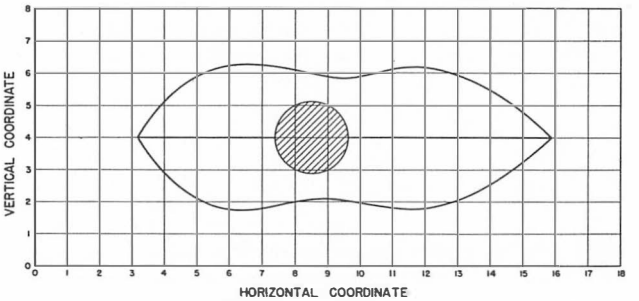

d. Isoclinic traced from b

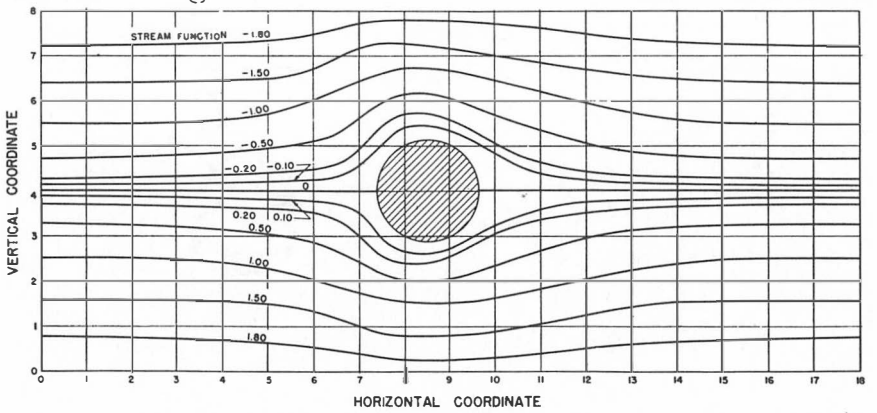

e. Developed streamlines about cylinder

Figure 16. Steps in the development of streamlines about a cylinder

$$Re = \frac{D\ U\ \rho}{\mu} \qquad (29)$$

where

Re = Reynolds number, dimensionless

D = diameter of cylindrical obstacle, cm.

U = average flow velocity cm./sec.

ρ = fluid density, gm./cu.cm.

μ = fluid viscosity, poises

A calculation of the viscous drag coefficient for flow about the cylinder was made as illustrated in Appendix G. Again checking was hampered by the lack of available measurements in the literature for flow about a cylinder in a closely bounded channel. The value of the viscous drag coefficient of 1.83 obtained from double refraction measurements was compared with the experimental value of 2.0 given by Goldstein (14) for flow in an unbounded channel at the same Reynolds number. The value of 1.86 calculated from the expression of Bairstow et al. (3)(4) for flow in a bounded channel at Reynolds numbers less than 0.1 gave better agreement.

CHAPTER VI

TABULATED RESULTS AND DISCUSSION

Some tabulations will now be presented to show the agreement obtained between the flow rates calculated from the flow double refraction measurements and those measured by the flow meter in the system. These and other results will be discussed along with various sources of error in the flow double refraction technique. Suggestions will be offered for the reduction of these errors, and brief mention will be made of present and future investigations on further properties of aqueous milling yellow solutions.

Flow in Straight Channels

The results for flow in straight channels are given in Table V. Twenty-six flow situations were analyzed and the calculated and measured flow rates compared. Agreement between calculated and measured flow rates was within a maximum deviation of + 7.3, -9.6 per cent, and a mean square deviation of 4.22 per cent. This information, coupled with the excellent agreement between velocity profiles from flow double refraction and viscous measurements shown in Figure 12, tends to confirm the validity of the technique when applied to unidirectional, laminar flow.

TABLE V

AGREEMENT BETWEEN OBSERVED DISCHARGES AND THOSE CALCULATED FROM DOUBLE REFRACTION MEASUREMENTS FOR FLOW IN STRAIGHT CHANNELS

*Page	Discharge Calculated from Flow Double Refraction Measurements cu.cm./sec.	Discharge Read from Flow Meter cu.cm./sec.	Per cent Deviation Calculated from Observed Value
115	159.0	155.7	2.1
116	23.2	23.2	0.0
117	115.9	116.7	-0.7
118	142.2	144.4	-1.5
119	142.1	143.3	-0.8
120	18.1	18.1	0.0
121	51.0	48.0	6.3
122	127.5	127.2	0.2
123	43.4	44.2	-1.8
124	138.0	134.6	2.5
125	59.6	55.8	6.8
126	85.4	81.2	3.9
129	74.3	77.9	-4.6
136	81.4	78.8	3.3
145	59.4	63.0	-5.7
146	31.3	33.5	-6.6
147	170.4	170.0	0.2
148	36.4	38.2	-4.7
149	27.0	27.0	0.0
150	30.5	30.8	-1.0
151	55.6	61.5	-9.6
152	33.9	35.4	-4.2
153	99.6	92.8	7.3
154	54.6	56.3	3.0
155	174.0	173.8	0.1
157	47.1	44.3	6.3

*Page numbers refer to those in the Original Record of Research, Department of Chemical Engineering, University of Tennessee

Since the method of treating the data from the double refraction measurements involved two graphical integrations it would be expected that any random errors in the measurements of the fringe locations themselves would tend to be averaged out and their effect minimized. There were several possible sources of error, however, which would not be so affected. These are: (a) misalignment of optical components due to the optical bench being made in two sections rather than one, (b) difference between the temperature indicated by the thermometer upstream from the test section and the actual temperature in the test section itself, (c) personal errors in reading the rotameter or thermometer, and (d) non-parallelism of the channel walls. The effect of errors from these sources is very difficult to estimate. Every precaution was taken to prevent their arising, but it is doubtful whether any of them were completely eliminated.

Convergent and Divergent Flow

Results for flow in convergent and divergent channels similar to those given above for flow in straight channels, are presented in Table VI. Agreement between calculated and measured flow rates was within a maximum deviation of +13.2, -11.2 per cent and a mean square deviation of 7.75 per cent.

It will be noted that the spread in results for the

TABLE VI

AGREEMENT BETWEEN OBSERVED DISCHARGES AND THOSE CALCULATED FROM DOUBLE REFRACTION MEASUREMENTS FOR FLOW IN CONVERGENT AND DIVERGENT CHANNELS

*Page	Type of Flow	Discharge Calculated from Flow Double Refraction Measurements cu.cm./sec.	Discharge Read from Flow Meter cu.cm./sec.	Per cent Deviation Calculated from Observed Value
130	Convergent	88.8	81.2	9.4
131	Convergent	91.9	81.2	13.2
132	Convergent	91.5	81.2	12.7
133	Divergent	138.7	134.6	3.0
134	Divergent	139.7	134.6	3.8
135	Divergent	136.4	134.6	1.2
137	Convergent	70.3	78.6	-10.6
138	Convergent	36.6	33.6	8.9
139	Convergent	63.6	61.6	3.2
140	Convergent	128.8	127.2	1.3
141	Divergent	97.8	91.1	6.9
142	Divergent	54.5	56.4	-3.4
143	Divergent	39.5	44.5	-11.2
144	Divergent	176.6	173.8	1.6

*Page numbers refer to those in the Original Record of Research, Department of Chemical Engineering, University of Tennessee

convergent and divergent flow cases is somewhat wider than that obtained for straight parallel flow. It is believed that the wider spread is due to an error introduced in measuring the convergent and divergent flow photographs. It will be recalled that these measurements were obtained by direct graphical extension of the channel walls to their point of intersection, striking a circular arc across the channel from this point as center, and measuring the angle of intersection of each isoclinic with this arc using a drafting machine protractor. The location of the exact point of intersection of the channel walls was an extremely difficult process. Slight irregularities in the photograph could move this point backward or forward as much as 0.2 inch. Then when measurements were made by lining up the drafting machine scale between the wall intersection point and the point of intersection of an isochromatic with the circular arc, a consistent error could have been introduced. The angular values from the drafting machine protractor would all have been too high or too low according as the measured point of intersection of the walls lay nearer to or farther from the channel than its true position.

An examination of the interference patterns in a convergent or divergent channel using both plane and circularly polarized light as shown in Figure 17 yields some extremely interesting results in support of the present analysis. As

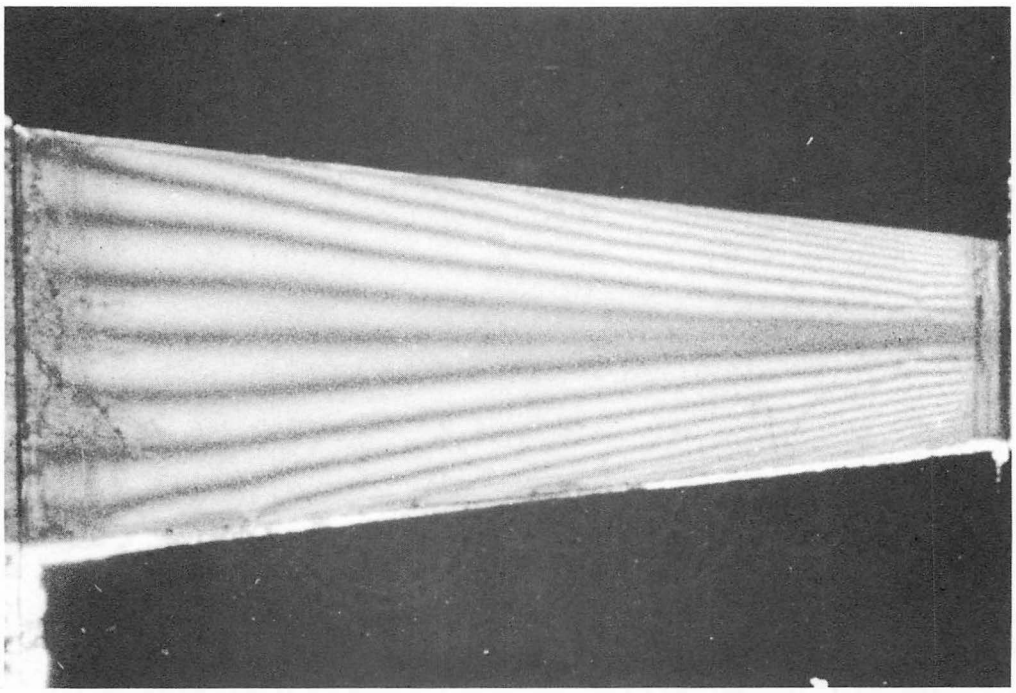

a. Plane polarized light

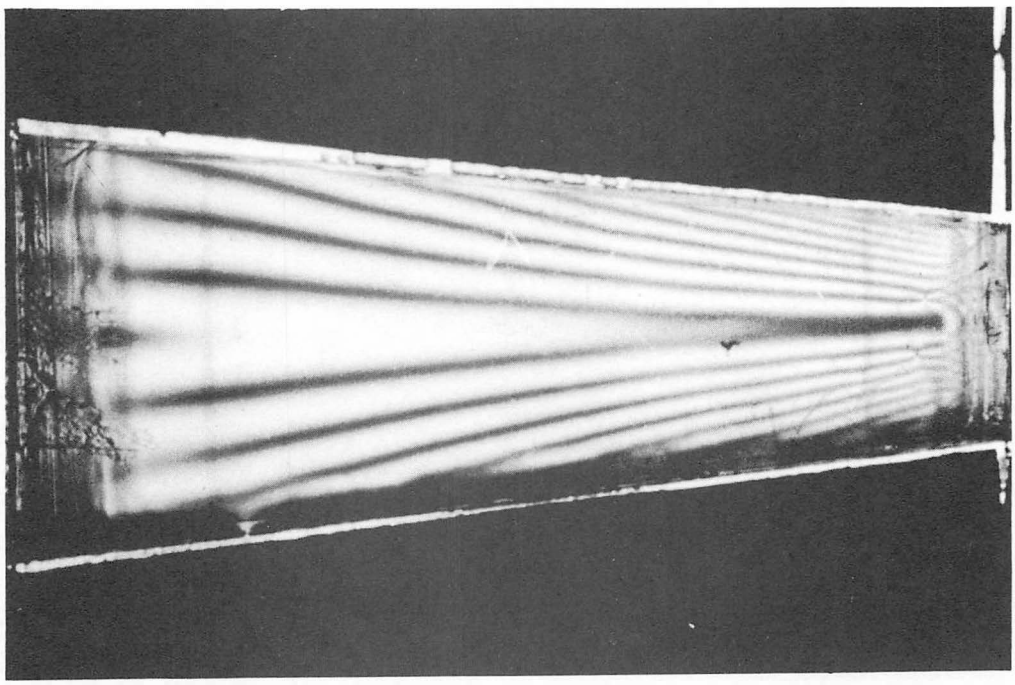

b. Circularly polarized light

Figure 17. Flow patterns produced in a converging channel from plane and circularly polarized light at comparable flow rates

can be seen from Figure 17(b), the pattern given by circularly polarized light has no zero order isochromatic along the center of the channel. If the amount of double refraction were dependent only upon the rate of pure shear, G, as has been suggested by some investigators (9)(15)(25)(34)(including the author), there would certainly be a zero order isochromatic along the center of the channel, for here the rate of pure shear vanishes. On the other hand, the rate of dilation, D, does not vanish and hence the total rate of deformation, E, is not zero. Therefore, the non-appearance of the zero order isochromatic tends to support the conclusion that the amount of double refraction is a function of the total rate of deformation, E (or the maximum shear stress, τ), for the doubly refracting liquids employed in the present study, viz., milling yellow dye solutions.

Figure 17(a) made in plane polarized light does show a dark band along the center line of the channel. This might lead one to suppose that it is, indeed, a zero order isochromatic. However, since the isochromatic must appear in circularly polarized light as well as in plane polarized light, one must conclude that this band is an isoclinic. Recalling equation (15)

$$\theta = \phi - \tfrac{1}{2} \arctan \left(\frac{D}{G}\right) \qquad (15)$$

and noting that G vanishes at the center of the convergent

channel while D does not, we see that here

$$\theta = \phi \pm \frac{\pi}{4} \tag{30}$$

with the sign determined by whether the rate of shear approaches zero from above or below the center line of the channel. Equation (30) states that the plane of maximum shear stress makes an angle of forty-five degrees with the horizontal streamlines at the center of the convergent and divergent channels. The total maximum rate of deformation is quite low, however, and the extinction angle is approximately forty-five degrees. Hence the optic axis of the fluid makes an angle of zero or ninety degrees with the vertical plane of polarization of the incident light, and an isoclinic appears along the channel center line. Now consider what would occur if the optical orientation of the doubly refracting liquid were determined by the streamlines. The horizontal streamline makes an angle of ninety degrees with the vertical plane of polarization of the incident light, the extinction angle is forty-five degrees, and hence the optic axis would be oriented at forty-five degrees to the light polarization. Hence no isoclinic would appear. Since the isoclinic does appear, it may be concluded that the optical orientation of the doubly refracting milling yellow solutions is determined by the direction of the maximum shear stress (or rate of

deformation) rather than by the streamline direction.

Flow about a Cylindrical Obstacle

Because of the lack of an adequate method of checking results, it is difficult to assess the validity of the streamline patterns developed about the cylindrical obstacle. The pattern as shown in Figure 16 satisfies one's intuitive notion as to what such a flow should look like. The wider separation of the streamlines on the downstream side suggests the existence of a stable pair of vortexes directly behind the cylinder. In order to demonstrate these from flow double refraction measurements, it would be necessary to refine the coordinate grid considerably, near the cylinder. Unfortunately, the isochromatic patterns are quite faint and distorted in this region, and it is doubtful that any consistent results could be obtained even if the grid were refined.

In order to obtain any precise indication of flow next to an obstacle of this nature it will probably be necessary to modify the details of channel construction somewhat. As pointed out by Frocht (13) for the case of photoelastic solids, the production of sharp accurate double refraction patterns next to solid boundaries requires that all corners be square and surfaces parallel within very close tolerances. In spite of extreme care exercised in construction of the

Plexiglas channels it is doubtful that the required tolerances could be attained and there was no way to check on this internally after the channel had been assembled. Another difficulty arose in the fixing of the cylindrical obstacle in the channel itself. In order to prevent leaks a rather tight fit was required, and some small amounts of residual stress were set up in the Plexiglas about the cylinder mount. Since Plexiglas is, itself, doubly refracting when stressed, this resulted in further distortion of the interference pattern in the immediate vicinity of the cylinder.

In addition to these sources of error the isoclinic patterns were somewhat diffuse, and it was difficult to locate accurately the center line of a given isoclinic curve for tracing (see Figure 16). This may, again, have been due in part to non-parallelism of the channel walls or to a slight misalignment of the optical components.

In view of these difficulties, it is rather encouraging to note the fairly close agreement in stream function values at the meeting-point for calculations started upstream and downstream from the cylinder (see Figure 15). The agreement within two per cent of the drag coefficients calculated from flow double refraction and the theoretical formula of Bairstow (3) is also encouraging, although there is considerable uncertainty as to the effect produced by using Bairstow's formula at a Reynolds number of 3.81 which is considerably

higher than the maximum value of 0.1 for which it was derived.

It is hoped that eventually a more accurate check on these results can be made by determining the streamline patterns for flow about a cylindrical obstacle by some method other than from flow double refraction measurements. Direct injection of a dark colored dye, or a stream of tiny air bubbles would enable one to trace out the streamline pattern and compare it with that obtained in the present work as shown in Figure 16.

Recommended Improvements

In view of the sources of error mentioned above, it is recommended that a number of improvements and modifications be made on the experimental system described in the present work before further work of a similar nature is undertaken. The channel design should be modified to eliminate in so far as possible, all non-square corners, non-parallel walls, and residual stresses in the walls. This may require abandonment of Plexiglas as the sole material of construction for the channels. Converging and diverging flow sections should be provided with reference marks so that the point of intersection of the non-parallel channel walls can be determined in advance and appear in the flow photograph

itself. A method should be provided for positive alignment of the optical components.

In addition to those mentioned above, changes in the overall flow facility can be recommended which would materially increase the convenience of making flow double refraction measurements. The fluid circulation system should be modified to eliminate brass and copper materials in contact with the dye solution, and allow the dye to come in contact with only glass, plastic, or stainless steel. It is believed that this would stop the rapid darkening and clouding of the solution that occurred in the flow facility and necessitated the laborious preparation of 20-gallon batches of dye at three-week intervals. This aging effect is not observed when solutions are stored in glass containers, even over long periods of time. It would be helpful in maintaining a close temperature control if a smaller pump could be employed. For the present studies, a maximum flow of five or six gallons per minute was more than adequate in contrast with the thirty or forty available; and the additional pump capacity acted as a heater, overloading the refrigeration capacity of the constant temperature bath. A diaphragm or needle valve by-pass arrangement to permit closer flow control would also be desirable.

Parallel and Future Investigations

In spite of the encouraging experimental results, a complete justification of the present techniques requires a sound theoretical basis which is unavailable at present. Such a basis could only be provided by an understanding of the microscopic mechanisms responsible for the flow double refraction of aqueous milling yellow solutions. This mechanism could then be analyzed together with the forces arising from flow to yield theoretical relationships between the amount of double refraction, extinction angle, and rate of deformation in the liquid.

Investigations on the viscous and thermal properties of aqueous milling yellow solutions are now in progress and it is expected that these will be continued. It is hoped that further investigations using an electron microscope may be combined with these to yield information on the microscopic nature of these solutions, for use as a starting point in a future theoretical investigation.

CHAPTER VII

CONCLUSIONS AND RECOMMENDATIONS

From the results of the investigation, the following conclusions may be drawn.

a. The experimental quantities furnished by the flow double refraction technique, viz., magnitude and direction of maximum shearing stress throughout the field of flow, may be analyzed to yield the streamlines and velocity distribution in a two-dimensional laminar flow situation.

b. The results of such analyses are quantitatively accurate within plus or minus ten per cent for flow with straight, parallel streamlines, and within plus or minus fifteen per cent for flow with straight, non-parallel streamlines.

c. Quantitative results may be obtained for a general two-dimensional flow situation involving neither straight nor parallel streamlines. Absolute determination of the limits of error on these results will require further experimental effort.

It is therefore felt that this technique will be of real use in the analysis of complex laminar flow situations which can be idealized to two dimensions. The technique should be especially valuable in those situations where a measuring probe is undesirable, as in the narrow laminar

boundary layers formed next to solid objects in a turbulent stream.

Many refinements in experimental technique are possible which will doubtless improve the degrees of accuracy mentioned above. It is recommended that experimental work be continued to develop such refinements. It is also recommended that further theoretical investigations be undertaken on the microscopic mechanisms responsible for flow double refraction in milling yellow solutions. Such investigations would provide a sounder basis for the techniques of analysis employed.

LIST OF REFERENCES

LIST OF REFERENCES

1. Alcock, E. D. and Sadron, C. L., "An Optical Method for Measuring the Distribution of Velocity Gradients in a Two-Dimensional Flow" Physics 6, 92-95 (1935)

2. Allen, D. N. de G. and Southwell, R. V., "Relaxation Methods Applied to Determine the Motion in Two Dimensions of a Viscous Fluid Past a Fixed Cylinder" Quart. J. Mech. Appl. Math. 8, 129-145 (1955)

3. Bairstow, L., Cave, B. M. and Lang, E. D., "The Two-Dimensional Slow Motion of Viscous Fluids" Proc. Roy. Soc. A100, 394-413 (1922)

4. _____, "The Resistance of a Cylinder Moving in a Viscous Fluid" Phil. Trans. A 223, 383-432 (1923)

5. Balint, E., "Techniques of Flow Visualization" Aircraft Engineering 25, 161-167 (1953)

6. Binnie, A. M., "A Double Refraction Method of Detecting Turbulence in Liquids" Proc. Phys. Soc. (London) 57, 390-402 (1945)

7. Binnie, A. M. and Fowler, J. S., "A Study by a Double Refraction Method of the Development of Turbulence in a Long Circular Tube" Proc. Roy. Soc. A 192, 32-44 (1947)

8. Cerf, R. and Scheraga, H. A., "Flow Birefringence in Solutions of Macromolecules" Chem. Rev. 51, 185-261 (1952)

9. Dewey, D. R., "Visual Studies of Fluid Flow Patterns Resulting from Streaming Double Refraction," Doctoral dissertation, Massachusetts Institute of Technology, 1941

10. Edsall, J. T., "Streaming Birefringence and Its Relation to Particle Size and Shape" Advances in Colloid Science, Vol. I. New York: Interscience Publishers, Inc., (1942) pp. 269-316

11. Edsall, J. T. et al., "An Instrument for the Study of Double Refraction of Flow at Low and Intermediate Velocity Gradients" Rev. Sci. Inst. 23, 695-701 (1952)

12. Farrow, A. P. Jr., "Determination of the Velocity Profiles in Rectangular Channels Using a Doubly Refracting Liquid," Bachelor's Thesis, University of Tennessee, 1956

13. Frocht, M. M., Photoelasticity, Vol. I. New York: John Wiley and Sons, (1941)

14. Goldstein, S., Modern Developments in Fluid Dynamics, Vol. I. Oxford: The Clarendon Press, (1938)

15. Hauser, E. A. and Dewey, D. R., "Study of Liquid Flow" Ind. Eng. Chem. 31, 786 (1939)

16. _____, "Visual Studies of Flow Patterns" J. Phys. Chem. 46, 212-213 (1942)

17. Havewala, J. B., "The Viscous Behavior of Aqueous Milling Yellow Dye Solutions at Very Low Rates of Shear," Unpublished Bachelor's Thesis, University of Tennessee, 1957

18. Hildebrand, F. B., Methods of Applied Mathematics, New York: Prentice-Hall, Inc. (1952)

19. Honeycutt, E. H. Jr. and Peebles, F. N., "Rheological Properties of Aqueous Solutions of Milling Yellow Dye," Progress Report 3 under Contract Number Nonr - 811(04), Knoxville, Tennessee, The Engineering Experiment Station and the Department of Chemical Engineering of the University of Tennessee (1955)

20. Humphry, R. H., "Demonstration of the Double Refraction Due to Motion of a Vanadium Pentoxide Sol and Some Applications" Proc. Phys. Soc. (London) 35, 217-218 (1923)

21. Leaf, W., "Fluid Flow Study of Locomotive Fire Box Design" Mech. Engr. 67, 586-590 (1945)

22. Maron, S. H., Krieger, I. M. and Sisko, A. W., "A Capillary Viscometer with Continuously Varying Pressure Head" J. Appl. Phys. 25, 971-976 (1954)

23. Peebles, F. N., Garber, H. J. and Jury, S. H., "Preliminary Studies of Flow Phenomena Utilizing a Doubly Refracting Liquid" Proc. Third Midwestern Conference on Fluid Mechanics. Minneapolis: The University

of Minnesota Press. 1953

24. Peebles, F. N., Prados, J. W. and Honeycutt, E. H. Jr., "A Study of Laminar Flow Utilizing a Doubly Refracting Liquid" Progress Report 1 under Contract Number Nonr - 811(04), Knoxville, Tennessee, The Engineering Experiment Station and the Department of Chemical Engineering of the University of Tennessee (1954)

25. Prados, J. W. and Peebles, F. N., "Determination of the Flow Double Refraction Properties of Aqueous Milling Yellow Dye Solutions" Progress Report 2 under Contract Number Nonr - 811(04), Knoxville, Tennessee, The Engineering Experiment Station and the Department of Chemical Engineering of the University of Tennessee (1955)

26. Purday, H. F. P., An Introduction to the Mechanics of Viscous Flow, New York: Dover Publications, Inc. (1949)

27. Rosenberg, B., "The Use of Doubly Refracting Solutions in the Investigation of Fluid Flow Phenomena" Navy Dept., David W. Taylor Model Basin, Washington 7, D. C., Report No. 617 (1952)

28. Scarborough, J. B., Numerical Mathematical Analysis, Third Edition. Baltimore: The Johns Hopkins Press, (1955)

29. Streeter, V. L., Fluid Dynamics, New York: McGraw-Hill Book Company, Inc., (1948)

30. Taylor, G. I., "Stability of a Viscous Liquid Contained between Two Rotating Cylinders" Phil. Trans. A 223, 289-343 (1923)

31. Tomotiko, S and Aoi, T., "The Steady Flow of a Viscous Fluid Past a Sphere and Circular Cylinder at Small Reynolds Numbers" Quart. J. Mech. and Appl. Math. 3, 140-161 (1950)

32. Ullyott, P., "Investigation of Flow in Liquids by Use of Birefringent Colloidal Solutions of Vanadium Pentoxide" Trans. ASME 69, 245-251 (1947)

33. Wayland, H., "Streaming Birefringence as a Hydrodynamic Research Tool - Applied to a Rotating Cylinder Apparatus above the Transition Velocity" J. Appl.

Phys. 26, 1197-1205 (1955)

34. Weller, R., "The Optical Investigation of Fluid Flow" J. Appl. Mech. 14, 103-107 (1947)

35. Weller, R., Middlehurst, D. J. and Steiner, R., "The Photoviscous Properties of Fluids" NACA Tech. Note No. 841 (1942)

APPENDIXES

APPENDIX A

THE SHEARING STRESS IN A VISCOUS FLUID IN TERMS OF VELOCITY SPACE DERIVATIVES

Consider a square element in a plane continuum, subjected to a generalized two-dimensional stress system and oriented parallel to a pair of x, y coordinate axes. Such an element is shown in Figure 18 below.

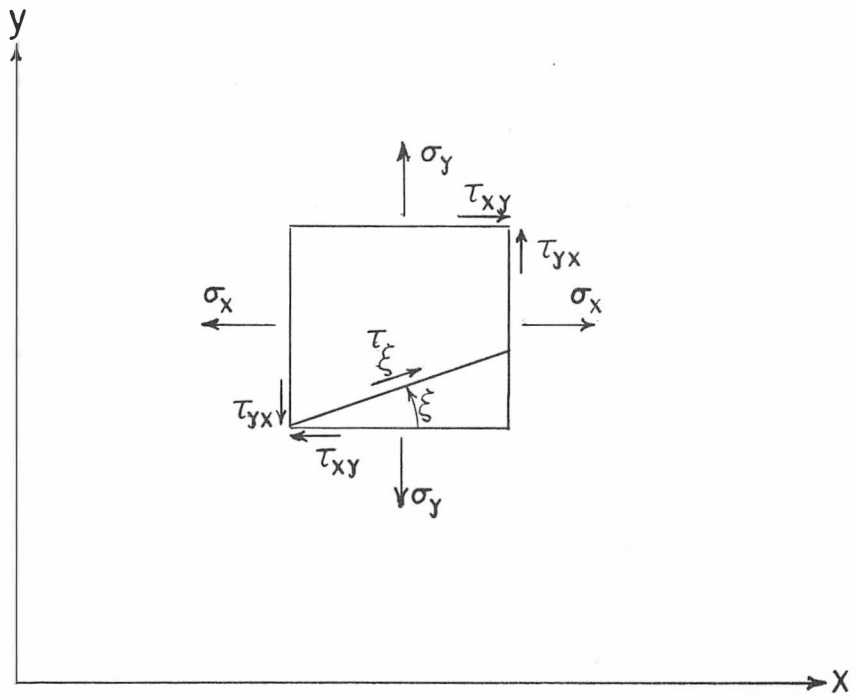

Figure 18. Square element of a continuum, subjected to a generalized two-dimensional stress system

The shear stress acting on a plane of unit length inclined at an angle of ξ to the horizontal in such an element may be obtained by a force balance on the element. (See Frocht

(13) or a strength of materials text for details.)

$$\tau_\xi = \frac{\sigma_y - \sigma_x}{2} \sin 2\xi + \tau_{xy} \cos 2\xi \qquad (30)$$

where

τ_ξ = shearing stress acting on plane inclined at angle ξ to the horizontal

σ_x = normal stress on element in x direction

σ_y = normal stress on element in y direction

τ_{xy} = shear stress acting in x direction on element side facing y direction

It may be remarked that the entire stress system shown in Figure 18 is considered as positive in sign. From the Navier-Stokes development of shear and normal stresses in terms of velocity component derivatives, one may obtain expressions for σ_x, σ_y, and τ_{xy}. These may be found in many references on fluid mechanics, such as that by Streeter (29) and are presented below for the case of two-dimensional, incompressible flow.

$$\sigma_x = -p - 2\mu \frac{\partial u}{\partial x} \qquad (31)$$

$$\sigma_y = -p - 2\mu \frac{\partial v}{\partial y} \qquad (32)$$

$$\tau_{xy} = \mu \left(\frac{\partial u}{\partial y} + \frac{\partial v}{\partial x}\right) \qquad (20)$$

where

p = hydrostatic pressure in fluid

μ = fluid viscosity

u = fluid velocity component in x direction

v = fluid velocity component in y direction

Substitution of equations (31), (32), and (20) into equation (30) yields the following expression:

$$\tau_{\xi} = \mu\left(\frac{\partial v}{\partial y} - \frac{\partial u}{\partial x}\right) \sin 2\xi + \mu\left(\frac{\partial u}{\partial y} + \frac{\partial v}{\partial x}\right) \cos 2\xi \quad (1)$$

which provides the desired relationship between the shearing stress acting in a specified direction in a moving viscous liquid, and the space derivatives of the x and y velocity components. Equation (1) is the starting point for the mathematical considerations of Chapter II.

APPENDIX B

TRANSFORMATION OF DEFORMATION COMPONENTS FROM CARTESIAN TO STREAM COORDINATES

The transformation of equation (1) from rectangular Cartesian coordinates to stream coordinates requires the transformation of the velocity component derivatives:

$$\frac{\partial u}{\partial x}, \quad \frac{\partial v}{\partial y}, \quad \frac{\partial u}{\partial y}, \quad \text{and} \quad \frac{\partial v}{\partial x}$$

To do so one must first write the transformation equations between the two coordinate systems. These equations may be obtained graphically from Figure 19 below.

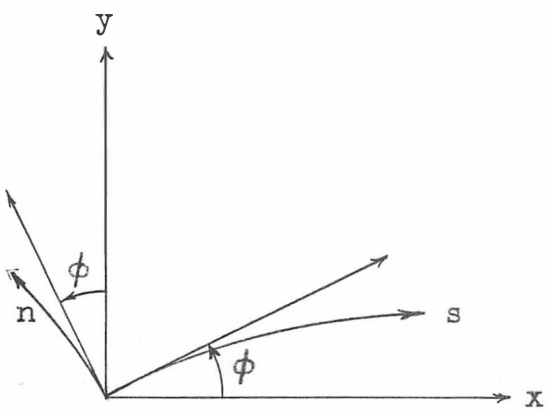

a. Coordinate relationships

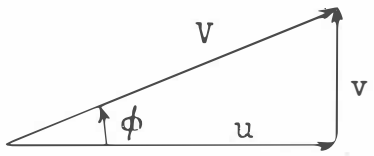

b. Velocity component relationships

Figure 19. Relationships between coordinates and velocity components for Cartesian and stream coordinates

These transformation relations are:

$$s = x \cos\phi + y \sin\phi \tag{33a}$$

$$n = -x \sin\phi + y \cos\phi \tag{33b}$$

$$u = V \cos\phi \tag{34a}$$

$$v = V \sin\phi \tag{34b}$$

where

ϕ = angle made by streamline with the horizontal

s = distance along a streamline

n = distance along a curve normal to a set of streamlines

V = velocity along a streamline

Now if f is a function of s and n, which are in turn functions of x and y (all functions being continuous with continuous first derivatives) one may write that

$$df = \frac{\partial f}{\partial s} \cdot ds + \frac{\partial f}{\partial n} \cdot dn \tag{35}$$

$$\frac{\partial f}{\partial x} = \frac{\partial f}{\partial s} \cdot \frac{\partial s}{\partial x} + \frac{\partial f}{\partial n} \cdot \frac{\partial n}{\partial x} \tag{36a}$$

$$\frac{\partial f}{\partial y} = \frac{\partial f}{\partial s} \cdot \frac{\partial s}{\partial y} + \frac{\partial f}{\partial n} \cdot \frac{\partial n}{\partial y} \tag{36b}$$

where

$f = f(s,n)$

If the derivatives of s and n with respect to x and y are calculated from equations (33a) and (33b), these relations become

$$\frac{\partial f}{\partial x} = \cos\phi \frac{\partial f}{\partial s} - \sin\phi \frac{\partial f}{\partial n} \tag{37a}$$

$$\frac{\partial f}{\partial y} = \sin\phi \frac{\partial f}{\partial s} + \cos\phi \frac{\partial f}{\partial n} \tag{37b}$$

Now one may substitute for the x and y velocity components in the desired expression with the following results.

$$\begin{aligned} \frac{\partial v}{\partial y} - \frac{\partial u}{\partial x} &= \frac{\partial(V \sin\phi)}{\partial y} - \frac{\partial(V \cos\phi)}{\partial x} \\ &= V \cos\phi \frac{\partial \phi}{\partial y} + \sin\phi \frac{\partial V}{\partial y} \\ &\quad + V \sin\phi \frac{\partial \phi}{\partial x} - \cos\phi \frac{\partial V}{\partial x} \end{aligned} \tag{38}$$

Use is now made of (37a) and (37b) with $V = f$ and $\phi = f$, and it is seen that

$$\begin{aligned} \frac{\partial v}{\partial y} - \frac{\partial u}{\partial x} &= V \cos\phi \left[\sin\phi \frac{\partial \phi}{\partial s} + \cos\phi \frac{\partial \phi}{\partial n}\right] \\ &\quad + \sin\phi \left[\sin\phi \frac{\partial V}{\partial s} + \cos\phi \frac{\partial V}{\partial n}\right] \\ &\quad + V \sin\phi \left[\cos\phi \frac{\partial \phi}{\partial s} - \sin\phi \frac{\partial \phi}{\partial n}\right] \\ &\quad - \cos\phi \left[\cos\phi \frac{\partial V}{\partial s} - \sin\phi \frac{\partial V}{\partial n}\right] \end{aligned} \tag{39}$$

After terms are collected and the trigonometric double angle

identities applied, the result,

$$\frac{\partial v}{\partial y} - \frac{\partial u}{\partial x} = \sin 2\phi \left[\frac{\partial V}{\partial n} + V \frac{\partial \phi}{\partial s}\right] - \cos 2\phi \left[\frac{\partial V}{\partial s} - V \frac{\partial \phi}{\partial n}\right] \quad (40)$$

is obtained.

A similar technique is now applied to the terms $\frac{\partial u}{\partial y}$, $\frac{\partial v}{\partial x}$, to yield

$$\begin{aligned} \frac{\partial u}{\partial y} + \frac{\partial v}{\partial x} &= \partial\left(\frac{V \cos\phi}{\partial y}\right) + \partial\left(\frac{V \sin\phi}{\partial x}\right) \\ &= -V \sin\phi \frac{\partial \phi}{\partial y} + \cos\phi \frac{\partial V}{\partial y} \\ &\quad + V \cos\phi \frac{\partial \phi}{\partial x} + \sin\phi \frac{\partial V}{\partial x} \end{aligned} \quad (41)$$

Again use is made of equations (37a) and (37b) and

$$\begin{aligned} \frac{\partial u}{\partial y} + \frac{\partial v}{\partial x} &= -V \sin\phi \left[\sin\phi \frac{\partial \phi}{\partial s} + \cos\phi \frac{\partial \phi}{\partial n}\right] \\ &\quad + \cos\phi \left[\sin\phi \frac{\partial V}{\partial s} + \cos\phi \frac{\partial V}{\partial n}\right] \\ &\quad + V \cos\phi \left[\cos\phi \frac{\partial \phi}{\partial s} - \sin\phi \frac{\partial \phi}{\partial n}\right] \\ &\quad + \sin\phi \left[\cos\phi \frac{\partial V}{\partial s} - \sin\phi \frac{\partial V}{\partial n}\right] \end{aligned} \quad (42)$$

is obtained. The collection of terms and application of the double angle identities results in:

$$\frac{\partial u}{\partial y} + \frac{\partial v}{\partial x} = \cos 2\phi \left[\frac{\partial V}{\partial n} + V \frac{\partial \phi}{\partial s}\right] + \sin 2\phi \left[\frac{\partial V}{\partial s} - V \frac{\partial \phi}{\partial n}\right] \quad (43)$$

Equations (40) and (43) provide the transformed results desired. They are used in the formulation of equation (3), Chapter II.

APPENDIX C

EXPERIMENTAL DATA

The following tables show the data taken at the time the flow photographs were made, and the locations of the isochromatic and isoclinic fringes in the channels. Page numbers refer to the Original Record of Research, Department of Chemical Engineering, University of Tennessee. The page number given under "Data Reference" refers to the page on which the data, taken at the time the photographs were made, were originally recorded. The page number given under "Calculation Reference" refers to the page on which measurements taken from the photographs and calculations are recorded.

TABLE VII

EXPERIMENTAL DATA RECORDED WHILE PHOTOGRAPHING ISOCHROMATIC PATTERNS

Photograph Designation	Data Reference	Calculation Reference	Test Sol'n	Measured Temperature °C	Measured Flow Rate cu.cm./sec.	Type Channel
98B1	10298	115	T-7	24.80	155.7	Cylinder
98B17	10298	116	T-7	24.95	23.2	Diverging
98T19	10298	117	T-7	34.95	116.7	Converging
97B12	10297	118	T-7	25.00	144.4	Converging
97B13	10297	119	T-7	24.80	143.3	Converging
98T11	10298	120	T-7	25.00	18.1	Converging
99-11	10299	121	T-7	24.90	48.0	Cylinder
98T14	10298	122,140	T-7	24.80	127.2	Converging
98B16	10298	123,143	T-7	24.95	44.2	Diverging
98B19	10298	124,133-135	T-7	24.85	134.6	Diverging
98B9	10298	125	T-7	24.95	55.8	Cylinder
97B14	10297	126,130-132	T-7	24.90	81.2	Converging
98T16	10298	129	T-7	24.90	77.9	Converging
98T7	10298	136,137	T-7	24.90	78.8	Converging
97B16	10297	138	T-7	24.90	33.6	Converging
98T17	10298	139	T-7	24.90	61.6	Converging
98B14	10298	141	T-7	24.80	91.1	Diverging
98B15	10298	142	T-7	24.90	50.4	Diverging
98B18	10298	144	T-7	24.80	173.8	Diverging
18-3a	22018	157-163	T-8	25.00	44.3	Cylinder
97B15	10297	145	T-7	24.90	63.0	Converging
97B16	10297	146	T-7	24.90	33.5	Converging
98T1	10298	147	T-7	24.90	170.0	Cylinder

TABLE VII (continued)

EXPERIMENTAL DATA RECORDED WHILE PHOTOGRAPHING ISOCHROMATIC PATTERNS

Photograph Designation	Data Reference	Calculation Reference	Test Sol'n	Measured Temperature °C	Measured Flow Rate cu.cm./sec.	Type Channel
98T8	10298	148	T-7	24.95	38.2	Converging
98T9	10298	149	T-7	25.00	27.0	Converging
98T12	10298	150	T-7	25.00	30.8	Converging
98T17	10298	151	T-7	24.90	61.5	Converging
98T18	10298	152	T-7	24.90	35.4	Converging
98B14	10298	153	T-7	24.80	92.8	Diverging
98B15	10298	154	T-7	24.90	56.3	Diverging
98B18	10298	155	T-7	24.80	173.8	Diverging

TABLE VIII

EXPERIMENTAL DATA RECORDED WHILE PHOTOGRAPHING ISOCLINIC PATTERNS*

Photograph Designation	Data Reference	Measured Temperature °C	Measured Flow Rate cu.cm./sec.	Isoclinic Angle degrees
18-19	22018	25.00	44.3	0
18-20	22018	25.05	44.3	15
18-21	22018	24.95	44.3	30
18-22	22018	24.95	44.3	45
18-23	22018	24.95	44.3	60
18-24	22018	25.00	44.3	75
18-25	22018	25.00	44.3	90
18-26	22018	25.00	44.3	15

*Test solution T-8 used in all cases.

TABLE IX

MEASURED POSITIONS OF ISOCHROMATIC FRINGES IN STRAIGHT CHANNELS

Photograph Designation	Calculation Reference	Isochromatic Order	Vertical Distance from Channel Bottom cm.
98B1	115	6	0.177
98B1	115	5	0.360
98B1	115	4	0.540
98B1	115	3	0.724
98B1	115	2	0.910
98B1	115	1	1.092
98B1	115	0	1.276
98B1	115	1	1.468
98B1	115	2	1.647
98B1	115	3	1.826
98B1	115	4	2.005
98B1	115	5	2.184
98B1	115	6	2.360
98B17	116	3	0.136
98B17	116	2	0.300
98B17	116	1	0.466
98B17	116	0	0.620
98B17	116	1	0.782
98B17	116	2	0.944
98B17	116	3	1.104
98T19	117	4	0.216
98T19	117	3	0.482
98T19	117	2	0.738
98T19	117	1	1.001
98T19	117	0	1.273
98T19	117	1	1.540
98T19	117	2	1.803
98T19	117	3	2.059
98T19	117	4	2.323
97B12	118	5	0.135
97B12	118	4	0.370
97B12	118	3	0.589
97B12	118	2	0.817
97B12	118	1	1.042
97B12	118	0	1.274
97B12	118	1	1.506

TABLE IX (continued)

MEASURED POSITIONS OF ISOCHROMATIC FRINGES IN STRAIGHT CHANNELS

Photograph Designation	Calculation Reference	Isochromatic Order	Vertical Distance from Channel Bottom cm.
97B12	118	2	1.735
97B12	118	3	1.955
97B12	118	4	2.177
97B12	118	5	2.406
97B13	119	5	0.252
97B13	119	4	0.452
97B13	119	3	0.653
97B13	119	2	0.855
97B13	119	1	1.059
97B13	119	0	1.268
97B13	119	1	1.472
97B13	119	2	1.682
97B13	119	3	1.883
97B13	119	4	2.085
97B13	119	5	2.287
98T11	120	2	0.188
98T11	120	1	0.404
98T11	120	0	0.618
98T11	120	1	0.832
98T11	120	2	1.054
99-11	121	2	0.100
99-11	121	1	0.652
99-11	121	0	1.273
99-11	121	1	1.894
99-11	121	2	2.446
98T14	122	5	0.134
98T14	122	4	0.355
98T14	122	3	0.584
98T14	122	2	0.815
98T14	122	1	1.049
98T14	122	0	1.273
98T14	122	1	1.501
98T14	122	2	1.741
98T14	122	3	1.960
98T14	122	4	2.184
98T14	122	5	2.403

TABLE IX (continued)

MEASURED POSITIONS OF ISOCHROMATIC FRINGES IN STRAIGHT CHANNELS

Photograph Designation	Calculation Reference	Isochromatic Order	Vertical Distance from Channel Bottom cm.
98B16	123	6	0.102
98B16	123	5	0.186
98B16	123	4	0.274
98B16	123	3	0.362
98B16	123	2	0.452
98B16	123	1	0.539
98B16	123	0	0.625
98B16	123	1	0.713
98B16	123	2	0.799
98B16	123	3	0.885
98B16	123	4	0.974
98B16	123	5	1.062
98B16	123	6	1.148
98B19	124	5	0.179
98B19	124	4	0.414
98B19	124	3	0.643
98B19	124	2	0.858
98B19	124	1	1.072
98B19	124	0	1.273
98B19	124	1	1.481
98B19	124	2	1.689
98B19	124	3	1.907
98B19	124	4	2.128
98B19	124	5	2.367
98B9	125	2	0.229
98B9	125	1	0.729
98B9	125	0	1.273
98B9	125	1	1.809
98B9	125	2	2.323
97B14	126	3	0.197
97B14	126	2	0.564
97B14	126	1	0.913
97B14	126	0	1.270
97B14	126	1	1.623
97B14	126	2	1.968
97B14	126	3	2.346

TABLE IX (continued)

MEASURED POSITIONS OF ISOCHROMATIC FRINGES IN STRAIGHT CHANNELS

Photograph Designation	Calculation Reference	Isochromatic Order	Vertical Distance from Channel Bottom cm.
98T16	129	2	0.443
98T16	129	1	0.853
98T16	129	0	1.273
98T16	129	1	1.694
98T16	129	2	2.101
98T7	136	3	0.149
98T7	136	2	0.524
98T7	136	1	0.909
98T7	136	0	1.273
98T7	136	1	1.639
98T7	136	2	2.032
98T7	136	3	2.398
97B15	145	8	0.119
97B15	145	7	0.182
97B15	145	6	0.246
97B15	145	5	0.308
97B15	145	4	0.369
97B15	145	3	0.435
97B15	145	2	0.496
97B15	145	1	0.559
97B15	145	0	0.625
97B15	145	1	0.688
97B15	145	2	0.752
97B15	145	3	0.811
97B15	145	4	0.875
97B15	145	5	0.937
97B15	145	6	1.000
97B15	145	7	1.062
97B15	145	8	1.135
97B16	146	4	0.159
97B16	146	3	0.272
97B16	146	2	0.390
97B16	146	1	0.506
97B16	146	0	0.625
97B16	146	1	0.746
97B16	146	2	0.861

TABLE IX (continued)

MEASURED POSITIONS OF ISOCHROMATIC FRINGES IN STRAIGHT CHANNELS

Photograph Designation	Calculation Reference	Isochromatic Order	Vertical Distance from Channel Bottom cm.
97B16	146	3	0.978
97B16	146	4	1.091
98T1	147	6	0.192
98T1	147	5	0.369
98T1	147	4	0.547
98T1	147	3	0.731
98T1	147	2	0.910
98T1	147	1	1.090
98T1	147	0	1.273
98T1	147	1	1.454
98T1	147	2	1.636
98T1	147	3	1.818
98T1	147	4	1.999
98T1	147	5	2.172
98T1	147	6	2.341
98T8	148	5	0.110
98T8	148	4	0.212
98T8	148	3	0.317
98T8	148	2	0.420
98T8	148	1	0.521
98T8	148	0	0.625
98T8	148	1	0.727
98T8	148	2	0.832
98T8	148	3	0.935
98T8	148	4	1.040
98T8	148	5	1.141
98T9	149	3	0.193
98T9	149	2	0.338
98T9	149	1	0.484
98T9	149	0	0.625
98T9	149	1	0.769
98T9	149	2	0.911
98T9	149	3	1.057
98T12	150	4	0.120
98T12	150	3	0.241
98T12	150	2	0.366

TABLE IX (continued)

MEASURED POSITIONS OF ISOCHROMATIC FRINGES IN STRAIGHT CHANNELS

Photograph Designation	Calculation Reference	Isochromatic Order	Vertical Distance from Channel Bottom cm.
98T12	150	1	0.498
98T12	150	0	0.625
98T12	150	1	0.755
98T12	150	2	0.878
98T12	150	3	1.006
98T12	150	4	1.132
98T17	151	8	0.089
98T17	151	7	0.152
98T17	151	6	0.223
98T17	151	5	0.289
98T17	151	4	0.352
98T17	151	3	0.424
98T17	151	2	0.495
98T17	151	1	0.557
98T17	151	0	0.625
98T17	151	1	0.692
98T17	151	2	0.760
98T17	151	3	0.828
98T17	151	4	0.894
98T17	151	5	0.963
98T17	151	6	1.030
98T17	151	7	1.096
98T17	151	8	1.160
98T18	152	5	0.094
98T18	152	4	0.186
98T18	152	3	0.300
98T18	152	2	0.412
98T18	152	1	0.519
98T18	152	0	0.625
98T18	152	1	0.731
98T18	152	2	0.838
98T18	152	3	0.950
98T18	152	4	1.051
98T18	152	5	1.161
98B14	153	4	0.109
98B14	153	3	0.410

TABLE IX (continued)

MEASURED POSITIONS OF ISOCHROMATIC FRINGES IN STRAIGHT CHANNELS

Photograph Designation	Calculation Reference	Isochromatic Order	Vertical Distance from Channel Bottom cm.
98B14	153	2	0.706
98B14	153	1	0.991
98B14	153	0	1.273
98B14	153	1	1.558
98B14	153	2	1.853
98B14	153	3	2.139
98B14	153	4	2.430
98B15	154	8	0.073
98B15	154	7	0.141
98B15	154	6	0.215
98B15	154	5	0.279
98B15	154	4	0.347
98B15	154	3	0.418
98B15	154	2	0.486
98B15	154	1	0.554
98B15	154	0	0.625
98B15	154	1	0.696
98B15	154	2	0.763
98B15	154	3	0.828
98B15	154	4	0.907
98B15	154	5	0.967
98B15	154	6	1.038
98B15	154	7	1.112
98B15	154	8	1.173
98B18	155	6	0.245
98B18	155	5	0.449
98B18	155	4	0.632
98B18	155	3	0.808
98B18	155	2	0.971
98B18	155	1	1.129
98B18	155	0	1.273
98B18	155	1	1.419
98B18	155	2	1.574
98B18	155	3	1.732
98B18	155	4	1.909
98B18	155	5	2.100

TABLE IX (continued)

MEASURED POSITIONS OF ISOCHROMATIC FRINGES IN STRAIGHT CHANNELS

Photograph Designation	Calculation Reference	Isochromatic Order	Vertical Distance from Channel Bottom cm.
98B18	155	6	2.295
18-3a	157	2	0.393
18-3a	157	1	0.816
18-3a	157	0	1.273
18-3a	157	1	1.726
18-3a	157	2	2.160

TABLE X

MEASURED POSITIONS OF ISOCHROMATIC FRINGES
IN CONVERGING CHANNELS

Photograph Designation	Calculation Reference	Isochromatic Order	Distance from Center along Circular Arc* cm.	Radius of Circular Arc cm.
97B14	130	5	-1.132	10.97
97B14	130	4	-0.935	10.97
97B14	130	3	-0.769	10.97
97B14	130	2	-0.565	10.97
97B14	130	1	-0.284	10.97
97B14	130	1	0.284	10.97
97B14	130	2	0.561	10.97
97B14	130	3	0.769	10.97
97B14	130	4	0.938	10.97
97B14	130	5	1.132	10.97
97B14	131	6	-1.033	10.00
97B14	131	5	-0.838	10.00
97B14	131	4	-0.722	10.00
97B14	131	3	-0.585	10.00
97B14	131	2	-0.419	10.00
97B14	131	1	-0.204	10.00
97B14	131	1	0.204	10.00
97B14	131	2	0.416	10.00
97B14	131	3	0.591	10.00
97B14	131	4	0.722	10.00
97B14	131	5	0.838	10.00
97B14	131	6	1.033	10.00
97B14	132	8	-0.868	8.40
97B14	132	7	-0.706	8.40
97B14	132	6	-0.638	8.40
97B14	132	5	-0.650	8.40
97B14	132	4	-0.477	8.40
97B14	132	3	-0.374	8.40
97B14	132	2	-0.259	8.40
97B14	132	1	-0.108	8.40
97B14	132	1	0.112	8.40
97B14	132	2	0.257	8.40
97B14	132	3	0.376	8.40

*Positive distances are above center line, negative distances, below.

TABLE X (continued)

MEASURED POSITIONS OF ISOCHROMATIC FRINGES
IN CONVERGING CHANNELS

Photograph Designation	Calculation Reference	Isochromatic Order	Distance from Center along Circular Arc cm.	Radius of Circular Arc cm.
97B14	132	4	0.474	8.40
97B14	132	5	0.562	8.40
97B14	132	6	0.638	8.40
97B14	132	7	0.709	8.40
97B14	132	8	0.868	8.40
98T7	137	7	-0.858	8.34
98T7	137	6	-0.752	8.34
98T7	137	5	-0.657	8.34
98T7	137	4	-0.572	8.34
98T7	137	3	-0.473	8.34
98T7	137	2	-0.330	8.34
98T7	137	1	-0.153	8.34
98T7	137	1	0.138	8.34
98T7	137	2	0.306	8.34
98T7	137	3	0.449	8.34
98T7	137	4	0.560	8.34
98T7	137	5	0.660	8.34
98T7	137	6	0.752	8.34
98T7	137	7	0.858	8.34
97B16	138	4	-0.776	7.54
97B16	138	3	-0.555	7.54
97B16	138	2	-0.395	7.54
97B16	138	1	-0.197	7.54
97B16	138	1	0.195	7.54
97B16	138	2	0.392	7.54
97B16	138	3	0.555	7.54
97B16	138	4	0.776	7.54
98T17	139	6	-0.863	8.38
98T17	139	5	-0.726	8.38
98T17	139	4	-0.607	8.38
98T17	139	3	-0.480	8.38
98T17	139	2	-0.344	8.38
98T17	139	1	-0.154	8.38
98T17	139	1	0.161	8.38
98T17	139	2	0.332	8.38

TABLE X (continued)

MEASURED POSITIONS OF ISOCHROMATIC FRINGES
IN CONVERGING CHANNELS

Photograph Designation	Calculation Reference	Isochromatic Order	Distance from Center along Circular Arc cm.	Radius of Circular Arc cm.
98T17	139	3	0.483	8.38
98T17	139	4	0.609	8.38
98T17	139	5	0.726	8.38
98T17	139	6	0.863	8.38
98T14	140	8	-1.100	10.68
98T14	140	7	-0.941	10.68
98T14	140	6	-0.857	10.68
98T14	140	5	-0.767	10.68
98T14	140	4	-0.662	10.68
98T14	140	3	-0.534	10.68
98T14	140	2	-0.363	10.68
98T14	140	1	-0.165	10.68
98T14	140	1	0.183	10.68
98T14	140	2	0.382	10.68
98T14	140	3	0.538	10.68
98T14	140	4	0.656	10.68
98T14	140	5	0.771	10.68
98T14	140	6	0.861	10.68
98T14	140	7	0.938	10.68
98T14	140	8	1.100	10.68

TABLE XI

MEASURED POSITIONS OF ISOCHROMATIC FRINGES IN DIVERGING CHANNELS

Photograph Designation	Calculation Reference	Isochromatic Order	Distance from Center along Circular Arc* cm.	Radius of Circular Arc cm.
98B19	133	6	-1.061	10.31
98B19	133	6	-0.621	10.31
98B19	133	5	-0.435	10.31
98B19	133	4	-0.312	10.31
98B19	133	3	-0.227	10.31
98B19	133	2	-0.135	10.31
98B19	133	1	-0.042	10.31
98B19	133	1	0.042	10.31
98B19	133	2	0.132	10.31
98B19	133	3	0.225	10.31
98B19	133	4	0.306	10.31
98B19	133	5	0.432	10.31
98B19	133	6	0.609	10.31
98B19	133	6	1.061	10.31
98B19	134	5	-1.164	11.31
98B19	134	4	-0.631	11.31
98B19	134	3	-0.418	11.31
98B19	134	2	-0.181	11.31
98B19	134	1	-0.066	11.31
98B19	134	1	0.069	11.31
98B19	134	2	0.181	11.31
98B19	134	3	0.293	11.31
98B19	134	4	0.424	11.31
98B19	134	5	0.631	11.31
98B19	134	5	1.164	11.31
98B19	135	8	-0.908	8.81
98B19	135	8	-0.592	8.81
98B19	135	7	-0.433	8.81
98B19	135	6	-0.346	8.81
98B19	135	5	-0.274	8.81
98B19	135	4	-0.215	8.81
98B19	135	3	-0.141	8.81
98B19	135	2	-0.087	8.81
98B19	135	1	-0.031	8.81
98B19	135	1	0.036	8.81

*Positive distances above center line, negative, below.

TABLE XI (continued)

MEASURED POSITIONS OF ISOCHROMATIC FRINGES
IN DIVERGING CHANNELS

Photograph Designation	Calculation Reference	Isochromatic Order	Distance from Center along Circular Arc cm.	Radius of Circular Arc cm.
98B19	135	2	0.097	8.81
98B19	135	3	0.136	8.81
98B19	135	4	0.213	8.81
98B19	135	5	0.269	8.81
98B19	135	6	0.344	8.81
98B19	135	7	0.426	8.81
98B19	135	8	0.554	8.81
98B19	135	8	0.908	8.81
98B14	141	5	-0.738	9.80
98B14	141	4	-0.488	9.80
98B14	141	3	-0.336	9.80
98B14	141	2	-0.202	9.80
98B14	141	1	-0.083	9.80
98B14	141	1	0.086	9.80
98B14	141	2	0.200	9.80
98B14	141	3	0.336	9.80
98B14	141	4	0.482	9.80
98B14	141	5	0.758	9.80
98B15	142	4	-0.884	8.59
98B15	142	3	-0.502	8.59
98B15	142	2	-0.300	8.59
98B15	142	1	-0.125	8.59
98B15	142	1	0.125	8.59
98B15	142	2	0.307	8.59
98B15	142	3	0.510	8.59
98B15	142	4	0.884	8.59
98B16	143	3	-0.737	8.47
98B16	143	2	-0.417	8.47
98B16	143	1	-0.182	8.47
98B16	143	1	0.192	8.47
98B16	143	2	0.422	8.47
98B16	143	3	0.725	8.47
98B18	144	7	-1.065	10.34
98B18	144	7	-0.463	10.34
98B18	144	6	-0.353	10.34

TABLE XI (continued)

MEASURED POSITIONS OF ISOCHROMATIC FRINGES
IN DIVERGING CHANNELS

Photograph Designation	Calculation Reference	Isochromatic Order	Distance from Center along Circular Arc cm.	Radius of Circular Arc cm.
98B18	144	5	-0.286	10.34
98B18	144	4	-0.213	10.34
98B18	144	3	-0.159	10.34
98B18	144	2	-0.087	10.34
98B18	144	2	0.090	10.34
98B18	144	3	0.156	10.34
98B18	144	4	0.217	10.34
98B18	144	5	0.289	10.34
98B18	144	6	0.367	10.34
98B18	144	7	0.472	10.34
98B18	144	7	1.065	10.34

TABLE XII

MEASURED POSITION OF ISOCHROMATIC FRINGES ALONG VERTICAL GRID LINES ABOUT CYLINDER

Horizontal Grid Number	Isochromatic Order	Vertical Distance from Channel Bottom cm.
0	2	0.393
0	1	0.816
0	0	1.273
0	1	1.726
0	2	2.160
1	2	0.303
1	1	0.816
1	0	1.273
1	1	1.726
1	2	2.160
2	2	0.387
2	1	0.808
2	0	1.273
2	1	1.748
2	2	2.168
3	3	0.043
3	2	0.382
3	1	0.813
3	1	1.812
3	2	2.164
3	3	2.490
5	3	0.156
5	2	0.340
5	1	0.524
5	0	0.722
5	1	0.979
5	1	1.538
5	0	1.780
5	1	1.970
5	2	2.157
5	3	2.344
6	5	0.014
6	4	0.133
6	3	0.263
6	2	0.437
6	2	0.798

TABLE XII (continued)

MEASURED POSITION OF ISOCHROMATIC FRINGES ALONG VERTICAL GRID LINES ABOUT CYLINDER

Horizontal Grid Number	Isochromatic Order	Vertical Distance from Channel Bottom cm.
6	3	0.972
6	4	1.156
6	4	1.358
6	3	1.540
6	2	1.710
6	2	2.070
6	3	2.237
6	4	2.370
6	5	2.512
7	6	0.072
7	5	0.159
7	4	0.254
7	3	0.433
7	3	0.768
7	4	0.859
7	5	0.930
7	6	0.992
7	7	1.045
7	7	1.438
7	6	1.491
7	5	1.558
7	4	1.638
7	3	1.747
7	3	2.100
7	4	2.261
7	5	2.374
7	6	2.462
8	7	0.087
8	6	0.152
8	5	0.228
8	4	0.320
8	3	0.436
8	2	0.548
8	1	0.635
8	1	0.693
8	2	0.749

TABLE XII (continued)

MEASURED POSITION OF ISOCHROMATIC FRINGES ALONG VERTICAL GRID LINES ABOUT CYLINDER

Horizontal Grid Number	Isochromatic Order	Vertical Distance from Channel Bottom cm.
8	3	0.780
8	4	0.835
8	5	0.956
8	5	1.592
8	4	1.672
8	3	1.708
8	2	1.749
8	1	1.806
8	1	1.862
8	2	1.951
8	3	2.066
8	4	2.202
8	5	2.295
8	6	2.365
8	7	2.444
9	8	0.014
9	7	0.087
9	6	0.152
9	5	0.228
9	4	0.310
9	3	0.390
9	3	0.739
9	4	0.803
9	5	0.852
9	5	1.648
9	4	1.704
9	3	1.748
9	3	2.137
9	4	2.215
9	5	2.295
9	6	2.365
9	7	2.444
9	8	2.526
10	6	0.087
10	5	0.179
10	4	0.284

TABLE XII (continued)

MEASURED POSITION OF ISOCHROMATIC FRINGES ALONG VERTICAL GRID LINES ABOUT CYLINDER

Horizontal Grid Number	Isochromatic Order	Vertical Distance from Channel Bottom cm.
10	3	0.364
10	2	0.520
10	2	0.597
10	3	0.759
10	4	0.910
10	4	1.273
10	4	1.640
10	3	1.765
10	2	1.878
10	2	2.021
10	3	2.134
10	4	2.235
10	5	2.335
10	6	2.434
11	5	0.043
11	4	0.202
11	3	0.342
11	2	0.469
11	2	0.729
11	3	0.980
11	3	1.595
11	2	1.800
11	2	2.037
11	3	2.180
11	4	2.301
11	5	2.435
12	4	0.036
12	3	0.242
12	2	0.404
12	1	0.567
12	1	0.794
12	2	1.177
12	2	1.510
12	1	1.782
12	1	1.928
12	2	2.092

TABLE XII (continued)

MEASURED POSITION OF ISOCHROMATIC FRINGES ALONG VERTICAL GRID LINES ABOUT CYLINDER

Horizontal Grid Number	Isochromatic Order	Vertical Distance from Channel Bottom cm.
12	3	2.240
12	4	2.421
13	3	0.139
13	2	0.361
13	1	0.560
13	0	0.751
13	1	1.008
13	1	1.533
13	0	1.776
13	1	1.938
13	2	2.036
13	3	2.342
14	3	0.064
14	2	0.368
14	1	0.604
14	1	1.891
14	2	2.036
14	3	2.424
15	3	0.022
15	2	0.368
15	1	0.698
15	1	1.840
15	2	2.036
15	3	2.459
16	3	0.006
16	2	0.368
16	1	0.765
16	1	1.770
16	2	2.036
16	3	2.480
17	2	0.368
17	1	0.812
17	o	1.273
17	1	1.642
17	2	2.036

TABLE XII (continued)

MEASURED POSITION OF ISOCHROMATIC FRINGES
ALONG VERTICAL GRID LINES ABOUT CYLINDER

Horizontal Grid Number	Isochromatic Order	Vertical Distance from Channel Bottom cm.
18	2	0.393
18	1	0.816
18	0	1.273
18	1	1.726
18	2	2.160

TABLE XIII

VALUES OF THE ISOCLINIC ANGLE ALONG VERTICAL GRID LINES ABOUT CYLINDER

Horizontal Grid Number	Isoclinic Angle degrees	Vertical Coordinate
4	45	1.92
4	30	2.54
4	15	2.71
4	0,90	2.80
4	75	2.86
4	60	3.03
4	45	3.15
4	30	3.42
4	15	3.63
4	0,90	4.00
4	75	4.37
4	60	4.59
4	45	4.83
4	30	4.89
4	15	5.06
4	0,90	5.18
4	75	5.25
4	60	5.52
4	45	6.06
5	45	1.02
5	30	1.47
5	15	1.74
5	0,90	2.13
5	75	2.27
5	60	2.47
5	45	2.69
5	30	3.06
5	15	3.37
5	0,90	4.00
5	75	4.66
5	60	4.97
5	45	5.32
5	30	5.46
5	15	5.70
5	0,90	5.85
5	75	6.22

TABLE XIII (continued)

VALUES OF THE ISOCLINIC ANGLE ALONG VERTICAL GRID LINES ABOUT CYLINDER

Horizontal Grid Number	Isoclinic Angle degrees	Vertical Coordinate
5	60	6.65
5	45	6.98
6	45	0.48
6	30	0.89
6	15	1.26
6	0,90	1.84
6	75	2.00
6	60	2.11
6	45	2.52
6	30	2.91
6	15	3.18
6	0,90	4.00
6	75	4.80
6	60	5.10
6	45	5.49
6	30	5.74
6	15	5.98
6	0,90	6.14
6	75	6.69
6	60	7.15
6	45	7.51
7	45	0.22
7	30	0.87
7	15	1.35
7	0,90	1.80
7	75	1.93
7	60	2.20
7	45	2.56
7	30	2.87
7	15	3.13
7	0,90	4.00
7	75	4.87
7	60	5.15
7	45	5.42
7	30	5.85
7	15	6.09

TABLE XIII (continued)

VALUES OF THE ISOCLINIC ANGLE ALONG VERTICAL GRID LINES ABOUT CYLINDER

Horizontal Grid Number	Isoclinic Angle degrees	Vertical Coordinate
7	0,90	6.20
7	75	6.65
7	60	7.17
7	45	7.78
8	45	0.38
8	30	1.62
8	15	1.85
8	0,90	1.93
8	75	2.02
8	60	2.14
8	45	2.76
8	30	2.95
8	60	5.06
8	45	5.19
8	30	5.90
8	15	6.00
8	0,90	6.06
8	75	6.25
8	60	6.37
8	45	7.50
9	45	0.07
9	60	1.96
9	75	1.98
9	90,0	2.00
9	15	2.01
9	30	2.25
9	45	2.72
9	60	2.91
9	30	5.04
9	45	5.27
9	60	5.78
9	75	5.87
9	90,0	5.91
9	15	6.01
9	30	6.13
9	45	7.94

TABLE XIII (continued)

VALUES OF THE ISOCLINIC ANGLE ALONG VERTICAL GRID LINES ABOUT CYLINDER

Horizontal Grid Number	Isoclinic Angle degrees	Vertical Coordinate
10	45	0.12
10	60	1.67
10	75	1.84
10	90,0	1.96
10	15	2.08
10	30	2.15
10	45	2.40
10	60	2.72
10	75	3.02
10	90,0	4.00
10	15	5.00
10	30	5.25
10	45	5.55
10	60	5.76
10	75	5.84
10	90,0	5.95
10	15	6.11
10	30	6.43
10	45	7.87
11	45	0.25
11	60	1.25
11	75	1.56
11	90,0	1.77
11	15	1.93
11	30	2.04
11	45	2.33
11	60	2.67
11	75	3.02
11	90,0	4.00
11	15	4.98
11	30	5.33
11	45	5.61
11	60	5.88
11	75	6.00
11	90,0	6.17
11	15	6.34

TABLE XIII (continued)

VALUES OF THE ISOCLINIC ANGLE ALONG VERTICAL GRID LINES ABOUT CYLINDER

Horizontal Grid Number	Isoclinic Angle degrees	Vertical Coordinate
11	30	6.73
11	45	7.75
12	45	0.43
12	60	1.20
12	75	1.60
12	90,0	1.77
12	15	2.00
12	30	2.13
12	45	2.42
12	60	2.75
12	75	3.07
12	90,0	4.00
12	15	4.93
12	30	5.27
12	45	5.53
12	60	5.77
12	75	5.99
12	90,0	6.18
12	15	6.32
12	30	6.72
12	45	7.56
13	45	0.72
13	60	1.43
13	75	1.83
13	90,0	2.04
13	15	2.24
13	30	2.36
13	45	2.62
13	60	2.94
13	75	3.20
13	90,0	4.00
13	15	4.81
13	30	5.07
13	45	5.33
13	60	5.55
13	75	5.75

TABLE XIII (continued)

VALUES OF THE ISOCLINIC ANGLE ALONG VERTICAL GRID LINES ABOUT CYLINDER

Horizontal Grid Number	Isoclinic Angle degrees	Vertical Coordinate
13	90,0	5.92
13	15	6.07
13	30	6.42
13	45	7.28
14	45	1.17
14	60	2.00
14	75	2.32
14	90,0	2.54
14	15	2.66
14	30	2.79
14	45	3.00
14	60	3.24
14	75	3.42
14	90,0	4.00
14	15	4.62
14	30	4.78
14	45	4.98
14	60	5.13
14	75	5.33
14	90,0	5.43
14	15	5.57
14	30	5.87
14	45	6.84
15	45	1.87
15	60	2.80
15	75	3.07
15	90,0	3.25
15	15	3.28
15	30	3.35
15	45	3.50
15	60	3.65
15	75	3.72
15	90,0	4.00
15	15	4.22
15	30	4.31
15	45	4.50

TABLE XIII (continued)

VALUES OF THE ISOCLINIC ANGLE ALONG VERTICAL GRID LINES ABOUT CYLINDER

Horizontal Grid Number	Isoclinic Angle degrees	Vertical Coordinate
15	60	4.63
15	75	4.67
15	90,0	4.73
15	15	4.85
15	30	4.98
15	45	6.14

APPENDIX D

SAMPLE CALCULATION: STRAIGHT PARALLEL FLOW

The following table contains a complete sample of the calculations made for each of the straight parallel flow situations analyzed. Each column is keyed to a legend below the table in order to show the procedure for obtaining the values in a given column. General data are given below. See Appendix C for a fuller explanation of the headings.

Photograph Designation	98B16
Data Reference	10298
Calculation Reference	123
Channel Dimensions	1.250 cm. x 12.49 cm.
Measured Temperature	24.95°C
Measured Flow Rate	44.2 cu.cm./sec.
Test Fluid Designation	T-7

TABLE XIV

SAMPLE CALCULATIONS FOR STRAIGHT PARALLEL FLOW

(1) Isochromatic Order	(2) Measured Distance from Bottom y', in.	(3) Vertical Distance in Channel y, cm.	(4) E sec^{-1}	(5) y, cm.
Bottom	0	0	-	0
6	0.100	0.102	11.15	0.1
5	0.183	0.186	9.24	0.2
4	0.270	0.274	7.46	0.3
3	0.356	0.362	5.58	0.4
2	0.445	0.452	3.70	0.5
1	0.530	0.539	1.88	0.6
0	0.615	0.625	0	0.625
1	0.702	0.713	1.88	0.7
2	0.786	0.799	3.70	0.8
3	0.871	0.885	5.58	0.9
4	0.958	0.974	7.46	1.0
5	1.045	1.062	9.24	1.1
6	1.130	1.148	11.15	1.250
Top	1.230	1.250	-	

Legend:

(1) From flow photograph
(2) Measured from photograph
(3) By ratio, $\frac{1.250}{1.230}$ (y')
(4) From optical calibration curve for T-7
(5) Arbitrary

TABLE XIV (continued)

SAMPLE CALCULATIONS FOR STRAIGHT PARALLEL FLOW

(6) Δy, cm.	(7) $\overline{\frac{du}{dy}}$, sec^{-1}	(8) $\overline{\frac{du}{dy}}\Delta y$, $\frac{cm.}{sec.}$	(9) v, $\frac{cm.}{sec.}$	(10) $\bar{v}$, $\frac{cm.}{sec.}$	(11) $\bar{v}\Delta y$, $\frac{cm.^2}{sec.}$
			0		
0.1	12.20	1.220		0.61	0.061
			1.220		
0.1	10.07	1.007		1.73	0.173
			2.227		
0.1	8.00	0.800		2.66	0.266
			3.027		
0.1	5.88	0.588		3.35	0.335
			3.615		
0.1	3.74	0.374		3.83	0.383
			3.989		
0.1	1.62	0.162		4.09	0.409
			4.151		
0.025	0.24	0.006		4.15	0.104
			4.157 / 4.175		
0.075	0.80	0.060		4.14	0.311
			4.115		
0.1	2.64	0.264		4.00	0.400
			3.851		
0.1	4.77	0.477		3.62	0.362
			3.374		
0.1	6.95	0.695		3.05	0.305
			2.679		
0.1	9.12	0.912		2.24	0.224
			1.767		
0.150	11.78	1.767		0.95	0.143
			0		

(6) Arbitrary
(7) Graphically from Figure 10
(8) (7) x (6)
(9) Sum of values of (8) from wall outward
(10) Graphically from Figure 10
(11) Sum of values of (10) from wall outward

Calculated flow rate = 43.4 cc./sec.
Per cent deviation from measured flow rate = 1.8

APPENDIX E

SAMPLE CALCULATION: CONVERGING FLOW

The development of the velocity profile for converging or diverging flow requires the numerical solution of the first order differential equation

$$\frac{\partial V}{\partial n} = \pm \sqrt{E^2 - \frac{4\,V^2}{r'^2}} \qquad (18)$$

along a line of constant s (i.e., a stream normal) and subject to the boundary conditions of zero velocity at the channel walls. This equation is of the form

$$\frac{dV}{dn} = g(V,n) \qquad (44)$$

and was solved numerically by the method of Runge and Kutta (28). This method requires the calculation of five difference approximations for each increment in the independent variable, n. The last of these is the desired increment in V. Let Δn be the chosen increment in n and let n_o and V_o be the values of n and V respectively at the beginning of the increment. Then the five difference approximations in terms of equation (18) are given by:

$$k_1 = \left(\sqrt{E^2(n_o) - \frac{4V_o^2}{r'^2}}\right)\Delta n \qquad (45a)$$

$$k_2 = \left(\sqrt{E^2(n_o + \frac{\Delta n}{2}) - \frac{4}{r'^2}(V_o + \frac{k_1}{2})^2}\right)\Delta n \qquad (45b)$$

$$k_3 = \left(\sqrt{E^2(n_o + \frac{\Delta n}{2}) - \frac{4}{r'^2}(V_o + \frac{k_2}{2})^2}\right)\Delta n \qquad (45c)$$

$$k_4 = \left(\sqrt{E^2(n_o + \Delta n) - \frac{4}{r'^2}(V_o + k_3)^2}\right)\Delta n \qquad (45d)$$

$$\Delta V = \frac{1}{6}(k_1 + 2k_2 + 2k_3 + k_4) \qquad (45e)$$

where

k_1, k_2, k_3, k_4 = difference approximations required by Runge-Kutta integration method

Δn = increment in n, distance along stream normal

ΔV = increment in V corresponding to Δn

n_o = value of n at beginning of increment

V_o = value of V at beginning of increment

Starting with the known velocity of zero along the channel walls, equation (18) was integrated by this method working from both walls out to the center. The method is illustrated for a specific integration in Table XV on the following pages. General data are given below with headings as explained in Appendix C. An interpolation plot for calculating E at

various values of n is given in Figure 20.

Photograph Designation	97B16
Data Reference	10297
Calculation Reference	138
Channel Type	Convergent
Measured Temperature	24.90°C
Measured Flow Rate	33.6 cu.cm./sec.
Test Fluid Designation	T-7
Stream Normal Radius	7.538 cm.

$$\frac{4}{r'^2} = \frac{4}{(7.538)^2} = 0.07040 \text{ cm}^{-2}$$

TABLE XV

SAMPLE CALCULATION FOR CONVERGENT FLOW

(1) Isochromatic Order	(2) Angle of Isochromatic Intersection with Stream Normal radians	(3) Distance from Center of Channel along Stream Normal n cm.	(4) Rate of Deformation E_{-1} $sec.^{-1}$	(5) n_o cm.	(6) Δn cm.	(7) $E(n_o)$ $sec.^{-1}$
4 (Top)	0.10298	0.776	7.21	-0.776		7.21
					0.116	
3	0.07359	0.555	5.41	-0.660		6.37
					0.160	
2	0.05207	0.392	3.60	-0.500		4.84
					0.200	
1	0.02589	0.195	1.79	-0.300		2.62
					0.300	
				0		0.746
					0.300	
1	0.02618	0.197	1.79	0.300		2.63
					0.200	
2	0.05236	0.395	3.60	0.500		4.84
					0.160	
3	0.07359	0.555	5.41	0.660		6.39
					0.116	
4 (Bottom)	0.10298	0.776	7.21	0.760		7.21

Legend:
(1) From flow photograph
(2) Measured from photograph
(3) 7.538 x (2)
(4) From T-7 optical calibration
(5) Arbitrary
(6) Arbitrary
(7) From plot of E vs. n (Fig. 20) made from (3) and (4)

TABLE XV (continued)

SAMPLE CALCULATION FOR CONVERGENT FLOW

(8) $E^2(n_o)$ $sec.^{-2}$	(9) $\frac{4}{r'^2} V_o^2$	(10) $E^2(n_o)-\frac{4}{r'^2}V_o^2$	(11) $\sqrt{E(n_o)^2-\frac{4}{r'^2}V_o^2}$	(12) k_1	(13) $E(n_o+\frac{\Delta n}{2})$	(14) $E^2(n_o+\frac{\Delta n}{2})$
51.90	0	51.98	7.21			
				0.8364	6.81	46.38
40.58	0.0438	40.54	6.367			
				1.0187	5.68	32.26
23.43	0.2015	23.23	4.820			
				0.9640	3.68	13.54
6.970	0.4133	6.557	2.561			
				0.7683	1.51	2.280
				0.7650	1.50	2.250
6.917	0.4133	6.504	2.550			
				0.9640	3.67	13.47
23.43	0.2020	23.23	4.820			
				1.0219	5.68	32.26
40.83	0.0439	40.70	6.387			
				0.8364	6.82	46.51
51.98	0	51.98	7.21			

(8) $(7)^2$
(9) $0.07040 \times (31)^2$
(10) (8) - (9)
(11) $\sqrt{(10)}$
(12) (10) x Δn
(13) From plot of E vs. n
(14) $(13)^2$

TABLE XV (continued)

SAMPLE CALCULATION FOR CONVERGENT FLOW

(15) $V_o + \frac{k_1}{2}$	(16) $\frac{4}{r'^2}(V_o + \frac{k_1}{2})^2$	(17) $E^2(n_o + \frac{\Delta n}{2}) - \frac{4}{r'^2}(V_o + \frac{k_1}{2})^2$	(18) $\sqrt{E^2(n_o + \frac{\Delta n}{2}) - \frac{4}{r'^2}(V_o + \frac{k_1}{2})^2}$
0.4182	0.0123	46.37	6.810
1.298	0.1186	32.14	5.669
2.174	0.3327	13.21	3.635
2.807	0.5547	1.725	1.3135
2.806	0.5543	1.696	1.302
2.176	0.3333	13.14	3.625
1.301	0.1192	32.14	5.669
0.4182	0.0123	46.50	6.819

(15) (31)+ $(\frac{12}{2})$ (17) (14) - (16)

(16) 0.07040 x $(15)^2$ (18) $\sqrt{(17)}$

TABLE XV (continued)

SAMPLE CALCULATION FOR CONVERGENT FLOW

(19) k_2	(20) $V_o + \frac{k_2}{2}$	(21) $\frac{4}{r'^2}(V_o + \frac{k_2}{2})^2$	(22) $E^2(n_o + \frac{\Delta n}{2}) - \frac{4}{r'^2}(V_o + \frac{k_2}{2})^2$	(23) $\sqrt{E^2(n_o + \frac{\Delta n}{2}) - \frac{4}{r'^2}(V_o + \frac{k_2}{2})^2}$
0.7900	0.3950	0.0110	46.37	6.810
0.9070	1.243	0.1088	32.15	5.670
0.7270	2.056	0.2976	13.24	3.639
0.3941	2.620	0.4833	1.797	1.3405
0.3906	2.618	0.4825	1.767	1.3295
0.7250	2.057	0.2979	13.17	3.629
0.9070	1.244	0.1089	32.15	3.670
0.7910	0.3955	0.0110	46.50	6.819

(19) (18) x Δn
(20) (31) + $\frac{(19)}{2}$
(21) 0.007040 x $(20)^2$
(22) (14) - (21)
(23) $\sqrt{(22)}$

TABLE XV (continued)

SAMPLE CALCULATION FOR CONVERGENT FLOW

(24) k_3	(25) $V_o + k_3$	(26) $\frac{4}{r'^2}(V_o + k_3)^2$	(27) $E^2(n_o + \Delta n) - \frac{4}{r'^2}(V_o + k_3)^2$	(28) $\sqrt{E^2(n_o + \Delta n) - \frac{4}{r'^2}(V_o + k_3)^2}$
0.7900				
	0.7900	0.0440	40.54	6.367
0.9072				
	1.696	0.2025	23.23	4.820
0.7298				
	2.420	0.4123	6.558	2.561
0.4022				
	2.825	0.5618	0	0
	2.822	0.5606	0	0
0.3989				
	2.420	0.4123	6.505	2.551
0.7258				
	1.697	0.2027	23.23	4.820
0.9072				
	0.7910	0.0440	40.79	6.387
0.7910				

(24) (23) x Δn (26) $0.07040 \times (25)^2$ (28) $\sqrt{(27)}$
(25) (31) ÷ (24) (27) (8) - (26)

TABLE XV (continued)

SAMPLE CALCULATION FOR CONVERGENT FLOW

(29) k_4	(30) ΔV	(31) V_o	(32) $\overline{V}$	(33) $\overline{V}\,\Delta n$
		0		
0.7386	0.789		0.41	0.048
		0.781		
0.7712	0.903		1.26	0.202
		1.692		
0.5122	0.731		2.07	0.414
		2.423		
0	0.393		2.69	0.807
		2.816		
		2.814		
0	0.391		2.68	0.804
		2.433		
0.5101	0.729		2.07	0.414
		1.694		
0.7712	0.904		1.24	0.198
		0.790		
0.7409	0.790		0.39	0.045
		0		

(29) (28) $x\Delta n$

(30) $\frac{1}{6}\left[(12) + 2(19) + 2(24) + (29)\right]$

(31) Previous (31) + (30)

(32) From curve of V vs. n (See Figure 14)

(33) (32) $x\,\Delta n$

Calculated Flow Rate = 36.6 cu.cm./sec.

Per cent Deviation from Measured Flow Rate = +8.9

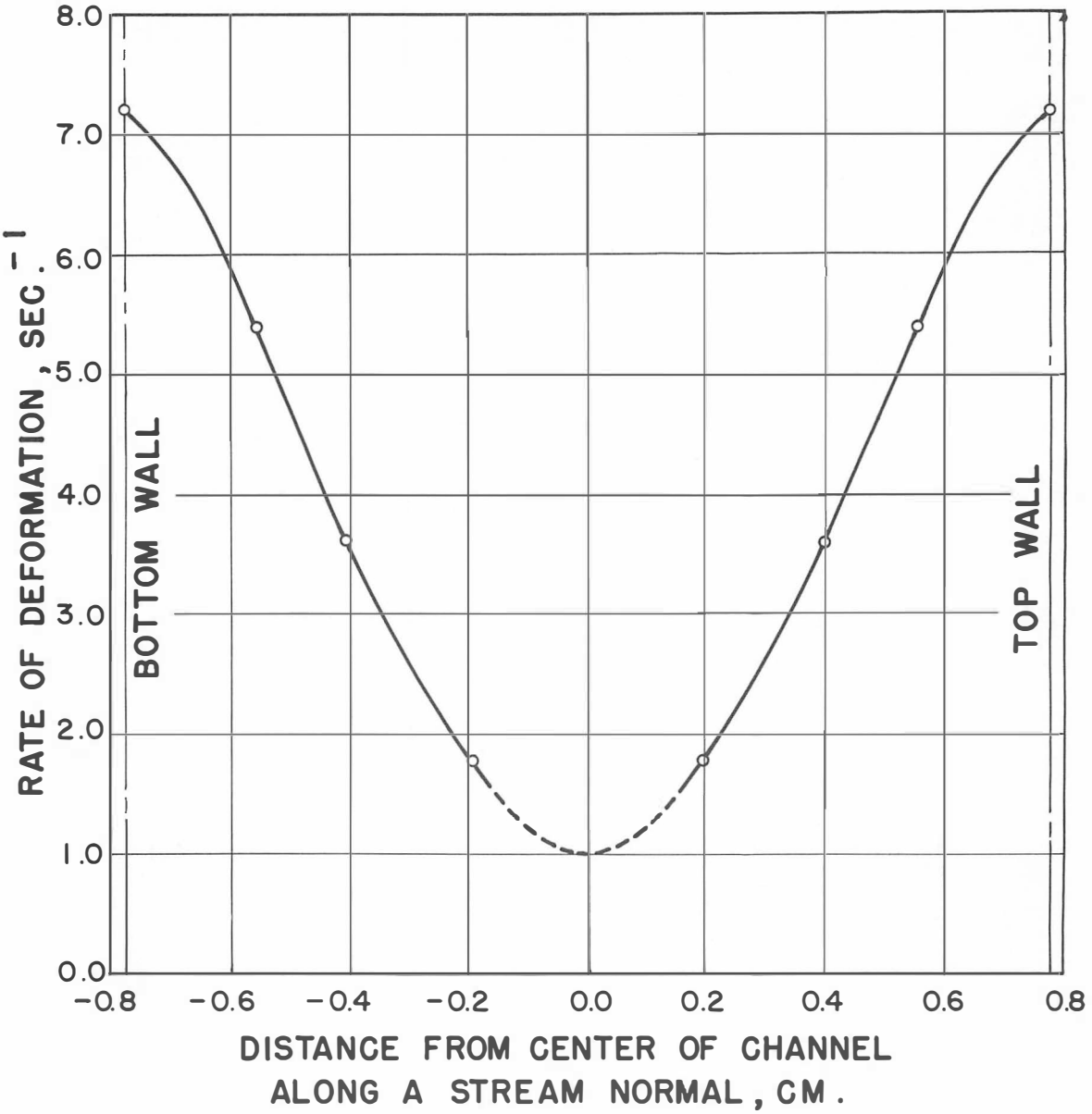

Figure 20. Interpolation plot of rate of deformation versus distance from center of channel along a circular arc; convergent flow

APPENDIX F

SAMPLE CALCULATIONS: THE CYLINDRICAL OBSTACLE

The fairly extensive calculations required for the determination of the stream function are presented here in sample and tabular form. The order of presentation follows that in which the calculations were made, i.e.: (a) calculation of the stream function upstream from the cylinder (Table XVI); (b) determination of the isoclinic angle and rate of deformation at certain points from the flow pattern photographs, and throughout the field by interpolation (Figure 21); (c) determination of the x-component of the deformation rate at the corners of the coordinate grid (Figure 22 and following page); and (d) determination of the stream function at the corners of the coordinate grid by iteration from equation (24) (results in Figure 15, Chapter V). It should be noted here that original data used in these calculations and sample plots are given in Tables XII and XIII, Appendix C.

Calculation of the Stream Function, ψ, across the Channel Upstream from the Cylindrical Obstacle

This calculation is identical with that shown in Appendix D for flow in a straight channel. Hence only those columns corresponding to (5) and (11) in Appendix D will be

TABLE XVI

STREAM FUNCTION, ψ , UPSTREAM FROM CYLINDER

Distance from Bottom y, cm.	$\bar{u}\,\Delta y$ cm.^{2}/sec.	ψ cm.^{2}/sec.
0		1.893
	0.165	
0.318		1.728
	0.434	
0.637		1.294
	0.604	
0.955		0.690
	0.690	
1.273		0
	0.690	
1.591		-0.690
	0.609	
1.910		-1.299
	0.432	
2.228		-1.731
	0.169	
2.546		-1.900

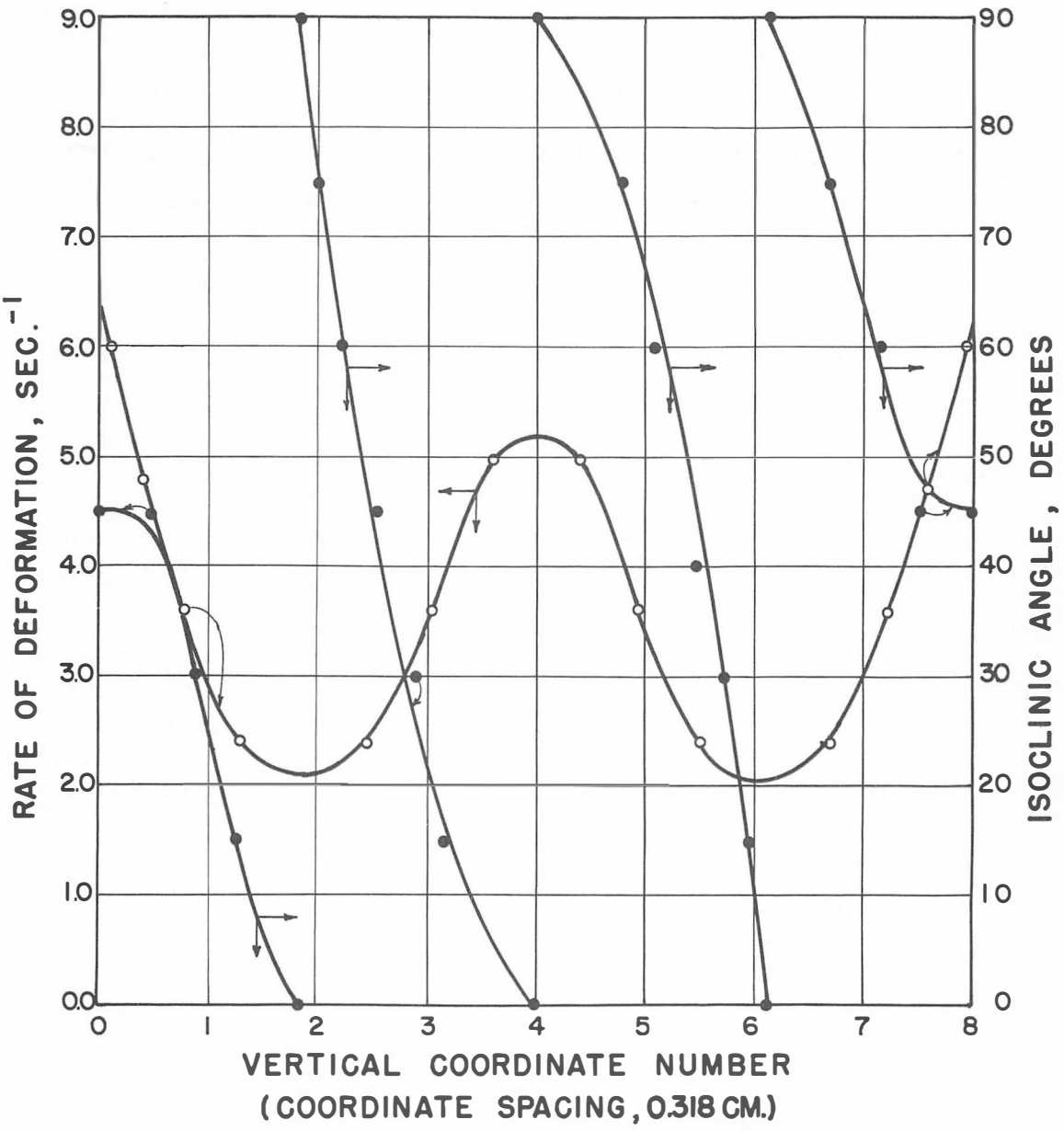

Figure 21. Interpolation plot for isoclinic angle and rate of deformation along vertical grid line number 6

8	3.59 0	3.59 0	3.61 0	3.72 0	4.05 0	4.62 0	6.09 0	8.19 0	9.50 0	9.50 0	8.33 0	6.27 0	4.99 0	4.32 0	3.82 0	3.67 0	3.60 0	3.59 0	3.59 0
7	2.62 0	2.62 0	2.58 0	2.56 39.7 45.0 5.3	2.54 39.7 45.0 5.3	2.55 39.7 45.0 5.3	3.19 38.3 64.0 25.7	4.47 36.6 64.2 27.6	4.80 36.1 48.1 12.0	4.70 36.3 37.3 1.0	4.35 36.7 36.0 -0.7	3.82 36.5 34.1 -2.4	3.07 38.7 35.2 -3.5	2.62 39.5 40.8 1.3	2.62 0	2.62 0	2.62 0	2.62 0	2.62 0
6	1.72 0	1.72 0	1.63 41.4 45.0 3.6	1.52 41.7 45.0 3.3	1.20 42.3 46.6 4.3	0.51 43.9 84.4 40.5	2.06 40.6 11.0 -29.6	3.25 38.4 20.0 -18.4	1.20 42.3 14.0 -28.3	2.87 39.1 10.0 -29.1	2.63 39.5 0.0 -30.5	2.11 40.5 74.8 34.3	0.97 42.8 75.0 32.2	0.66 43.5 10.0 -33.5	1.06 42.6 32.6 -10.0	1.38 42.0 43.6 1.6	1.55 41.6 45.0 3.4	1.70 0	1.72 0
5	0.82 0	0.82 0	0.83 43.2 45.0 1.8	0.64 43.5 45.0 1.5	1.00 42.8 20.5 -21.3	1.15 42.5 68.0 15.5	3.46 38.1 67.0 28.9	6.41 34.3 67.5 33.2	6.00 30	7.16 -30	4.96 35.9 15.0 -20.9	3.60 37.8 15.0 -22.8	1.93 40.9 18.3 -22.6	0.94 42.9 25.9 -17.0	0.68 43.4 48.0 4.6	0.57 43.7 30.0 -13.7	0.71 43.4 45.0 1.6	0.79 0	0.82 0
4	0 0	0 0	0 0	0.13 45.0	0.80 45.0	1.57 45.0	4.87 45.0	9.10 45.0			4.80 45.0	4.06 45.0	2.71 45.0	1.71 45.0	0.98 45.0	0.58 45.0	0.28 45.0	0 0	0 0
3	0.82 0	0.82 0	0.81 43.2 45.0 1.8	0.64 43.5 45.0 1.5	1.00 42.8 60.0 17.2	1.04 42.7 31.9 -10.8	3.24 38.4 22.0 -16.4	5.85 34.9 15.0 -19.9	6.00 -30	6.72 30	4.95 35.9 72.3 36.4	3.60 37.8 75.0 37.2	1.98 40.7 71.7 31.0	0.87 43.0 63.3 20.3	0.65 43.5 45.0 1.5	0.58 43.7 70.0 26.3	0.73 43.4 45.0 1.6	0.78 0	0.82 0
2	1.70 0	1.70 0	1.63 41.4 45.0 3.6	1.49 41.7 45.0 3.3	1.20 42.4 43.5 1.1	0.83 43.1 5.4 -37.7	1.77 41.1 74.0 33.9	3.16 38.6 31.0 32.4	1.85 41.0 76.0 35.0	3.16 38.6 0.0 -38.6	2.30 40.1 3.4 -36.7	2.09 40.5 13.0 -17.5	1.12 42.5 15.0 -27.5	0.98 42.8 85.7 42.9	1.26 42.2 60.0 17.8	1.43 41.9 46.0 5.0	1.63 41.4 45.0 3.6	1.70 0	1.70 0
1	2.62 0	2.62 0	2.62 0	2.59 39.6 45.0 5.4	2.65 39.5 45.0 5.5	2.87 39.1 45.0 5.9	3.55 37.9 25.3 -12.6	4.53 36.5 27.1 -9.4	5.15 35.7 41.3 5.6	4.53 36.5 52.5 16.0	4.80 36.1 53.7 17.6	4.04 37.1 56.2 19.1	3.52 38.0 56.2 18.2	2.97 38.9 49.4 10.5	2.79 39.2 45.0 5.8	2.76 39.3 45.0 5.7	2.68	2.62 0	2.62 0
0	3.61 0	3.61 0	3.69 0	3.72 0	4.20 0	4.77 0	6.12 0	8.22 0	9.60 0	9.60 0	8.48 0	6.63 0	5.31 0	4.53 0	4.03 0	3.83 0	3.68 0	3.61 0	3.61 0
	0	1	2	3	4	5	6	7	8	9	10	11	12	13	14	15	16	17	18

VERTICAL COORDINATE

HORIZONTAL COORDINATE

Vertical order of tabulation:
(top to bottom in a square, values not used are omitted)

maximum rate of deformation, E, sec^{-1}
extinction angle, degrees
isoclinic angle, degrees
angle between direction of E and horizontal, θ, degrees

Figure 22. Tabulation of intermediate data at the corners of the coordinate grid

reproduced here. It was shown in equation (28) that

$$\psi(y) = \psi(0) - \int_0^y u\,dy \qquad (28)$$

In the form for graphical integration, this becomes

$$\psi(y) = \psi(0) - \sum \bar{u} \Delta y \qquad (28a)$$

where $\bar{u}$ is obtained from a plot of u versus y similar to that in Figure 10. The values of y and $\psi(0)$ were arbitrarily set at zero at the center of the channel. General data are given below, with headings as explained in Appendix C.

Photograph Designation	18-3a
Data Reference	22018
Calculation Reference	157-160
Channel Dimensions	2.546 cm. x 12.41 cm.
Measured Temperature	25.00°C
Measured Flow Rate	44.3 cu.cm./sec.
Test Fluid Designation	T-8

Calculation of E_{xy} at a Corner of the Coordinate Grid

Point chosen: 51 (5-horizontal, 1-vertical)

Value of E: 2.87 $sec.^{-1}$ (from isochromatic photograph and optical calibration, by interpolation. See Figures 21 and 22)

Value of extinction angle: 39.1 degrees (from optical calibration)

Value of isoclinic angle: 45.0 degrees (from isoclinic photographs, by interpolation. See Figures 21 and 22)
(Angle between plane of polarization and horizontal, at which an isoclinic appears)

Value of h^2 = 0.1013 (from coordinate spacing)

Value of θ = (isoclinic angle) - (extinction angle)

= 45.0 - 39.1

= 5.9 degrees

$\cos 2\theta = \cos(10.6^{o}) = 0.979$

$E_{xy} = E \cos 2\theta = 2.87 \times 0.979 = 2.81$

$h^2 E_{xy} = 0.1013 \times 2.81 = 0.285$

Calculation of $\psi(x+h,y)$ by Iteration

Point chosen: 62 for $\psi(x+h,y)$

$\psi(x - h,y) = -1.294$ (from Table X)

$\psi(x,y - h) = -0.690$ (from Table X)

$\psi(x,y + h) = -1.728$ (from Table X)

$h^2 E_{xy} = -0.174$ (from calculation similar to above)

$$\psi(x+h,y) = \psi(x,y+h) + \psi(x,y - h) - \psi(x - h,y) + h^2 E_{xy} \quad (24)$$

$\psi(x+h,y) = -1.728 - 0.690 + 1.294 - 0.174 = -1.298$

APPENDIX G

CALCULATION OF THE VISCOUS DRAG COEFFICIENT

Consider the viscous drag force exerted on a long circular cylinder normal to the stream flow. The viscous drag force is defined as the force exerted per unit length of cylinder, in the direction of stream flow, by the viscous forces on the surface of the cylinder. For a differential surface element of cylinder, this force may be expressed as follows:

$$dD_f = \tau \cdot dS \cdot \cos\theta \tag{46}$$

and

$$dS = \frac{d}{2} \cdot d\beta \tag{47}$$

where

D_f = viscous drag force on cylindrical surface

τ = maximum shear stress in fluid along surface of cylinder

θ = angle made by τ with positive x axis (here τ must act tangent to surface of cylinder)

d = diameter of cylinder

β = polar angle inside cylinder

These relations may be seen in Figure 23. Since τ must lie in the plane of a solid boundary, one can find θ for any given value of β chosen. τ itself can be obtained from the

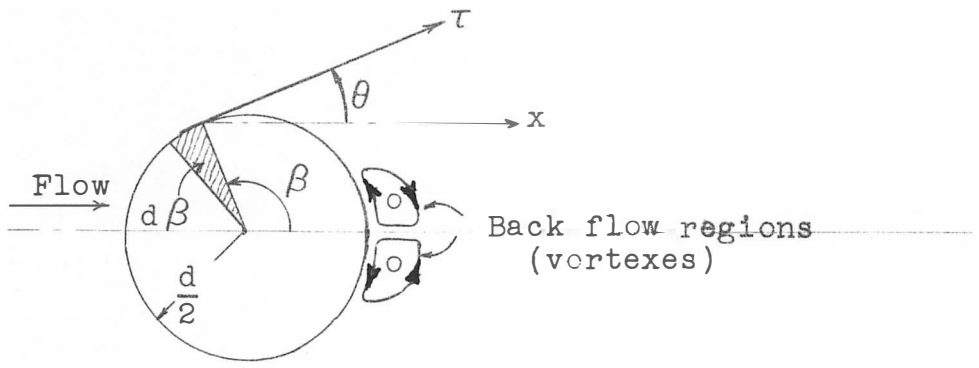

Figure 23. Viscous drag forces on a circular cylinder

photograph of the isochromatic patterns about the cylinder, since τ is specified at each point where an isochromatic touches the cylinder wall. Figure 16 shows such a situation.

It has been pointed out by Tomotiko (31) and others, that even at extremely low Reynolds numbers there exist two stable vortexes on the downstream side of a cylinder normal to the stream flow (See Figure 23). These vortexes would affect the direction of action of τ along the back side of the cylinder causing it to act π radians away from its direction of action were there no back flow. (In either case τ acts along the tangent plane to the cylinder.) The point at which these regions of back flow begin should be marked by a zero isochromatic on both upper and lower surfaces of the cylinder. Unfortunately the isochromatic patterns are too faint in the neighborhood of the cylinder to allow location of these points.

However, estimates of the isochromatic positions along

the cylinder were made from the photograph of Figure 16 and a graphical evaluation was made of the expression

$$D_f = \frac{d}{2}\int_0^{2\pi} \tau \cos\theta \cdot d\beta \qquad (48)$$

as indicated above. Values for E for each isochromatic were obtained from the optical calibration curve of solution T-8, and were multiplied by the viscosity of 0.265 poise to yield corresponding values of τ. θ was obtained from the tangent plane to the cylinder, with direction chosen in the direction of flow; forward over the upstream portion, and reverse over the downstream portion beyond the estimated points of vanishing shear. The calculations are tabulated in Table XVII. General data are the same as those in Appendix F.

From Table XVII, the sum of the values in column (11) multiplied by 0.359 cm., the radius of the cylinder, gives the total drag force per unit length, $D_f = 1.268 \frac{\text{dynes}}{\text{cm.}}$. For purposes of comparison, this is expressed in terms of the frictional drag coefficient, C_{D_f}, defined by the expression:

$$C_{D_f} = \frac{2 D_f}{\rho U^2 d} \qquad (49)$$

where

C_{D_f} = frictional drag coefficient

U = mean flow velocity in channel

TABLE XVII

CALCULATION OF THE VISCOUS DRAG FORCE
ON A CYLINDRICAL OBSTACLE

(1) Isochromatic Order	(2) β radians	(3) θ degrees, minutes	(4) $\cos\theta$	(5) E $sec.^{-1}$	(6) τ $\frac{dynes}{cm.^2}$
4	0.4698	116° 55'	-0.4527	4.80	1.274
3	0.8334	137 45	-0.7402	3.60	0.956
0	1.114	-	-	0	0
3	1.524	- 2 40	0.9989	3.60	0.956
4	1.737	9 30	0.9863	4.80	1.274
4	1.857	16 25	0.9592	4.80	1.274
5	2.006	24 55	0.9069	6.00	1.593
6	2.051	27 30	0.8870	7.20	1.912
7	2.180	34 55	0.8200	8.40	2.230
7	3.748	-55 15	0.5700	8.40	2.230
6	3.879	-47 45	0.6724	7.20	1.912
5	3.984	-41 45	0.7461	6.00	1.593
4	4.244	-26 0	0.8923	4.80	1.274
4	4.481	-13 15	0.9734	4.80	1.274
3	4.852	8 0	0.9903	3.60	0.956
0	5.166	-	-	0	0
3	5.377	-141 55	-0.7868	3.60	0.956
4	6.155	-97 20	-0.1276	4.80	1.274

Legend:

(1) From isochromatic photograph
(2) From isochromatic photograph
(3) $\beta \pm 90°$
(4) cos (3)
(5) From optical calibration curve of T-8
(6) 0.265 x (5)

TABLE XVII (continued)

CALCULATION OF THE VISCOUS DRAG FORCE
ON A CYLINDRICAL OBSTACLE

(7) $\tau\cos\theta$	(8) β	(9) $\Delta\beta$	(10) $\tau\cos\theta$	(11) $\Delta\beta \times \tau\cos\theta$
-0.577	0			
		0.4	-0.279	-0.112
-0.708	0.4	0.4	-0.644	-0.257
0	0.8	0.4	-0.310	-0.124
0.955	1.2	0.4	0.713	0.285
1.257	1.6	0.4	1.235	0.444
1.223	2.0	0.4	1.813	0.726
1.223	2.4	0.4	1.787	0.714
1.696	2.8	0.2	1.332	0.267
1.829	3.0	0.2	0.418	0.084
1.271	3.2	0.4	0.987	0.395
1.285	3.6	0.4	1.270	0.508
1.189	4.0	0.4	1.158	0.463
1.137	4.4	0.4	1.183	0.474
1.240	4.8	0.4	0.573	0.229
0.947	5.2	0.4	-o.685	-0.274
0	5.6	0.4	-0.564	-0.226
-0.752	6.0	0.28	-0.200	-0.056
-0.1626	6.28			

Legend:

(7) (6) x (4)
(8) Arbitrary
(9) Arbitrary
(10) From plot of $\tau\cos\theta$ vs. β
(11) (9) x (10)

The calculation is illustrated below: (Calculation reference 163)

$$U = \frac{44.2 \text{ cu.cm./sec.}}{12.41 \text{ cm.} \times 2.546 \text{ cm.}} = 1.402 \text{ cm./sec.}$$

$$C_{D_f} = \frac{2(1.268) \text{ (gm. cm.)/(cm. sec.}^2\text{)}}{1.002 \frac{\text{gm.}}{\text{cm.}^3} \; (1.402)^2 \; \frac{\text{cm.}^2}{\text{sec.}^2} \; 0.718 \text{ cm.}}$$

$$= 1.83$$

A value for comparison purposes may be obtained from the theoretical formula of Bairstow (3), derived for flow in a bounded channel at a Reynolds number less than 0.1. Bairstow's formula is as follows.

$$C_{D_f} = \frac{7.10}{Re} \qquad (50)$$

where

Re = Reynolds number, defined in equation (29)

For the present case of Re = 3.81 one obtains a value of

$$C_{D_f} = \frac{7.10}{3.81} = 1.86$$

which agrees quite well with the value 1.83 obtained from the flow double refraction measurements.

APPENDIX H

OPTICAL CALIBRATION DATA

All double refraction measurements reported in the present work were made using one of two test solutions, designated, respectively, T-7 and T-8. Optical calibration data for these solutions are presented in Figure 24 on the following page. Curves showing amount of double refraction versus rate of deformation are presented for solution T-7 at temperatures of 24.75°, 24.95°, and 25.20°C.; and for solution T-8 at 25.00°C. A curve of extinction angle versus rate of deformation is shown for solution T-8 at a temperature of 25.00°C. Data reference pages are 22015, 22022, and 156.

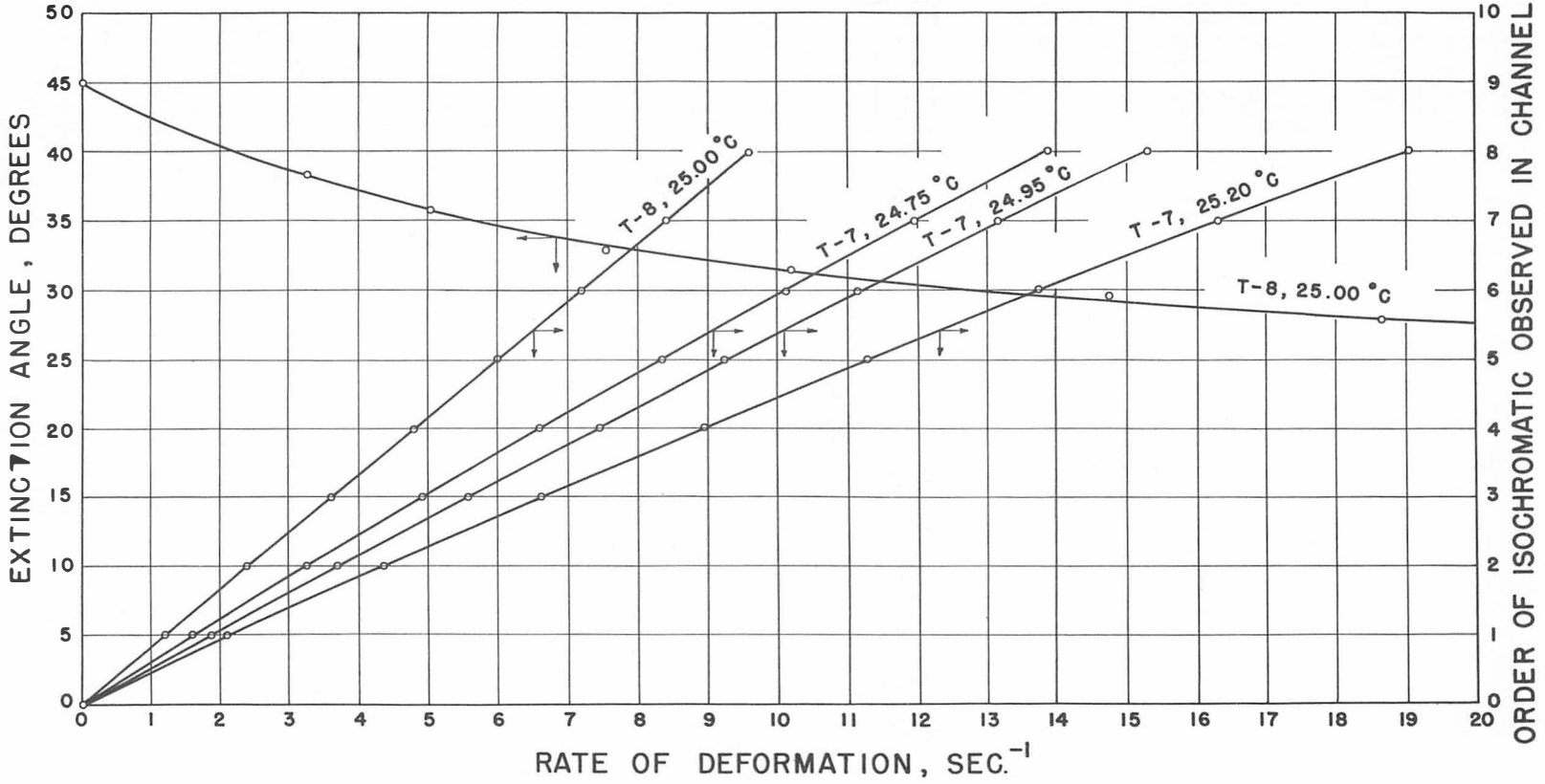

Figure 24. Optical calibration curves for test solutions T-7 and T-8

APPENDIX J

NOTATION

Symbol	Meaning
a	Distance from center to top or bottom of rectangular channel
b	Width of rectangular channel
C_{D_f}	Viscous drag coefficient for circular cylinder
d	Diameter of cylindrical obstacle
D	Rate of dilation in a viscous fluid
D_f	Viscous drag force, exerted in the direction of flow, on a unit length of circular cylinder with axis normal to the flow
E	Maximum rate of deformation at a point in a viscous fluid
E_ξ	Rate of deformation in a viscous fluid along a plane oriented at an angle ξ to the horizontal
E_{xy}	Rate of deformation in a viscous fluid along a horizontal plane
f	Focal length of camera lens
f	Functional notation
g	Functional notation
G	Rate of pure shear in a viscous fluid
h	Incremental distance in x and y coordinates for iterative solution of partial differential equation

Symbol	Meaning
	in difference form
k_1, k_2, k_3, k_4,	Difference approximations used in the numerical solution of a first order ordinary differential equation by the method of Runge and Kutta
n	Stream normal coordinate, distance along a curve normal to a set of streamlines
n_o	Value of stream normal at the start of an increment in the numerical solution of a differential equation by the Runge-Kutta method
Δn	Incremental distance normal to streamlines taken at each step of the Runge-Kutta method for numerical solution of a differential equation
N	Total distance from wall to wall of channel taken along a stream normal
p	Pressure in a moving viscous fluid
Q	Volumetric discharge through flow channel
r	Radius of curvature of a streamline
r'	Radius of curvature normal to a set of streamlines
Re	Reynolds number
s	Streamline coordinate, distance along streamline
S	Surface area per unit length of a circular cylinder
t	time
u	Fluid velocity component in x direction
U	Mean flow velocity of fluid in a channel, i.e., the

Symbol	Meaning
	ratio of volumetric discharge to channel cross sectional area
v	Fluid velocity component in y direction
V	Fluid velocity along a streamline
V_o	Value of fluid velocity along a streamline at the start of an increment in the numerical solution of a differential equation by the Runge-Kutta method
ΔV	Incremental streamline velocity change calculated by the Runge-Kutta procedure, corresponding to incremental distance, Δn, along stream normal
x	Horizontal coordinate-rectangular Cartesian system
y	Vertical coordinate - rectangular Cartesian system
β	Polar angle inside circular cylinder
θ	Angle made by direction of maximum shear stress with the horizontal in a moving viscous fluid
μ	Fluid viscosity
ξ	Angle measured from horizontal made by an arbitrary direction in a moving viscous fluid
π	Ratio of circumference to the diameter of a circle
ρ	Fluid density, mass per unit volume
σ_x	Normal stress exerted in x-direction in a moving viscous fluid
σ_y	Normal stress exerted in y-direction in a moving viscous fluid

Symbol	Meaning
τ	Maximum shear stress at a point in a moving viscous fluid
τ_{ξ}	Shear stress in a moving viscous fluid, acting on a plane oriented at angle ξ to the horizontal
τ_{xy}	Shear stress acting in positive x direction on a surface facing in positive y direction in a moving viscous fluid
τ_{yx}	Shear stress acting in positive y direction on a surface facing in positive x direction in a moving viscous fluid
ϕ	Angle made by a streamline with the horizontal
ψ	Stokes stream function